Doctoral Dissertation

Development of an agricultural robot with wheel and track locomotions based on soil condition

走行環境に応じて走行形態をホイール/トラックに変化させる農業用ロボットの開発

SUPAPHON KAMON
Department of Life Science and Systems Engineering
Graduate School of Life Science and Systems Engineering
Kyushu Institute of Technology

A Doctoral Dissertation

submitted to Graduate School of Life Science and Systems Engineering

Kyushu Institute of Technology

in partial fulfillment of the requirements for the degree of

Ph. D. in ENGINEERING

SUPAPHON KAMON

Thesis Committee:

Professor Kazuo Ishii	(Supervisor)
Professor Shinsuke Yasukawa	(Co-supervisor)
Professor Yuya Nishida	(Co-supervisor)
Professor Keisuke Watanabe	(Co-supervisor)
Professor Hiroyuki Miyamoto	(Co-Supervisor)

Abstract

The use of agricultural machinery has led to soil degradation and the consequent crop yield reduction and maintenance costs increase. During operations on the farm, the heavy vehicles cause damage of soil by compaction and distortion. The soil compaction is damage that occurs in topsoil and subsoil. It is determined by the reduction of soil volume by compressing the soil's pore space. The effect of pore space compressing affects the limitation for water to infiltrate and reach the nutrients in the plant's roots. The soil distortion is damage that occurs only at the topsoil because of the shear force and it destroys the soil's pore space thorough shear deformation. The farmers have to restore the original state of soil and use expensive costs because the soil is damaged.

The soil damage is affected by the state of the soil and by the contact area between soil and running gear. The commonly used running gear in agricultural tasks are wheel system and track system. The main difference between the wheel system and the track system is the contact area with the soil and the pressure distribution. A vehicle with small contact like wheels causes higher soil compaction while tracked system cause higher the soil distortion. This thesis presents a new reconfigurable agricultural vehicle that can switch between the wheeled system and the tracked system according to the terrain conditions. The wheel/track reconfigurable vehicle has 2 wheels on the rear axle and 2 tracks on the front axle. The wheel/track reconfigurable vehicle can adjust the vehicle's contact area by lifting a part of the front tracks off the ground, remaining parts contacting the ground as if they were wheels (wheeled mode), and pushing a part of the tracks to the ground (tracked mode). We present all of the mechanical and electronic parts of the wheel/track reconfigurable vehicle. The power system, system

architecture and a user-friendly graphical interface is presented. The user can control the vehicle by a user-friendly graphical interface.

A wheel/track robot is designed to minimize soil compaction, soil distortion and power consumption. Soil compaction can be defined as a cone index (CI) of soil. We use a cone penetrometer test to measure CI of soil before and after the vehicle pass. The soil distortion can be defined as shear displacement. We put the chalk and measure chalk displacement after vehicle pass. The power consumption of motors can be measured by angular velocity and torque sensor of motor. We compared the soil compaction, soil distortion and power consumption between wheeled mode and tracked mode, without payload and with payload, on firm soil, soft soil and wet soil conditions to define which locomotion mode is preferable in soil conditions. On firm soil, tracked mode causes higher soil distortion, but the power consumption is similar to wheeled mode, so wheeled mode is preferable. On soft soil and wet soil, wheeled mode causes higher power consumption and soil compaction, so tracked mode is preferable. After we decide which mode is better, we design the cost function to switch mode autonomously.

The cost function is used in this research to switch modes. The cost function is a function of soil compaction and soil distortion. The cost function is the tradeoff between wheel mode and track mode. Wheel mode causes higher soil compaction, and track mode causes higher soil distortion.

In the test, we tested wheeled mode, tracked mode, and autonomous switching mode on two different soil conditions (firm soil and soft soil). We compare the results of sinkage, power, and shear displacement between autonomous switching mode and single mode (wheel and track mode). Autonomous switching mode can reduce sinkage

and power if compared with wheel mode. Also, autonomous switching mode can reduce shear displacement if compared with track mode.

Keywords: Soil compaction, Soil distortion, Wheel robot, Track robot, Reconfigurable robot.

Table of Contents

List of Figures

List of Tables

Nomenclature

Symbol	Quantity [unit]
J	Shear displacement [m]
i	Slip [%/100]
x	Contact length [m]
τ_s	Shear stress [pascal]
R	Rolling resistance [N]
l	Lenth of running gear [m]
b	Width of running gear [m]
p	Pressure [pa]
z	sinkage [m]
F	Traction force [N]
A	Contact area [m^2]
c	Cohesion [Pa]
ϕ	Angle shearing resistance [degree]
W	Weight of vehicle [N]
h	Vertical displacement (Scott-Russell) [m]
d	Horizontal displacement (Scott-Russell) [m]
s	Length of Electro hydraulic actuator (Scott-Russell) [m]
k_c	Cohesive modulus of soil deformation [(kN/m^{n+1})]
k_ϕ	Frictional modulus of soil deformation [kN/m^{n+2}]
n	Exponent of soil deformation [unitless]
P	Power consumption [W]
τ	Torque [Nm]
ω	Angular velocity [rad/s]
V	Velocity of robot [m/s]
r	Radius of running gear [m]

Chapter 1
Introduction

Chapter 1. Introduction

This thesis is a research project carried out at the Ishii Laboratory of the Kyushu Institute of Technology in Kitakyushu, Fukuoka JAPAN [1]. Many researchers have developed new technologies to support farmers and agricultural tasks. Technology can solve many problems such as high-quality products, population and labor shortage. Many automation robots and technologies are developed to support agricultural tasks. For example, weeding robots for rice [2,3], navigation in narrow pathways for agricultural robots [4], harvest robots [5,6], etc.

In recent years, many researchers and farmers have attempted to increase the yield production and speed up the process of crops harvesting by increasing agricultural machinery [7,8]. However, increasing agricultural machinery has a detrimental effect/impact on the environment and productivity. The use of heavy agricultural machinery such as tractors [9],[10] affect to soil damage, increase in maintenance costs and crop yield reduction [11],[12],[13]. The wheel/track reconfigurable vehicle is designed to minimize soil damage and power consumption. The vehicle can adjust contact area by switching between wheeled mode and tracked mode to minimize soil damage and reduce power consumption.

1.1. Background

1.1.1 Agricultural soil nature and degradation

Soil is the surface material that includes a set of particles of different sizes and shapes. The size and shape of the soil can determine the mechanical properties and strength of the soil when the weight is loaded on soil surface. The sides of particles can divide the soil types. The particle size bigger than 2 mm is the gravel soil, the particle size between

0.05 mm and 2 mm is the sand soil, the particle size between 0.002 mm and 0.05 mm is the silt soil, and clay soil has particles smaller than 0.002 mm as shown in Table 1.

Soil Type	Particle size
Gravel	> 2 mm
Sand	0.05 mm to 2 mm
Silt	0.002 mm to 0.05 mm
Clay	< 0.002 mm

Table 1 Particle size of soil types

Not all soil types are used in the same way for farming. Each soil type has advantages and disadvantages [14]. The ability that can stand a load before soil failure is the soil strength. In coarse sandy soil, σ is the normal stress exchanged at the contact between particles, as shown in Figure 1-1. The shear stress τ exchanged at the contact of two soil particles and depends on the friction between the particles.

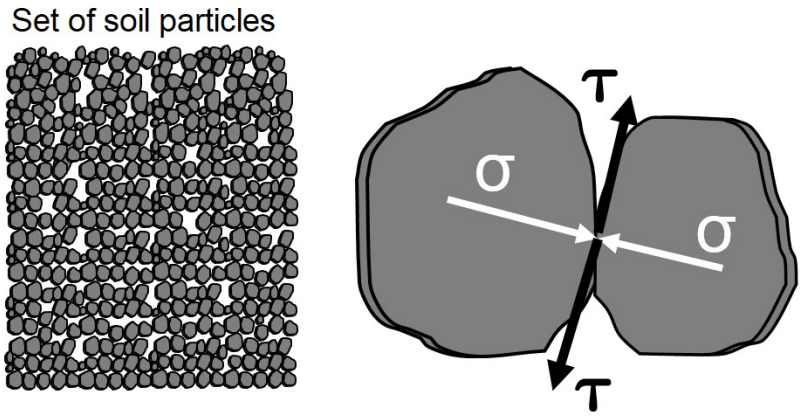

Figure 1-1 Soil structure and normal and shear stresses [1]

The soil consists of a set of particles and gaps between pores, as shown on the left in Figure 1-1. These pores are filled with air and water for root growth, and these gaps can get the nutrients for plants [15]. For the soil problem in farms, the use of heavy machinery destroys the natural state of the pores in two main ways: 1) soil compaction and 2) soil distortion

Soil Compaction: Running gear causes the pressure exerted on the ground that causes the volume reduction in the space between the soil particles. It can affect damage to both topsoil and subsoil, as shown in Figure 1-2 and 1-3. Soil compaction causes pore space reduction, loss of nutrients, and loss of air. It is difficult to access the water for plants. Table 2 shows the limits of suggestions for classifying resistance to penetration [16],[17].

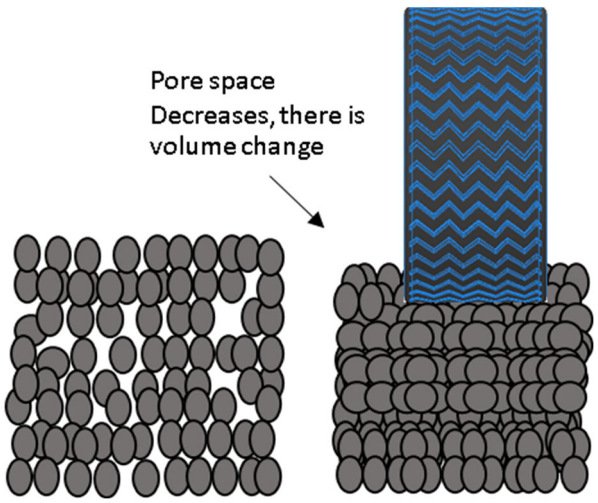

Figure 1-2 Soil before compaction (left) and after the compaction caused by a wheel pass (right) [1]

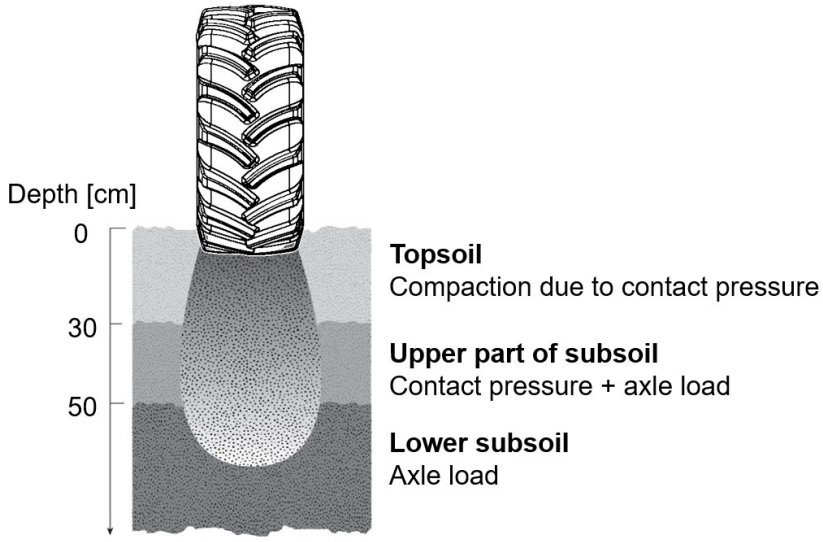

Figure 1-3 Axle load causes compaction in subsoil and contact pressure in the topsoil [1]

Resistance-to-penetration class	Limits (MPa)	Limitations for root growth
Very low	<= 1.0	No Limitations
Low	1.1-2.5	No Limitations
Medium	2.6-5.0	Some limitations
High	5.1-10.0	Some limitations
Very high	10.1-15.0	No root growth possible
Extremely high	>15.0	No root growth possible

Table 2 Suggested limits for classes of soil resistance to penetration [16]

Distortion: this is soil damage caused by the shearing action. The running gear of the vehicle develops at the contact area with the ground. Soil distortion is considered topsoil damage and is related to the shear displacements as shown in Figure 1-4. High slip and the length of the contact area cause topsoil damage in terms of soil cutting. In (1.1) and (1.2) the shear stress as a function of the shear displacement and the shear displacement as a function of the slip are shown respectively.

$$\tau_s = f(J) \tag{1.1}$$

$$J = ix \tag{1.2}$$

Where J is the shear displacement [m], i is the slip and x is the contact length along the moving direction [m].

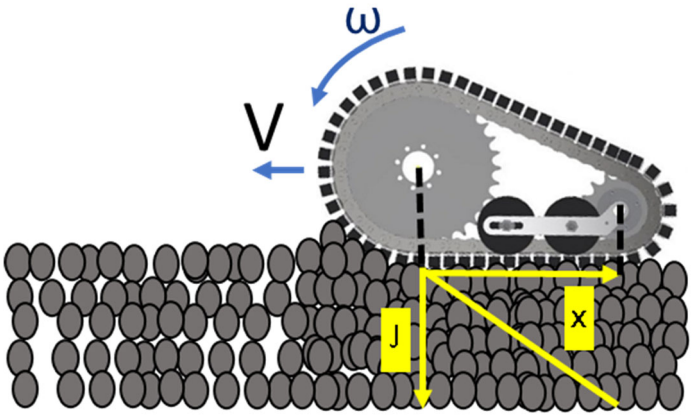

Figure 1-4 Example of shear displacement [1]

The use of heavy tractors causes progressive compaction and distortion [18],[19] on agricultural soil that affect many problems in agriculture. The most detectable problem is crop yield reduction. It is necessary to incur additional costs for restoring land productivity and soil maintenance [20]. The countermeasures of farmers include: 1) avoiding compaction, 2) alleviating methods and 3) no interventions. For the avoiding compaction countermeasure, the farmers use tracked tractor or low-pressure tires for this purpose. For alleviating countermeasure, the ploughing is used for this purpose. This strategy can temporarily restore the soil quality but it needs additional cost. Finally, no interventions, the soil is left in a compacted state, without any attempt to restore the soil.

For the gross margin, avoiding obtained the highest margin. No interventions obtain the lowest gross margin. Farmers' gross margin based on soil management strategy is shown in Figure 1-5.

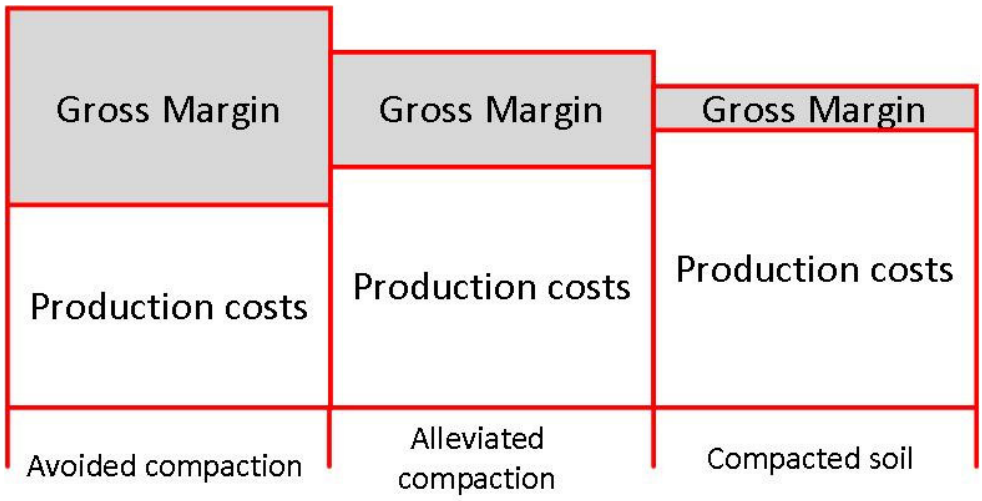

Figure 1-5 Farmers gross margins for different methods to mitigate soil degradation, [9].

The most used running gear for agricultural tasks are wheel and track running gear. The most significant different between two running gears is the contact area with the ground. Contact area also affects the vehicle's performance (traction force, rolling resistance, maneuverability). Rolling resistance on soft terrains can be seen as the work done in compacting the soil and making a rut of area A and depth z , as expressed below [11]

$$Rl = bl\int_0^{z_0} pdz \tag{1.3}$$

where l and b are the length and width of running gear. p is pressure and z is the sinkage. Maximum traction force is expressed as below [11]

$$F = Ac + W\tan\phi \tag{1.4}$$

where A is contact area, c and ϕ are cohesion and angle shearing resistance.

1.1.2 Track vs Wheel

Two different types of locomotion system, tracked and wheeled, are most frequently used in agricultural vehicles, as shown in Figure 1-6. The most significant different between two running gears is the contact area with the ground [21]. The wheel has a smaller contact area. The track has a bigger contact area. As a consequence, the peak pressure under the wheeled vehicle is higher than that under the tracked vehicle in the same weight condition, which leads to higher soil compaction. On the other hand, a tracked vehicle has a longer contact area that develops shear forces and shear displacement. So, tracked vehicles cause greater soil distortion in the top soil. A wheel has greater sinkage than a track. So, the wheel causes higher rolling resistance, and energy consumption. The situation is different on hard soils, track and wheel cause similar sinkage, rolling resistance and power consumption. On cohesive soils, like wet soil, a tracked system is preferable. On frictional soil, wheels may outperform tracks, depending on the diameter, because the area is not so important. Tracked and wheeled vehicle can turn left and right by skid steering [22]. Table 3 shows the comparison between wheel and track.

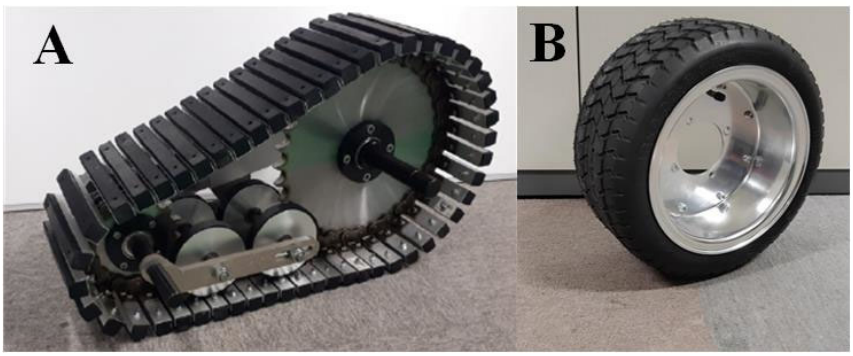

Figure 1-6 Running gear A) Track B) Wheel

Running gear types	Soil compaction	Soil distortion	Rolling resistance on soft soil	Rolling resistance on hard soil
Wheel	High	Low	High	Similar
Track	Low	High	Low	Similar

Table 3 Comparison between wheel and track running gear

1.2. Literature review

1.2.1 The Bekker Model Analysis for Small Robotic

The researcher developed a robotic model to compare different types of running gear on small robotic vehicle platforms. For example, the different types are evaluated in cohesive terrain, such as wet cray. Figure 1-7a shows a four-wheel robotic with 12-inch-diameter tires, and the tires are separated by a distance of 36 inches. The weight of the robot is 1000 lb. The rectangular foot print is 3x4 in. The total contact area of each tire is 12 sq. in. and the overall surface contact area is 48 sq. in. The ground pressure of the robot is 21 psi. The researcher can predict the sinkage, which is 2.3 in. The soil resistance is greater than the maximum soil thrust generated by the robot at this sinkage. A negative value for drawbar pulls (DP) indicates that the robot is incapable of moving forward at a nonzero speed.

Next, the researcher tried to increase the diameter of the tire, and the rectangular foot print of the robot was increased to 3x6 inches, as shown in Figure 1–7b. The total contact area of the robot is increased to 72 sq. in., so the robot causes soil sinkage that is reduced to 1.5 in. The soil resistance is reduced to the point that the vehicle can move with a positive DP. In summary, increasing the diameter of the tire and the contact area can increase the platform DP.

Figure 1-7d shows a robotic platform with a 6x6 wheel configuration. The diameter of the tire is 12 inches, and the foot print is 3x4 inches. The contact area of the robot has been increased to 108 sq. in. The ground pressure of the robot decreases to 9.1 psi, and the soil sinkage is reduced to 1 in. The net vehicle tractive force increases, and the DP increases to double in value.

Figure 1-7c show the track configuration. The length of the track is 25 inches, and the width of the track is 3 inches. The ground pressure is decreased to 6 psi, and the soil sinkage is decreased to 0.6 in. The DP of the track model is greater than that of the platform with the wheel model.

In summary, the performance of a vehicle depends on the overall design of the running gear configuration and contact area. The track has a larger contact area. In wet cray soil, the track has smaller soil sinkage and a higher DP if compared with another wheel robotic platform.

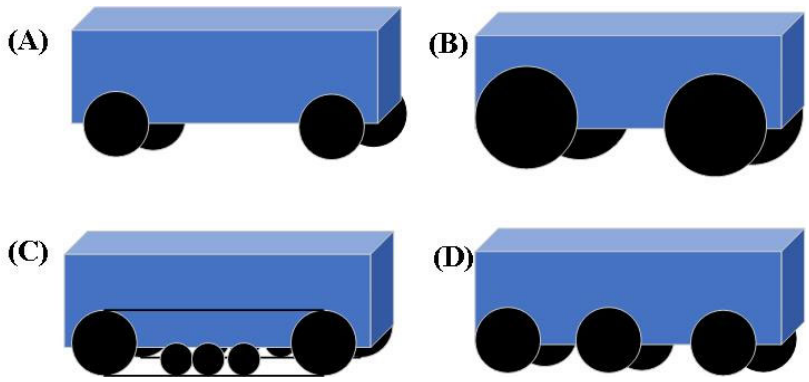

Figure 1-7 Robotic vehicles (a) 4-wheel (b) 4-wheel with larger tires (c) track (d) 6-wheel [76]

1.2.2 Running gear size selection of a wheel/track

In our previous work [1],[29], we tested wheel and track running gear to select the size of the vehicle. The size of running gears is the trade-off between performance weight and soil damage. The field experiments are conducted in a vineyard, and FEM is analyzed for a track and single wheel to evaluate the effect of different contact areas that are rolling resistance, sinkage, and pressure exerted onto the soil. A track is a complex system if compared with the wheel to analyze and simulate because it has a flexible chain, rubber, and peak pressures caused by the track's rollers.

We tested the track on mixed soil at the vinyl house of Kyushu Institute of Technology. The clay, sand, and slit are mixed in percentages of 20, 40, and 40 respectively, as shown in Figure 1-8. We mixed the soil to obtain a loam soil with the cohesive and frictional properties that is a typical of soil in agricultural fields. Then, we performed the pull tests, where the track was connected to a frame and loaded until 100 kg. The walking tractor pulled the track at constant velocity for 2.5 meters through a steel wire. A force gauge sensor was attached the steel wire to measure the rolling resistance. The sizes of the running gears are summarized in Table 4.

We tested different soil conditions: firm soil, soft soil, and wet soil. Table 5 shows results of tests. As we expected, the highest rolling resistance is obtained on deformable soil (soft soil and wet soil). In soft soil conditions, the soil has a higher fraction of pore space, which can cause a compaction and volume reduction. The pores are filled with water in wet soil conditions. It can make the soil incompressible, which leads to soil deformation by distortion. In soft and wet soil conditions, the volume of the soil is deformed, which can cause high rolling resistance.

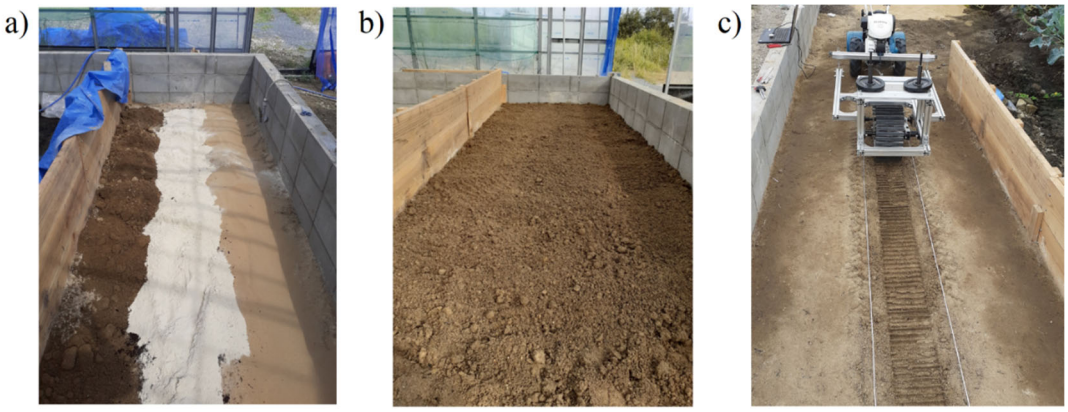

Figure 1-8 Soil bin preparation a), b) and pull test by using a walking tractor c). [1]

Running gear	Size
Sprocket diameter	330 mm
Idler diameter	175 mm
Track width	160 mm
Wheel diameter	300 mm
Wheel width	150 mm

Table 4 Running gear size

Soil Type	Mode	Moisture[%]	Rolling resistance [N]	Sinkage [mm]
Firm soil	Wheeled	42.3	82.3	8.8
	Tracked		78.2	9.5
Soft soil	Wheeled	53.8	120.5	20.3
	Tracked		183.3	24.7
Wet soil	Wheeled	82.7	170	21.2
	Tracked		202.7	31.9

Table 5 Summarization of moisture, rolling resistance, sinkage.

The summarization of results is explained in Table 5. On firm soil, the amount of soil deformed is the same for both track and wheel systems. The rolling resistance and sinkage is similar. There is no reason to use a tracked system when sinkage is limited. Tracked mode cause higher distortion of the soil. On soft and wet soil, track causes lower sinkage, which results in a lower rolling resistance. Track is preferable. We use these results to decide which locomotion mode is better for each soil condition. On firm soil, wheel is better because track causes higher soil distortion. On soft, and wet soil, track is better because wheel causes higher sinkage, which leads to higher compaction and rolling resistance.

1.2.3 Terrain classification

Recently, automatic control and sensing technologies are growing-up. Terrain characterization and classification is the popular challenge for mobile vehicle. Terrain characterization is determined as key parameters of the terrain when robot pass such as friction, roughness, etc. Terrain classification is determined as terrain categories such as glass, sand, gravel, etc. [30]. Robots move using their wheels [31], tracks [32] or legs [33] on terrain to get data from sensors for terrain classification. Once the robot identify terrain,

it can adapt to the new terrain condition through control system. Many researchers have developed control strategy for automatic terrain estimation and classification that can performed by agricultural robot during operations. Types of sensors for terrain classification can be divided into 2 types: 1) proprioceptive sensors and 2) exteroceptive sensors. The state of robot can be measured by proprioceptive sensors such as electrical current, voltage sensor, encoders, inertial measurement unit (IMU), accelerometer, etc. The state of the environment can be measured by exteroceptive sensors such as soil moisture, laser distance sensor, temperature etc.

Giulio et al. (2017) attached proprioceptive sensor (vertical accelerometer and wheel encoders and torque sensors) and exteroceptive sensors (a colour stereo-camera) [34] to get data for terrain estimation, improving the mobility of a mobile base as shown in Fig. The multi-class Support Vector Machine (SVM) was used to classify terrain. The pipeline of the supervised terrain classifier using exteroceptive and proprioceptive data is shown in Figure 1-9 [34]. This research is similar our works. Our vehicle will decide the locomotion mode autonomously based on data of proprioceptive sensors (motors' encoder and torque sensor) and data of exteroceptive sensors (soil moisture sensors and laser distance sensor) in wireless communication with the vehicle.

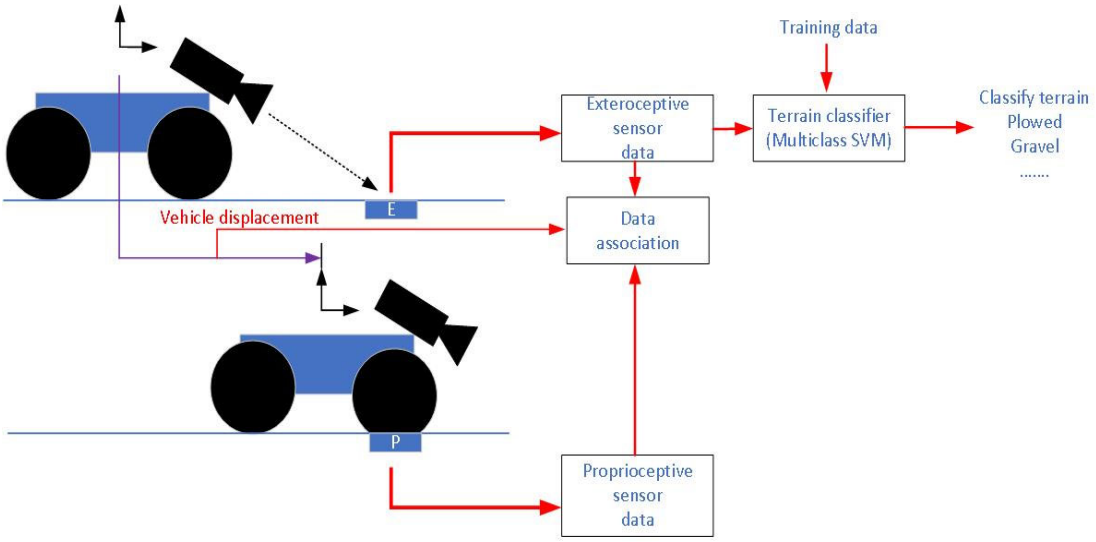

Figure 1-9 Pipeline of the supervised terrain classifier using exteroceptive and proprioceptive data [34]

1.3. Research objective

We therefore propose in this thesis the control strategy to switch locomotion mode to minimize soil damage and power consumption. The objectives of this research are described as below:

1. Minimizing soil damage (sinkage, soil compaction, soil distortion) using the new robot able to change the contact area based on soil condition.
2. Compare the results (soil damage, power) between two locomotion mode on agriculture soil (firm, soft, wet) to decide which locomotion mode (track or wheel) is preferable.
3. Implement a cost function using IF condition to make the robot decide autonomously the locomotion mode suited for the soil conditions.

Chapter 2
Agricultural Robot with Wheel and Track Locomotions

Chapter 2. Agricultural Robot with Wheel and Track Locomotions

2.1. Concept of Robot

The soil damage that is caused by heavy vehicles has two types: Soil compaction and soil distortion. The soil compaction is the result of the normal pressure exerted at the contact patch [23],[24]. It can compress pore spaces and reduce their volume. Soil compaction can reach deep soil layers in the subsoil. The soil distortion is caused by the shear forces exchanged with the soil that can destroy the pores space by a constant volume displacement. Soil distortion is considered topsoil damage [25] and is related to shear displacements. Soil distortion can be estimated by air permeability test [26].

Tracks and wheels are the common running gears used in agricultural vehicles. The main difference between a track and a wheel is the contact area with the ground. Track causes lower soil compaction because it has the better pressure distribution over a larger area. However, track causes higher soil distortion because it has peaks of pressure under the rollers and a higher traction force. Wheels cause higher compaction because they have a smaller contact area.

The different contact area between track and wheel also affects traction performance and power consumption. If the soil is cohesive (For example, clay), a larger contact area of running gear causes a higher traction force. On frictional soils, the soil strength can be increased by the normal stress of running gear, which leads to a higher draught. Moreover, the rolling resistance of running gear is determined by the volume of deformed soil. If the contact area of running gear is small, it can have high rolling resistance and sinkage on

highly deformable soil. Conversely, a large contact area causes lower sinkage and lower rolling resistance [27].

We combine the advantages of wheels and tracks and design the vehicle so that it can adjust the contact area based on soil conditions [28]. The idea of a locomotion system able to change contact area is considered. The name of the wheel/track reconfigurable vehicle is “Hadrian”. The vehicle has a locomotion switching system that can switch between wheeled and tracked modes, by partially lifting the idlers of the tracks and leaving only the sprockets in contact with the ground like a wheel. This concept is depicted in Figure 2-1.

The aim of a wheel/track reconfigurable vehicle is to minimize soil damage and adapt the vehicle’s performance (such as power consumption, torque, and rolling resistance). The aim of Hadrian is to transport the grapes in the vineyard during the harvesting period without using a heavy tractor. Also, Hadrian can be used for harvesting using a robotic arm and watering using a water tank. Hadrian can change its contact area to reduce soil damage and move autonomously using sensors. The wheel/track reconfigurable vehicle uses proprioceptive sensor data (motors’ angular velocity and power consumption) and exteroceptive sensor data (soil moisture sensors and velocity in wireless communication) to decide the locomotion mode autonomously. Humans can operate Hadrian in farms and offices using wireless communication, as shown in Figure 2-2.

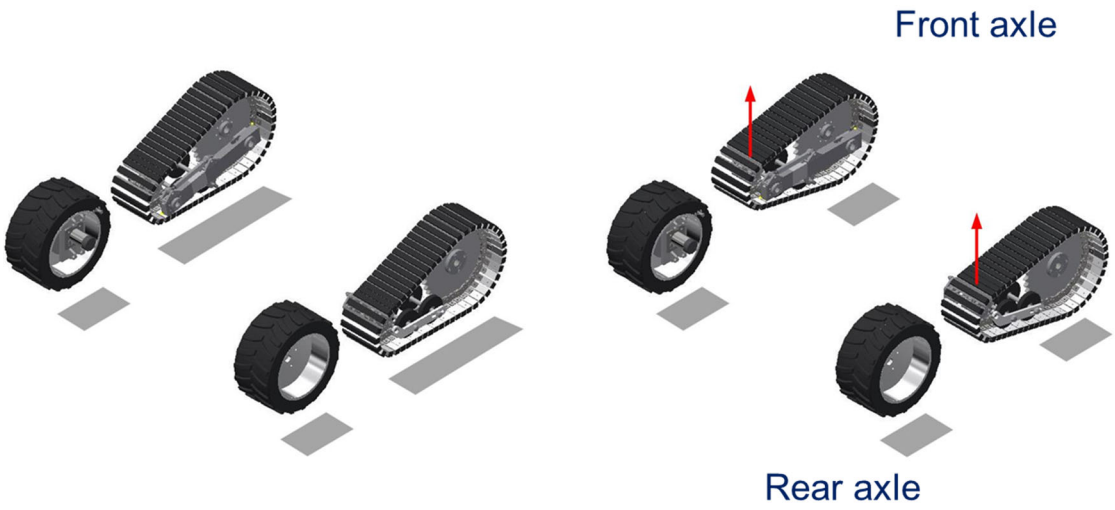

Figure 2-1 Reconfigurable system in tracked mode (left) and wheeled mode (right). [1]

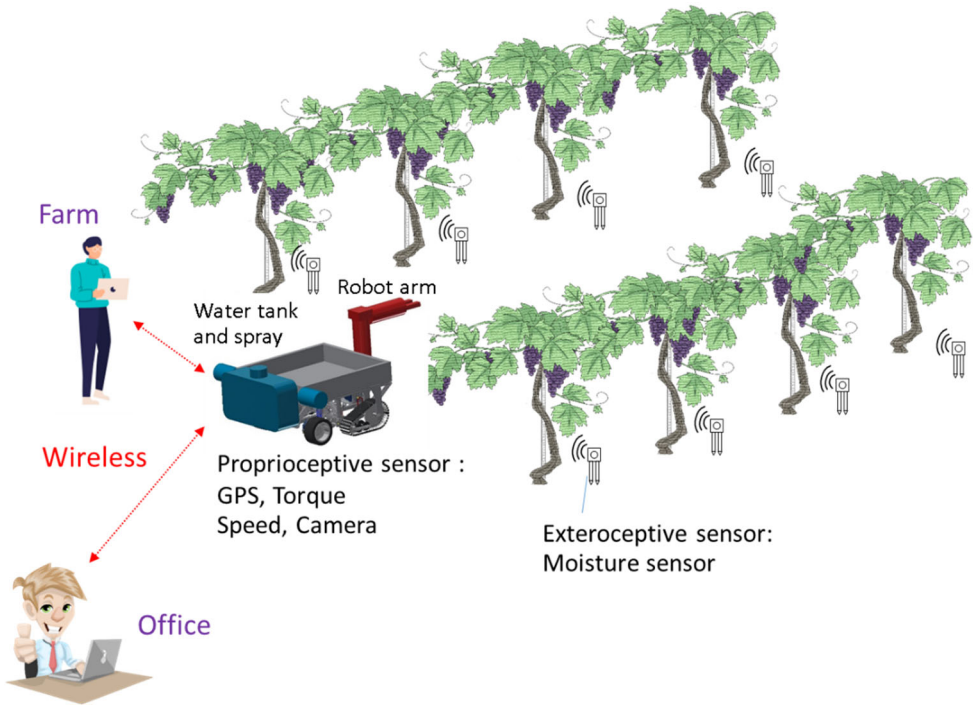

Figure 2-2 Concept design.

2.2. Hardware design

2.2.1 Mechanical design

The name of reconfigurable grape transporting vehicle is “Hadrian”. We can divide the vehicle into three main groups to describe mechanical solution that are rear axle, front axle and switching mechanism. Full vehicle and the three main groups are shown in Figure 2-3.

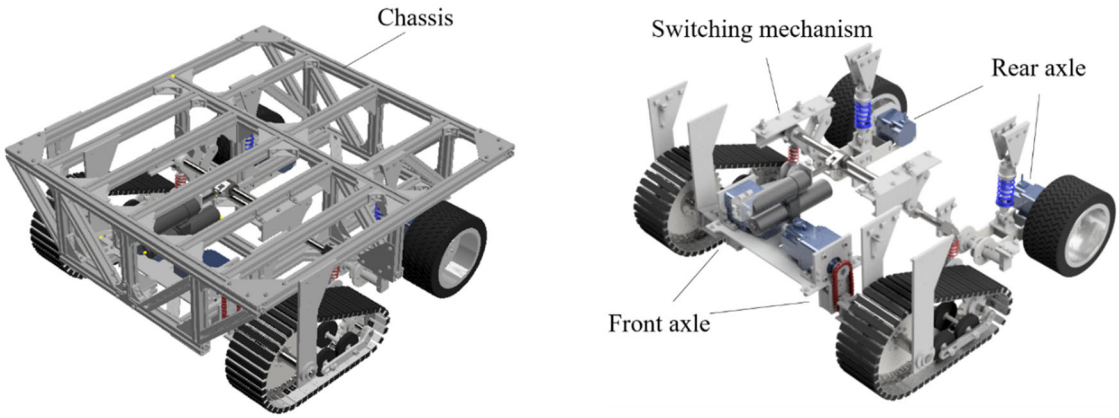

Figure 2-3 Hadrian's overview and main subsystems.[1]

The real axle consists two wheels that are connected to the chassis through a longitudinal trailing arm suspension system. The components of a wheel module are: outer tire, inner tube and rim. Outer tire is BRIDGESTONE PD 13×600-8 2P TL. Inner tube is G-Craft 8-inch 3.5/4.0-8 L and Rim is G-Craft 8 inch 5.5J. The wheel module is shown in Figure 2-4. The longitudinal trailing arm suspension system has the advantage of compact. The longitudinal trailing arm consists of welded plates, as shown in Figure 2-5.

Figure 2-4 Wheel module

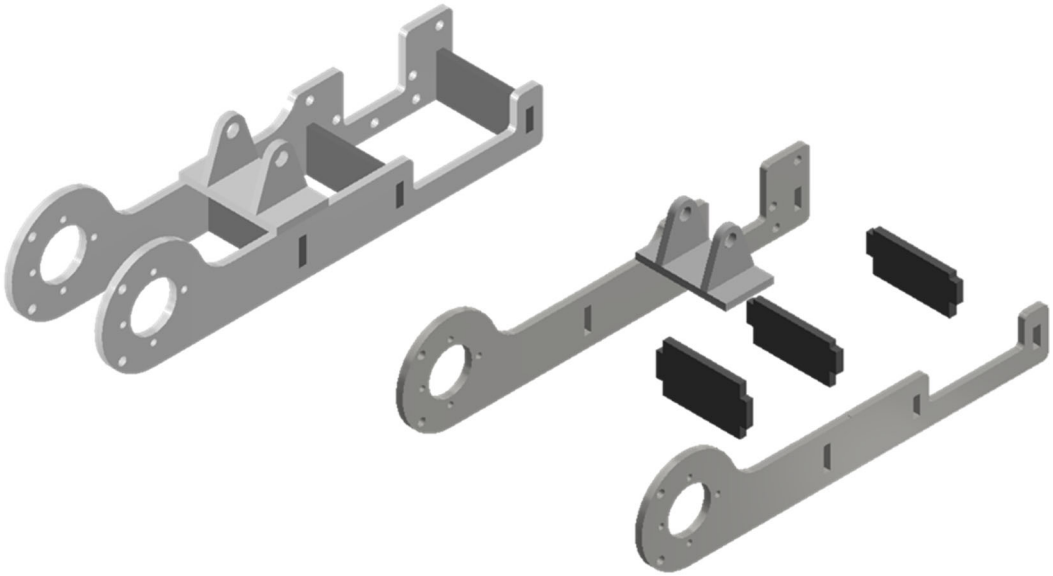

Figure 2-5 Trailing arm of the wheel suspension system.[1]

Wheel hup connected traction motor on each wheel. This configuration can save space for electrical system component that is located inside the chassis on the rear of the vehicle. The wheel system is shown in Figure 2-6.

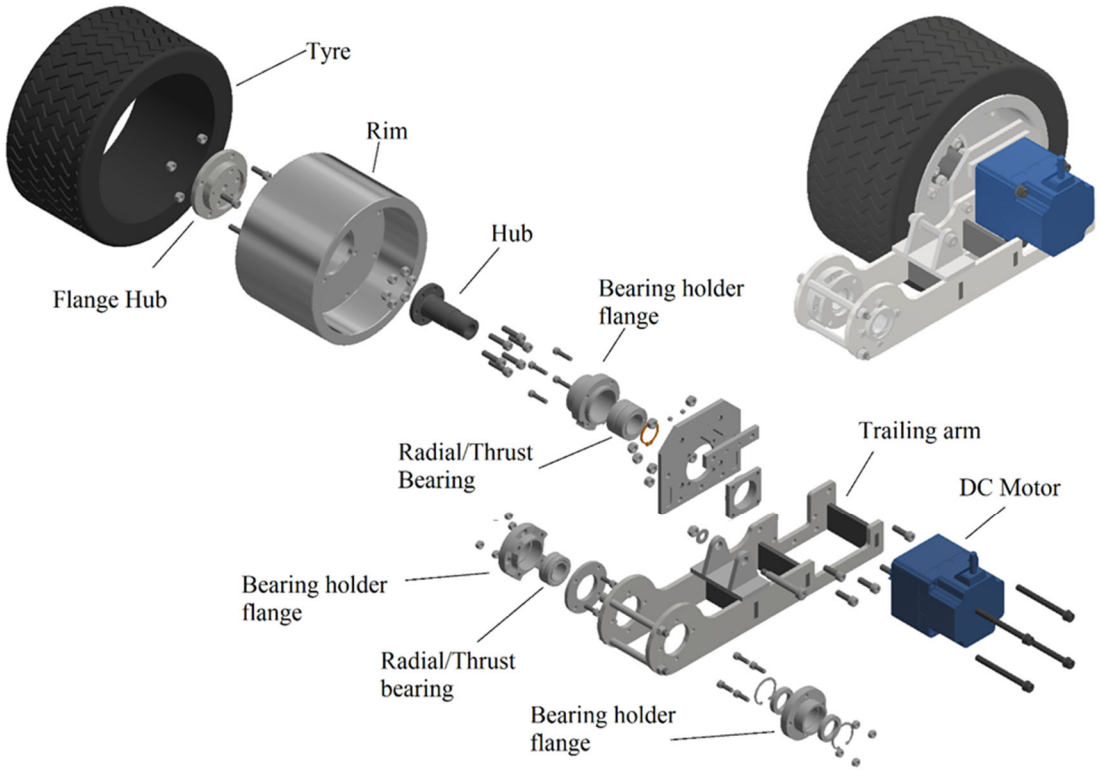

Figure 2-6 Wheel group's components. [1]

For the reasons for using the wheels at the rear, while vehicle is moving, the front running gears are compacting the soil and making the conditions more than the rear running gears. It is convenient to use wheels on the rear side because they cannot adjust their contact patch. In addition, the contact shape of sprocket front running gear still resembles a wheel, when the vehicle is sinking, avoiding the contact between the lifted portion of the track and the soil. The reasons can be explained in Figure 2-7.

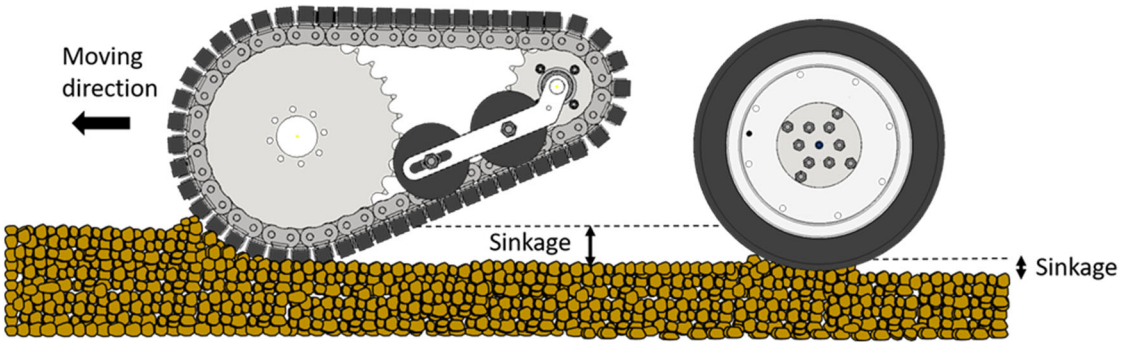

Figure 2-7 Tracks at the front axle improve the soil conditions for the wheels. [1]

The track module has been designed as shown in Figure 2-8 at the Ishii Laboratory of the Kyushu Institute of Technology. The components of a track module include: sprocket, idler, belt and rollers. In our track, the belt consists of a chain with attachments, as shown in Figure 2-9. The two bolt and a squared rubber lug inserted in to each aluminum U-channel as shown in Figure 2-10. The system main components are shown in Figure 2-11.

Components of the track module and final assembly are shown Figure 2-12. the track is made up of a chain engaging with a toothed drive sprocket and a toothed idler on the other. The drive sprocket is connected with motor and is used to move the track. The idler keeps the track straight. Sprocket has outer diameter of is 281 mm, pitch diameter of 267.21 and 33 teeth. Idler has outer diameter of 135 mm, pitch diameter of 122.17 mm and 15 teeth. An aluminum U-channel is fastened by two bolts on each one of the chain attachments, as shown in Figure 2-10. A squared rubber lug is inserted on inside each U–channel, fastened by two bolts and glued. These rubbers are used to contact the ground, exchange force and move the track. The chain has 52 links and pitch of 25.4mm.

Figure 2-8 Tracks module [1]

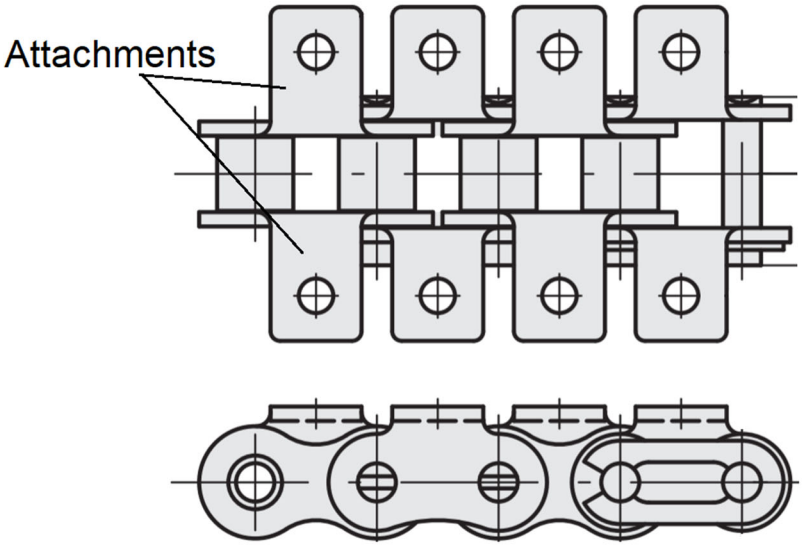

Figure 2-9 Chain and attachments. [1]

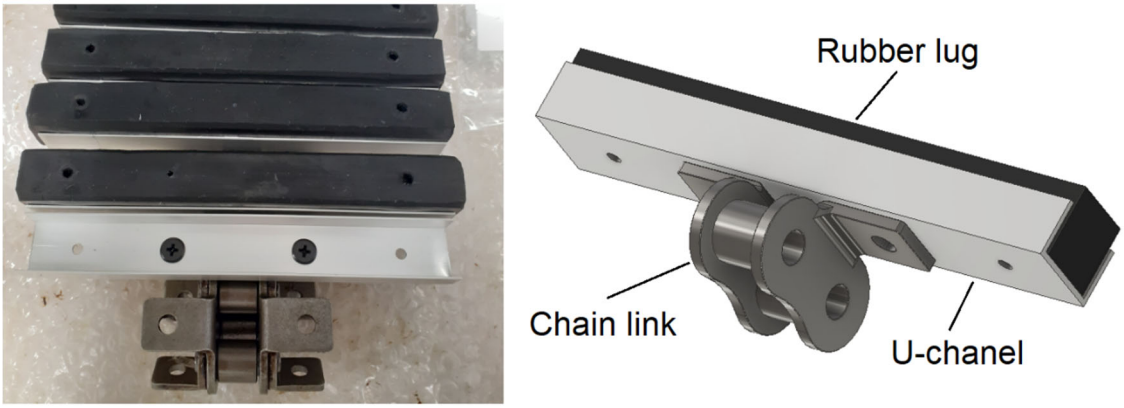

Figure 2-10 Connections between chain, U-chanel and rubber lugs. [1]

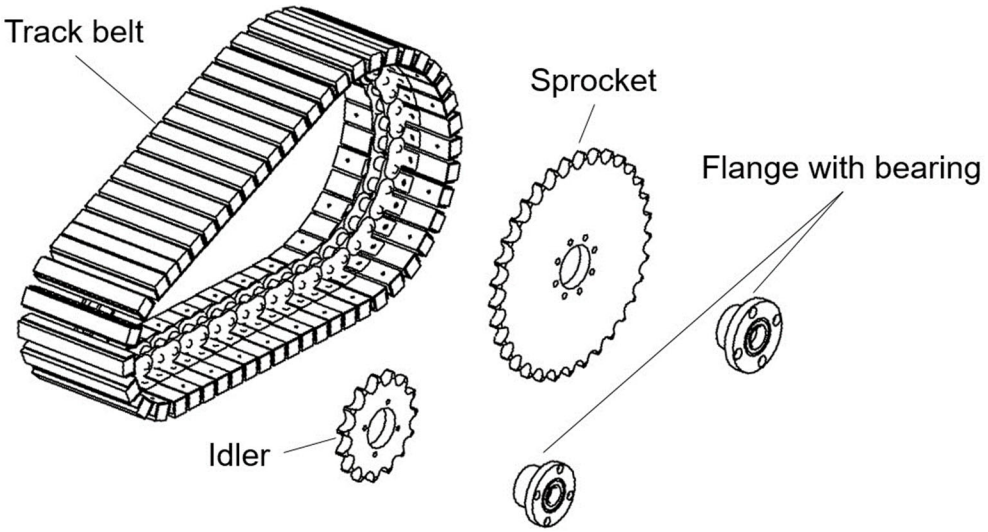

Figure 2-11 Track module main components. [1]

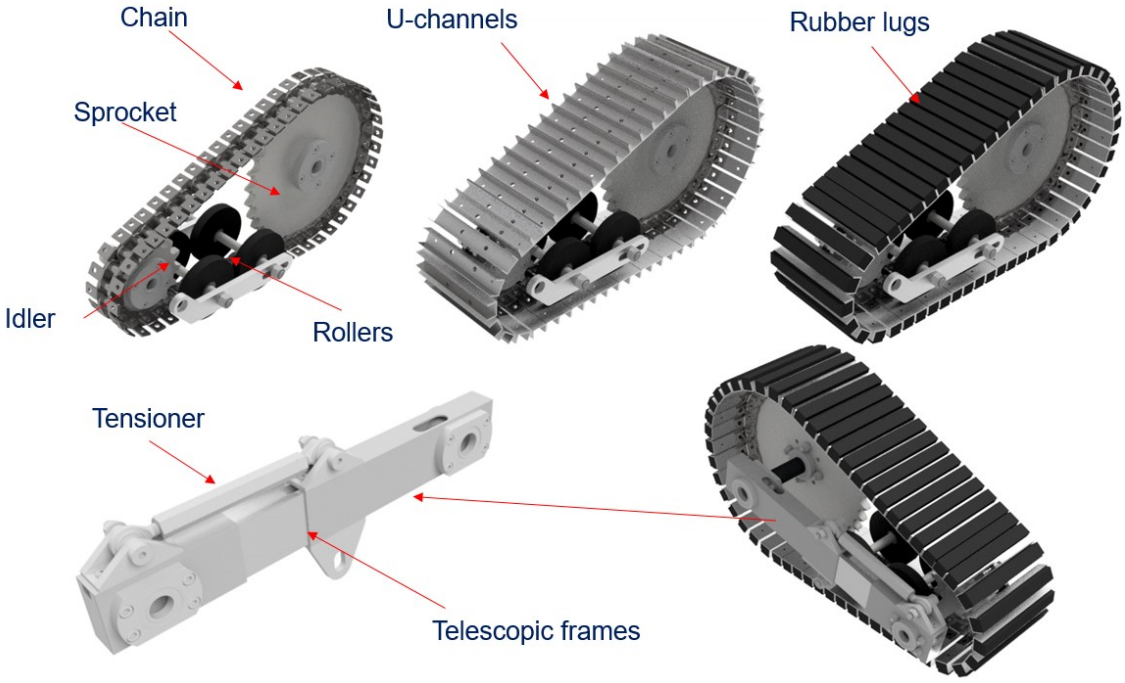

Figure 2-12 Components of the track module and final assembly.[1]

To distribute the weight of the vehicle, in the section of track belt that separate the sprocket from the idler must be pressed to the ground. Undercarriage is important component of track that can distribute the weight as shown in Figure 2-13. It consists of two rows carrying two rollers. The inserted shafts are free to rotate and are supported by two L–shaped support that are connected on one end to the sprocket shaft and idler shaft.

Figure 2-14 show track frame. Track frame is the arm that will be used to connect the sprocket shaft and the idler shaft. Track frame includes three telescopic squared aluminum frames. The central telescopic frame, it can slide inside the other two telescopic frames that are connected through hexagonal nut, ball joint and adjuster rod. Tension of track belt can adjust by adjuster rod. Flanges with bearing are positioned on the end of track frame on each side for sprocket shaft and idler shaft.

The traction motors of the front axle are positioned within the chassis. The traction motor drive the sprocket gear through a chain coupled with two sprocket gears, and the transmission ratio is 1. We rigidly connect each sprocket gear to the chassis by a pair of links. A shock absorber connects with the idler for switching mechanism. Two thrust bearing support on one end of the driven shaft. Figure 2-15 describe the design of the front axle. The track is connected to chassis by track supporting link. The triangular link connected to the tracks serve to increase overall stiffness of the system during the turning maneuvers.

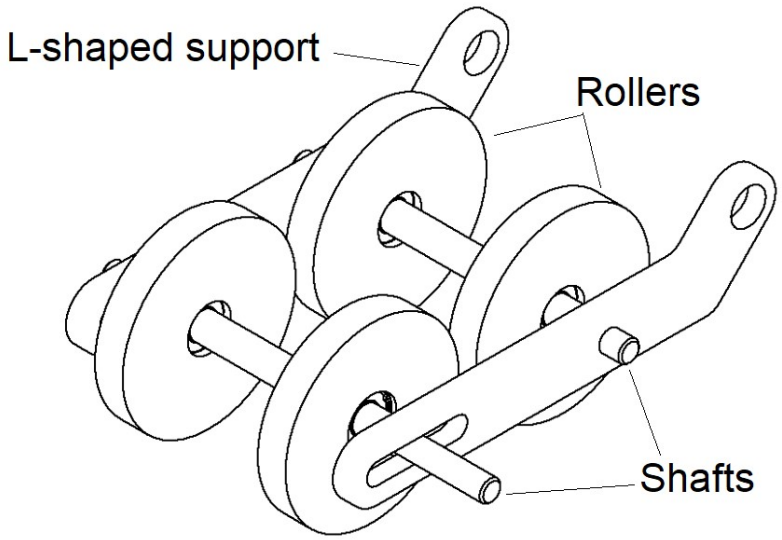

Figure 2-13 Undercarriage [1]

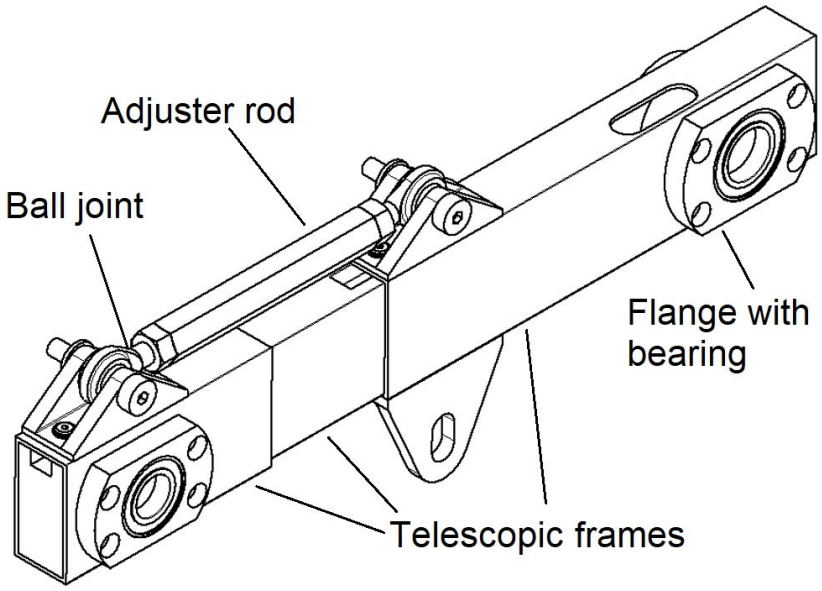

Figure 2-14 Track frame [1]

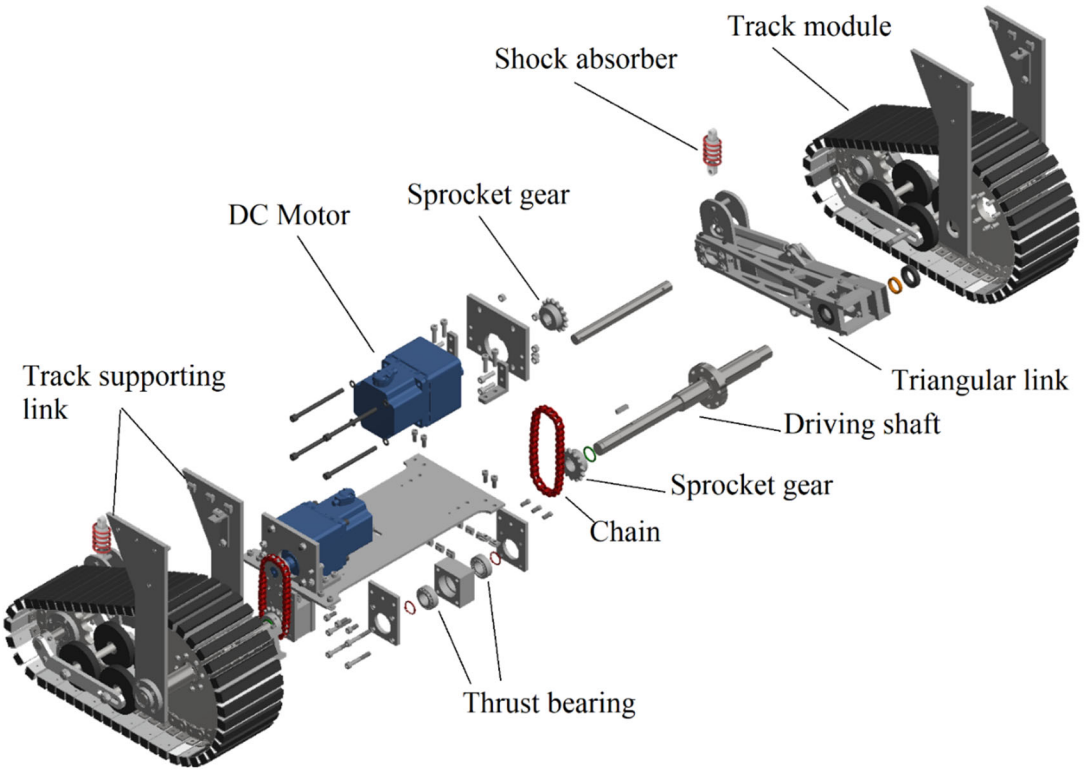

Figure 2-15 Track group's components [1]

Switching mechanism is described in the last group. Switching mechanism configurations and components are shown in Figure 2-16. Electro-hydraulic actuator is installed inside the robot to switch between tracked mode and wheeled mode. Electro-hydraulic actuator extends the stroke to switch tracked mode, and shortens the stroke to switch wheel mode. Scott Russel is used for switching mechanism which converts the horizontal displacement of an electro-hydraulic actuator (EHA) into a vertical linear movement of the idlers. A shaft (S1) with two bearing mounted at its ends is connected to EHA. Two bearings are inserted into two parallel linear guides. A shaft is connected with two long links of a scissor mechanism. The length of longest link is double the short

link. The middle of the long link is connected to one end the of short link by a revolute joint.

A second shaft (S2) connect the other end of the long link and connect to the idlers' shock absorbers. The displacements of EHA cause the shaft (S1) to move along the linear guide to lower or lift the shaft (S2) and the shock absorbers that is connected to the idler of track.

The kinematic model of the Scott-Russell mechanism[43],[44],[45] is shown in Figure 2-17. The relation equation between the vertical displacement and the horizontal displacement of the EHA can be calculated by the equation.

$$h = d\left(x\right) * tan(\alpha) \tag{2.1}$$

$$d = dmax - s \tag{2.2}$$

where α is the angle between scissor's links and the horizontal, as in Fig. 11 bmax is the maximum distance from the roller shaft and revolute joint of short scissor link. The desired vertical displacement of the idler is selected in the range 100 mm – 150 mm. We can confirm that this range is used for wheel mode. The contact area on the ground is circular that is similar to a wheel. Figure 2-17 describe the static analysis of the mechanism. Number 0 is the chassis, 1 is the actuator, 2 is the long scissor link ,3 is the short scissor link, and 4 is the linear guide. Small values of the angle α require a high actuator force and a higher reaction force on the links in track mode as shown in Figure 2-17. In wheel mode, EHA only lifts the idler, and small α angles can be accepted. Scoot Russell mechanism can help trade-off among the space available inside the chassis, decide the desired vertical displacement and avoid small angles in track mode. The α angle in track mode is of 53 deg in final design. For the alternative solution, we considered about

the lead screw mechanism by DC motor. However, we preferred to use the EHA because it has higher robustness under dynamic loads.

The three main groups (rear axle, front axle and switching mechanism) are connected to the chassis, which consists of aluminum frame. The aluminum frame of the chassis uses diagonal elements to triangulate. This design can improve the stiffness, avoiding rectangular arrangements of bars, which has low stiffness [46]. The final assembly of the vehicle is shown in Figure 2-18.

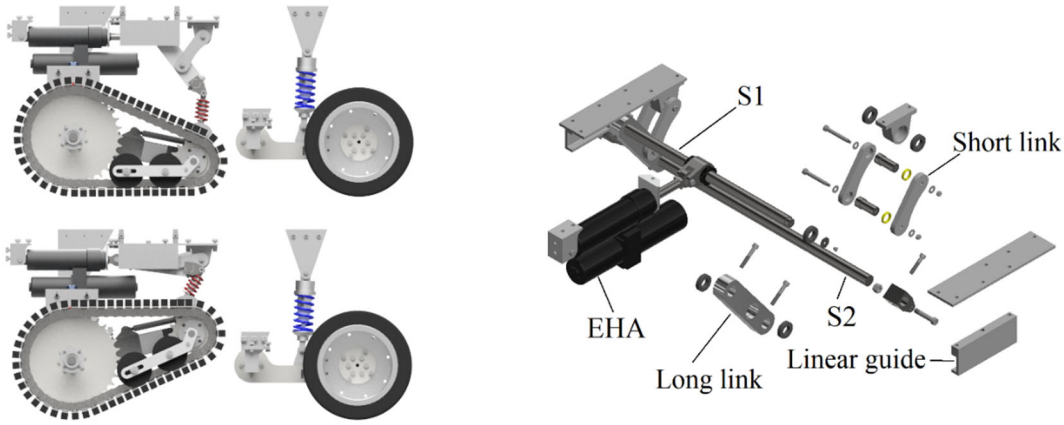

Figure 2-16 Switching mechanism configurations and components [1]

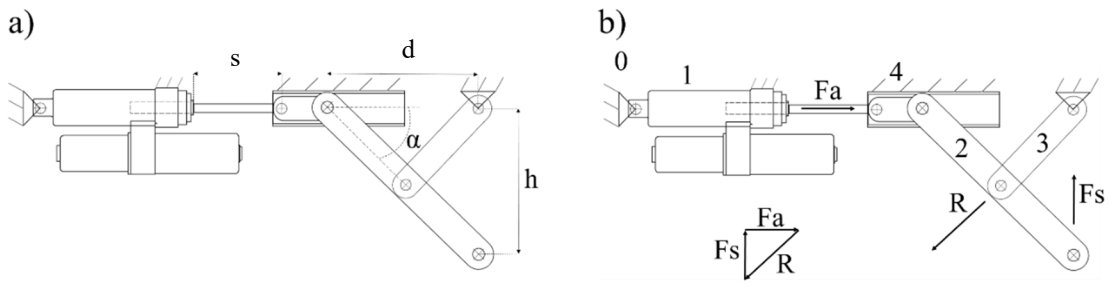

Figure 2-17 Scoot Rusell mechanism [1]
a) Relation between EHA stroke and vertical displacement. b) Static analysis.

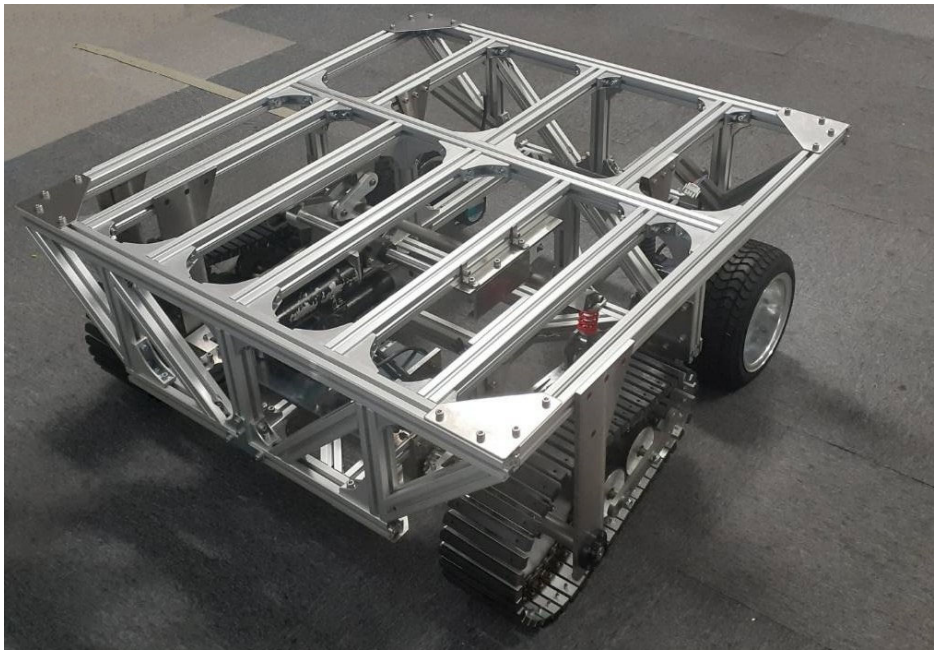

Figure 2-18 Final assembly of the vehicle

The total weight of the vehicle without any payload is 247 kg. We measure the weight distribution by using a weight scale as in Figure 2-19. We use this measurement to locate the center of gravity. The weight of front is 129 and rear is 118 kg. Total length of robot is 1260 mm. The center of gravity is 602 (measure from front side) and 658 mm (measure from rear side). The weight of left side is 123 and right side is124 kg. The width is 1230 mm. The center of gravity is 617 (measure from left side) and 613 mm (measure from right side). The summarization of characteristics of the vehicle is described in Table 6.

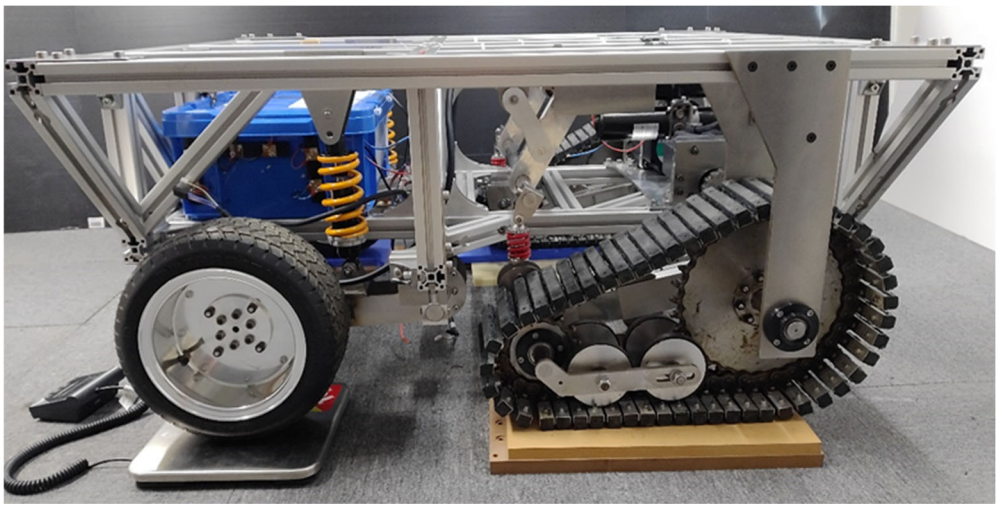

Figure 2-19 Weight distribution measurement by weight scale.

Vehicle characteristics	Specification
Mass	247 kg
Size	1230mm x 1260 mm x 540 mm
Velocity	0.4 m/s
Battery	Li-Ion 25.2 V 27 Ah x 2, mobile battery 5 V
EHA	MMP3 12 V, 5800 N
Motors	DCM 200 W x2, DCM 100 W x2

Table 6 Hadrian' main specifications

2.2.2 Traction motor

The wheel/track reconfigurable vehicle has 4 Blushless DC (BLDC) motor that are installed on 2 front tracks and 2 rear wheels. BLDC motor a synchronous motor that use DC electric power supply, and apply in many applications such as underwater robotic[47], electric vehicle[48],[49] etc. The BLV Series is a high-power blushless motor and DC power input motor driver package developed by Oriental motor corporation. The BLV Series has sensors for monitoring torque and angular speed of motor. Two Brushless DC Motors for tracks are BLV620K100S (200 W, DC24 V, 30 RPM, torque 52.7 N.m) and two Brushless DC Motors for wheels are BLV510K100S (100 W, DC24 V, 30 RPM, torque 27.4N.m). Traction motor for wheel and track are shown in Fig.6. We select BLDC

motor because it has higher power/weight ratio, higher speed and torque and higher efficiency if compared with blushed motor. Also, we can monitor torque and angular speed of motor in real-time Traction motor for wheel and track are shown in Figure 2-20.

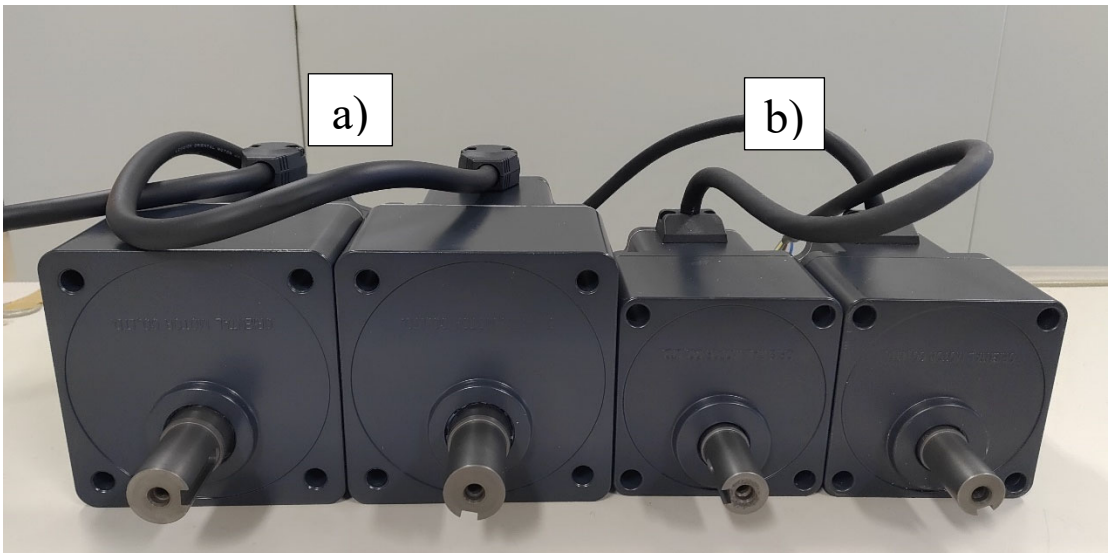

Figure 2-20 Brushless DC (BLDC) motor
a) Traction motor for track b) Traction motor for wheel

2.2.3 Electro-Hydraulic Actuator

Electro-hydraulic actuator (EHA) is actuator that operate a hydraulic fluid valve and use electrical energy to drive pump motor. Main source of energy is only electrical. EHA have ability that can impart large forces at high speeds and are used in many industrial [50]. The researchers challenge the nonlinear properties of EHA to design a suitable controller for motion control, position control, force control and tracking control [51],[52].

In our research, if Electro-hydraulic actuator extends the length of stroke, the robot will switch to tracked mode. If electro-hydraulic actuator shortens the length of stroke, the robot will switch to wheeled mode. The mini motion package (referred to as MMP) is series of electro-hydraulic actuator that was made by KYB company. The components

of MMP series includes electric motor, hydraulic pump, oil tank and cylinder as shown in Figure 2-21. MMP is used as actuator on agriculture vehicles such as combines with spraying machines. The major markets of MMP are Japan and North America. The EHA selected is the mini motion package MMP3-B1A100BA-GH, developed by KYB corporation, whose stroke is 0-100 mm, with a total minimum length of 280 mm and maximum length of 380 mm. The maximum force is 5800 N, and it has a piston pulling velocity of 33 mm/s and pushing velocity of 19 mm/s. Although the maximum force is oversized for this application, we preferred to use the Mini Motion Package because of its robustness and reliability in outdoor dirty environment, and its capacity to act as a rigid link once the desired position is reached. These kinds of actuators are often used on agricultural machinery, for example for adjusting the position of a plowing machine mounted behind a tractor

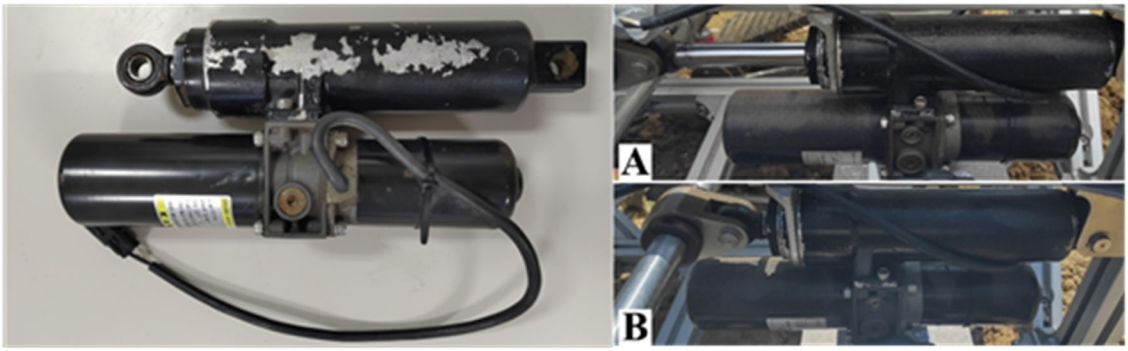

Figure 2-21 Electro-Hydarulic Actuator (EHA)
A) Maimum stroke B) Minimum stroke

2.2.4 Microcontroller

The ESP32 is a low-power and low-cost microcontroller. ESP32 support Wi-Fi and Bluetooth function. ESP32 is very small, and easy to use the ESP32 module with other components such as antenna, flash, etc. ESP32 is often used for tests and prototypes of

many projects such as Internet of things (IOT) [53],[54], robot [55], home automation[56],[57], photovoltaic system monitoring[58], etc. C is the common language for programming ESP32, and ESP32 has many libraries that provided in C. Also, ESP32 can be programmed in C++. Many libraries of Arduino can be used in C and C++ programming language. ESP32 is open source that everyone can develop operating system. ESP32 boards can be programmed using Arduino IDE. Figure 2-22 shows microcontroller ESP32.

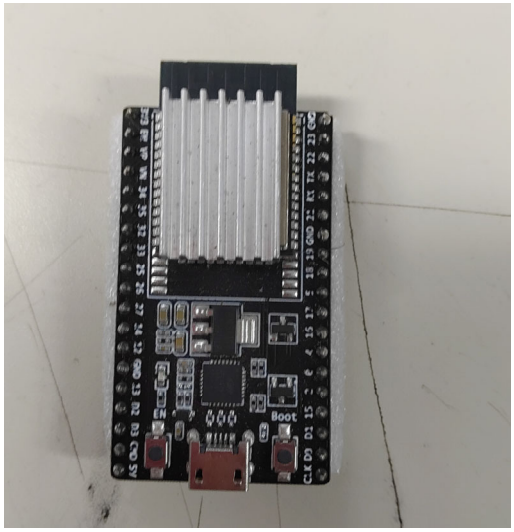

Figure 2-22 Microcontroller ESP32

ESP32 can receive Data from Multiple ESP32 Boards (many-to-one). ESP-NOW is the protocol that is developed by Espressif. ESP-NOW enables many ESP32 devices to communicate with one another ESP32 without using Wi-Fi [59]. Figure 2-23 shows the configuration. If we want to collect data from many devices into one ESP32. The concept of ESP-NOW. One board is a receiver and multiple board are transmitter. We connect soil moisture sensor with 2 ESP32 transmitter, and put them on field to measure soil moisture. Moreover, the laser distance sensor will be connected to one ESP32 transmitter, and put them on front and far from robot to measure distance and calculate velocity. If

the data from transmitter was successfully delivered or not, the transmitter will receive an acknowledge message. The one ESP32 receiver can receive the data from all ESP32 transmitter. The one ESP32 receiver can identify which board send the data.

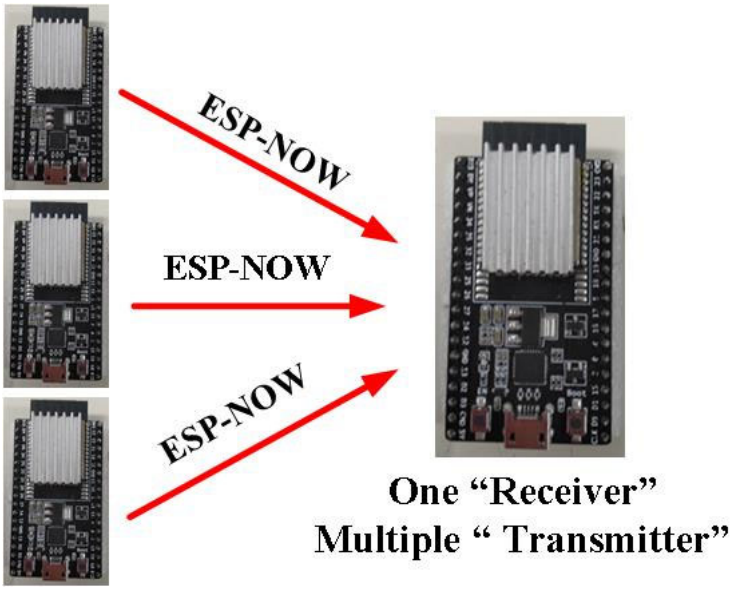

Figure 2-23 ESP-NOW communication protocol (many-to-one configuration)

2.2.5 Limit switch

Limit switch is an electromechanical device that can be operated by a physical force applied to it by an object [60]. These switches are used to detect the absence or presence of the object. Limit switch was used to define the limit of travel of the object, and as this reason, it was named Limit switch.

For configurations of limit switches, Limit switches has configurations that are a normally open and a normally closed as in Figure 2-24 [61]. A normally open of limit switch is one that is open when limit switch does not activate. It is unactivated state, and there is no path between the electrical contacts. When we push the button or lever, it closes the circuit and completes the current path, and allow the current to flow through

the circuit. Normally open of limit switch means the switch is off until it turns on. For a normally closed circuit, the switch is closed, completes the path, and the current flow freely through the circuit. Normally closed can be referred to the default state of the limit switch. In other words, when limit switch does not have input signal, the limit switch is in the closed position. Figure 2-24 shows configuration of limit switch and Figure 2-25 show limit switch in this research.

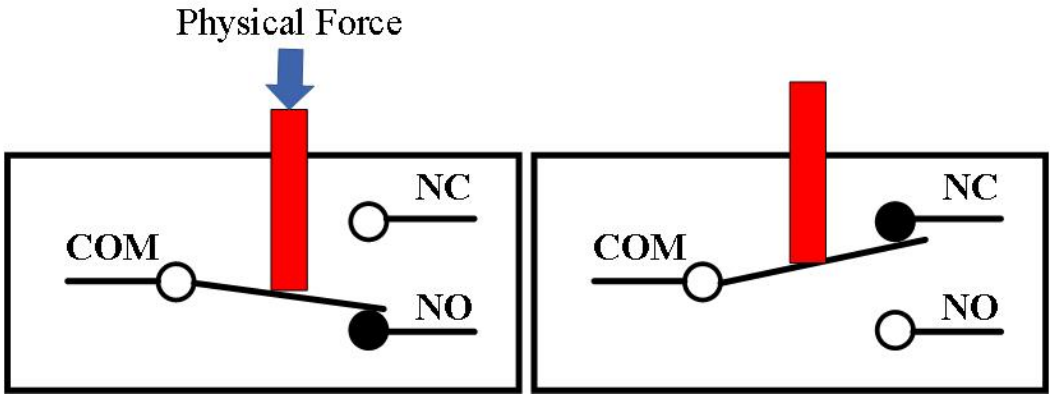

Figure 2-24 Configurations of limit switches normally closed (left) normally open (right)

Figure 2-25 Limit switch

2.2.6 Laser Distance Sensor

Laser distance sensors is used to measure distances to objects and their related parameters (displacements, position, and velocities) [62]. The laser distance sensor is used in this research is 100m JRT Laser Distance. Laser Distance Sensor is widely used in mapping, surveying and robots. hunting arrows, industrial monitoring and automated

measurement applications This sensor supports data communication via bluetooth, RS485, USB, and it can be applied to Arduino. This sensor is low price laser distance sensor if compared with other sellers. The laser distance sensors work on the basis of the Time-Of-Flight (ToF) principle. The transmitter of sensor emits a laser beam and the receiver of sensor receives the reflection of laser beam [63]. The laser distance sensor can determine the distance using the time that elapses between sending and receiving the laser light as shown in Figure 2-26. We connect the laser distance sensor with ESP32 to measure distance and calculate velocity. The laser distance sensor system is shown in Figure 2-27.

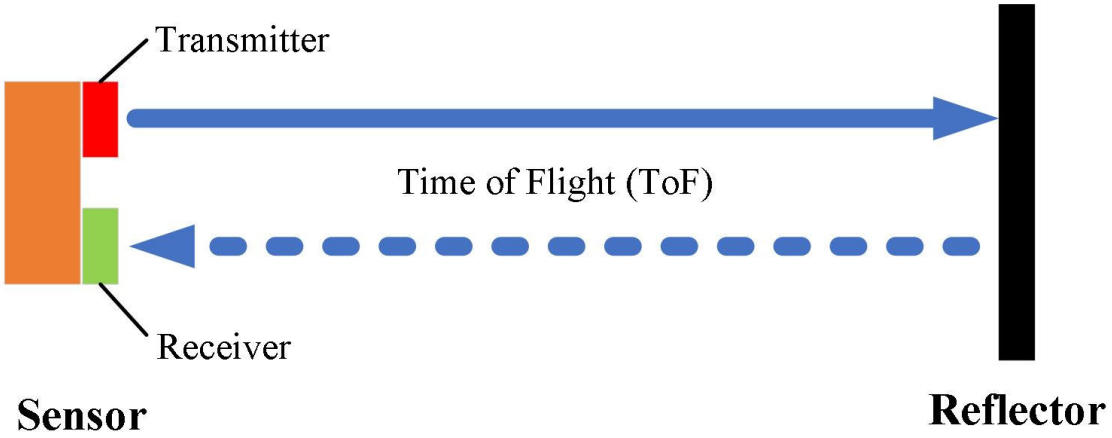

Figure 2-26 Laser distance sensor measurement

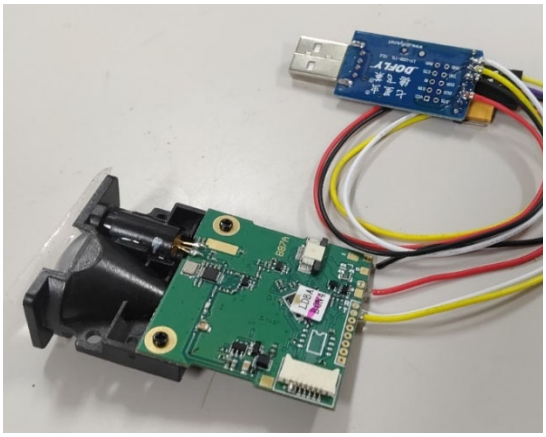

Figure 2-27 JRT laser distance sensor

2.2.7 Soil moisture sensor

Soil moisture is the water content in the soil. It is an essential parameter in agriculture. Soil moisture can determine several environmental and agricultural activities such as irrigation, climate change, etc [64]. Soil moisture sensor can measure water content in term of percentage of moisture (0% is moisture in air and 100% is moisture in water) can be expressed in term of percentage of water. Moreover, the soil moisture sensor should be calibrated to improve performance of sensor [65].

Soil moisture sensors and IoT application have become very popular nowadays to solve food shortages and global warming [66]. In this research we connect soil moisture and ESP32 to monitor data with wireless communication as shown in Figure 2-28. The soil moisture sensor that are used in this research is Analog Waterproof Capacitive Soil Moisture Sensor (SEN0308 DFRobot). We connect soil moisture sensor with ESP32 and OLED display module. Power supply of these module is mobile battery 5V. Kalman filter algorithm [67] is used to estimate the value of moisture. The system of soil moisture is shown in Figure 2-29.

Figure 2-28 Analog Waterproof Capacitive Soil Moisture Sensor (SEN0308 DFRobot)

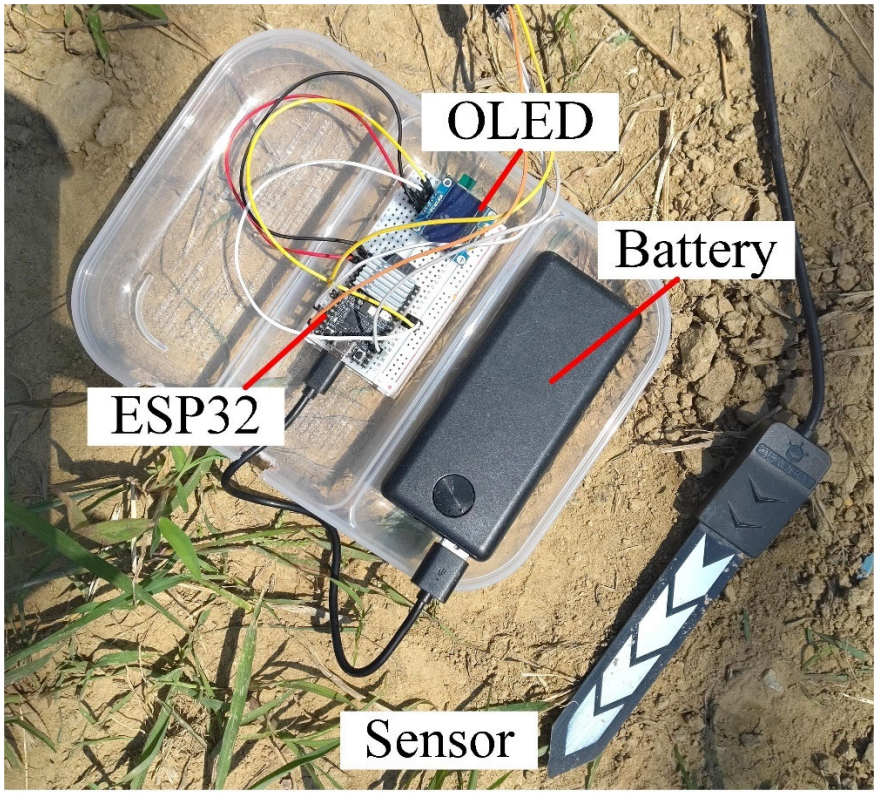

Figure 2-29 System of soil moisture

2.2.8 Power system

A flowchart of Hadrian's power system is provided as Figure 2-30. The system includes two Li-ion batteries of DC25.2 V that connect in parallel together. Two batteries supply four brushless DC (BLDC) motor that drive two tracks and two wheels. One DC-DC converter (from DC25.2 V to DC12V) is used for supplying energy to a Elec-tro-Hydraulic actuator (EHA). A microcontroller ESP32 is installed inside the vehicle, which has Wi-Fi integrated, and is used to receive the soil moisture data from the field. The ESP32 (Receiver) is connected to a PC by USB. Two soil moisture sensors in the field is connected to a separate ESP32 (Transmitter), and send soil moisture data in wireless communication with a ESP32 (Receiver) inside vehicle. DC 5V Mobile batteries is the power supply of the moisture sensors and ESP32 (Transmiter). The final number of soil

moisture sensors will depend on the expected variability of soil moisture and the size of the agricultural field.

In our preliminary tests, the vehicle moves on straight lanes, and the slip of running gear is evaluated using a laser distance sensor (LDS). The laser distance sensor is located at the end of the lane, and sensor points to a flat black panel that mounted on the front of Hadrian. We measure the position of vehicle and we can estimate velocity of moving using laser distance sensor (LDS) [68] and we measure angular velocity from encoder of motor, Then, we can evaluate slip.

The laser distance sensor connects to an ESP32 (Transmitter), and a battery of 3.3V. The Laser distance sensor is a temporary solution for the preliminary tests because it's simple and cheap. We will adopt a GPS [69] or DGPS in future work.

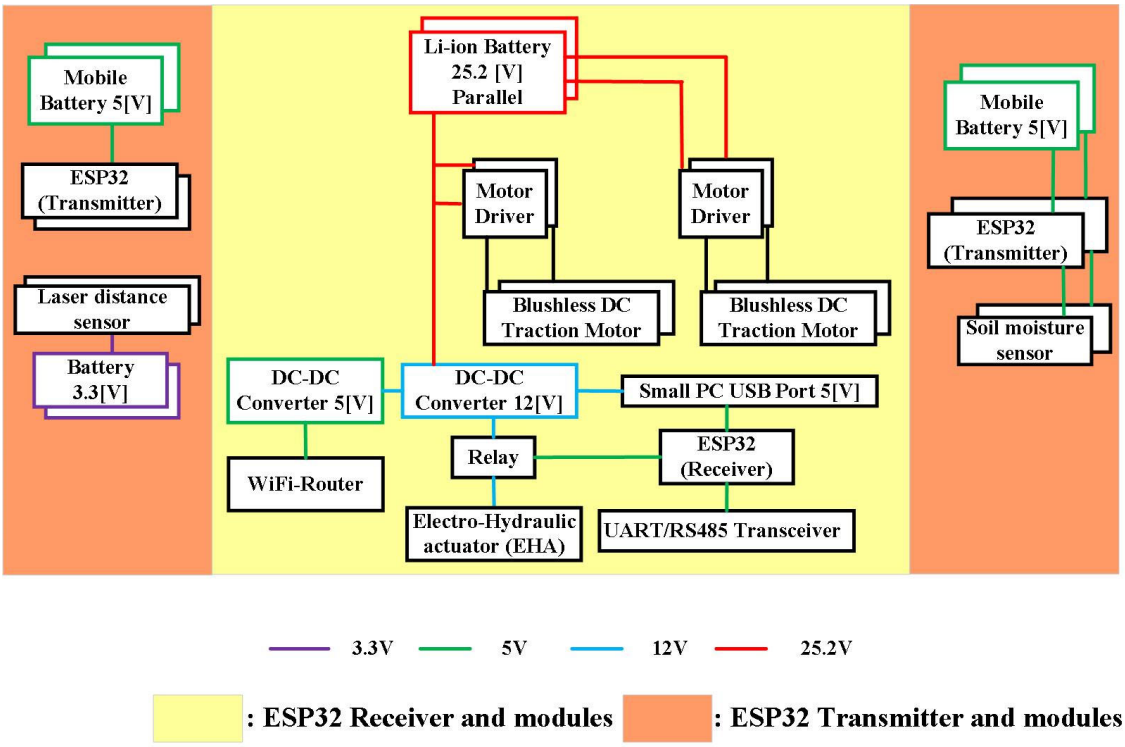

Figure 2-30 Power system

2.2.9 System architecture

We developed a user interface for easily operating the vehicle. To understand how user interface works, first we explained the system architecture as shown in Figure 2-31. Vehicle is equipped with PC from where it can be operated by using the user interface. A microcontroller ESP32 (Receiver) receives the soil moisture data from the ESP32 (transmitters) that connected to the soil moisture sensors in the field. The ESP32 (Receiver) is also interfaced with the four motor drivers and the relay to control directions of Electro-Hydraulic Actuator (EHA). The information of soil moisture is exteroceptive sensors that will be used, together with proprioceptive sensors data, to switch locomotion mode autonomously. The locomotion mode (tracked and wheeled mode) can also be switched manually by the user, and the switch relay control EHA. The BLDC motors use RS485 protocol. So, we use UART/RS485 converter for the communication with the ESP32.

The system components are grouped into modules depending on the function as shown in Fig. The MD module is the module of the four motor drivers, U/RT module is the UART/RS485 transceiver, MW/T module is the mechanical connection among motors and running gears (wheels and tracks), RL module is the relay to control EHA, EHA module is the electro-hydraulic actuator that is connected to the switching mechanism, and the SMS module is the soil moisture sensors.

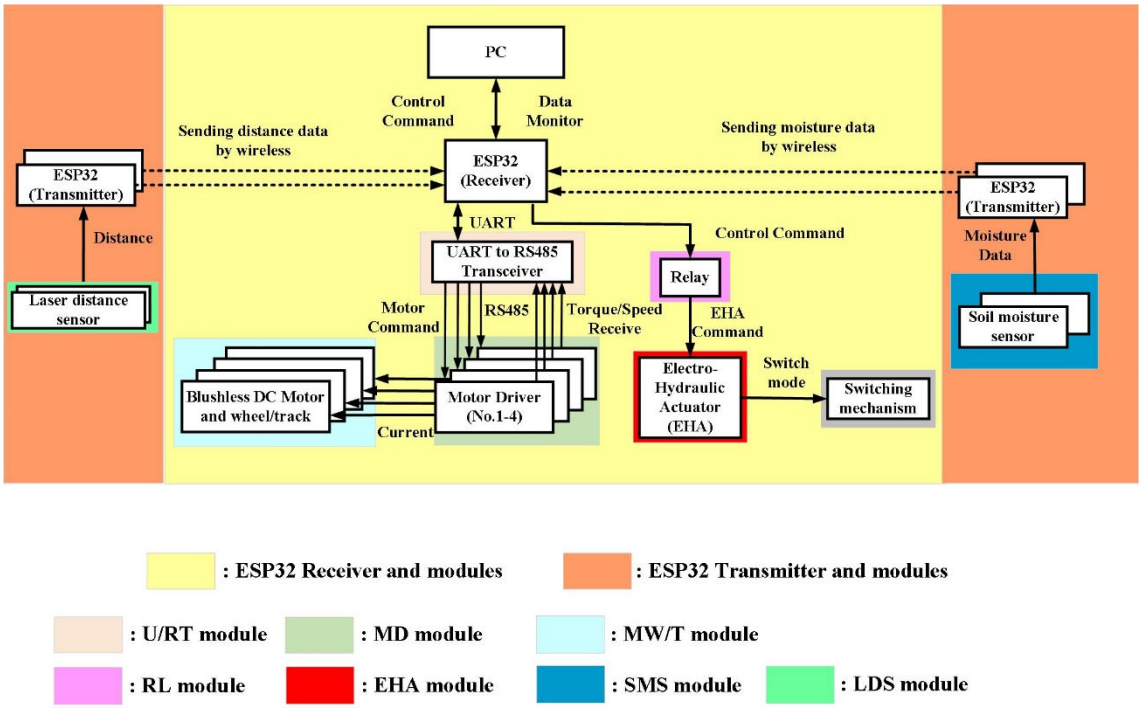

Figure 2-31 System architecture

2.3 Software design

2.3.1 Arduino and Visual basic

In this project, we use two software for controlling the robot that are Arduino (ESP32) and Visual basic 2022 (Personal computer). Arduino is used to upload into ESP32 microcontroller. Visual basic 2022 is used to design user interface and communicate with ESP32

Arduino software is an open-source software platform using C and C++ language. Arduino is designed to help computer programmers, industrial company, robotic engineering, etc. The Arduino software is used to write coding and upload to Arduino microcontroller such as Arduino UNO, ESP32. The screen of Arduino software is shown in Figure 2-32.

The layout include two main function that are void setup () and void loop (). The code that is put inside void setup() will be at the beginning of your program and only run once. For example, we setup initializes serial and the pin of sensor. The code that is put inside void loop() will run code repeatedly. For example, the robot will move forward and obtain velocity data from sensor to calculate slip forever. The open-source Arduino software is free to download. Arduino can make it easy for user to write code, upload it to the board for many projects.

Visual Basic (VB) is a programming language that was developed by Microsoft to operate window system. The VB was developed to design user interface. Figure 2-33 show toolbox and screen of Visual Basic. The main toolbox is described in Table 7. We use these toolbox to design user interface.

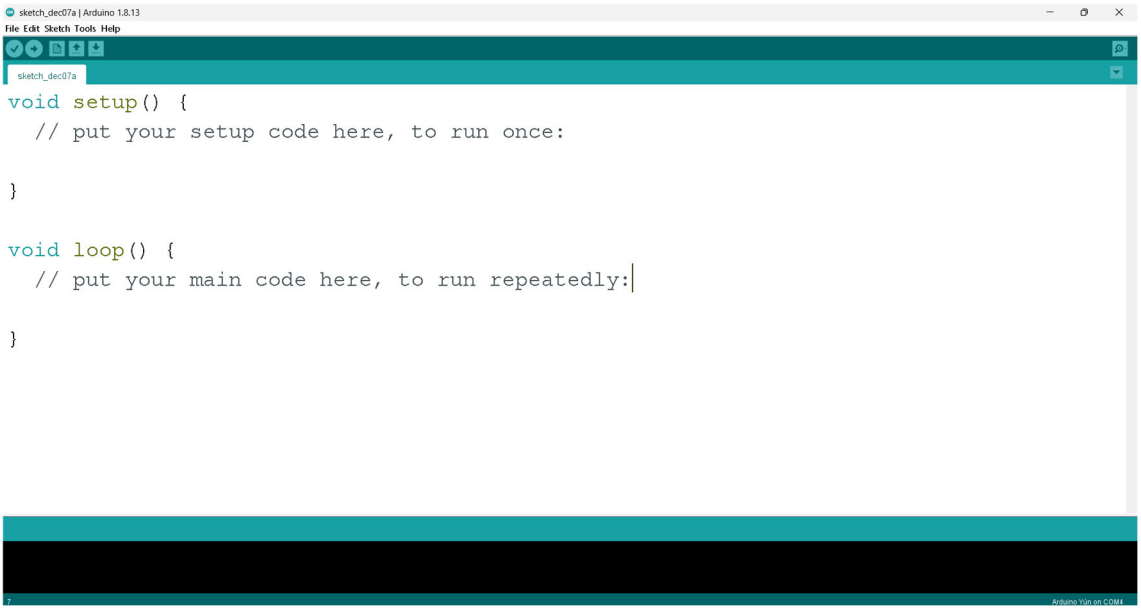

Figure 2-32 Screen of Arduino

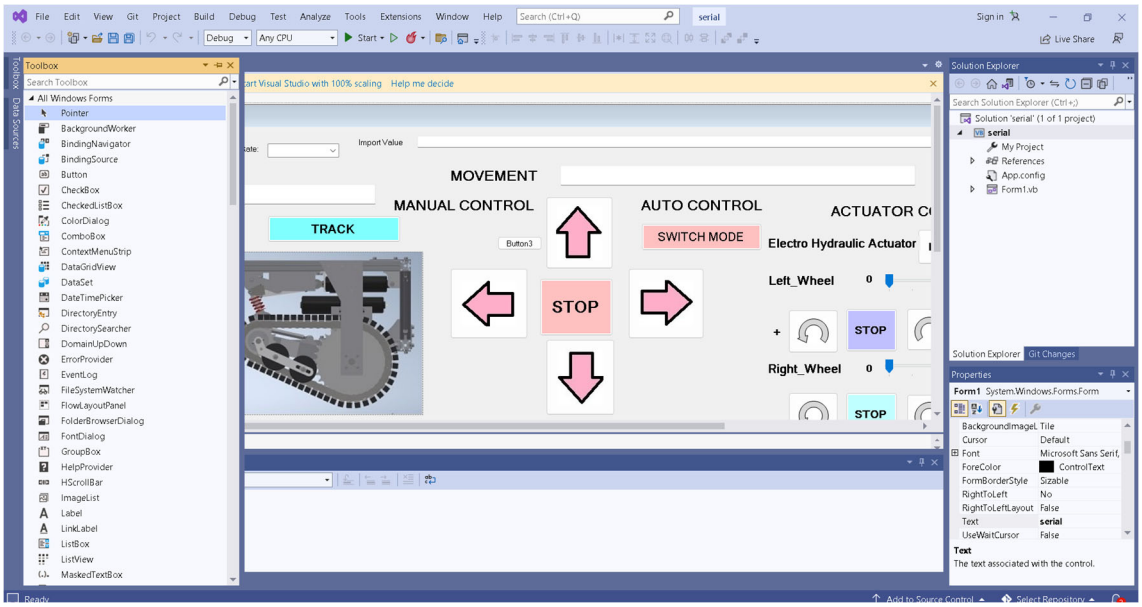

Figure 2-33 Screen of Visual basic

No.	ToolBox	Description
1	Button	- Create button to operate for scan port, connect and disconnect communication between visual basic - Create button send command from visual basic.NET to ESP32 for controlling robot
2	ComboBox	Create box for item selection
3	Label	Write comments on interface
4	TextBox	Create box to show values of sensor from ESP32
5	SerialPort	Creates SerialPort component that provides synchronous and event-driven I/O and access to serial driver properties.
6	Timer	Creates a Timer component. we can use to add time-based functionality.
7	PictureBox	Create box to add picture on user interface.
8	Chart	Create chart to show values from sensor in graph.

Table 7 Main Toolbox of Visual basic

2.3.2 User Interface

We develop the user interface using Visual Basic 2022 [70]. Visual Basic 2022 has many toolboxes that allow easy implementation of the required functions [71],[72]. The user can send commands to ESP32 to extend or shorten the Electro-Hydraulic Actuator (EHA) and control the velocity and direction of four BLDC motors through the user interface while monitoring the torque/angular velocity of motors and slip of running gears. Visual basic 2022 support user to design user interface using many toolboxes. The main toolboxes are "TextBox", "Button", " SerialPort " and " Chart ". These are used for operating the scan port and sending commands from visual basic.NET to the ESP32 controller, displaying the value from sensors, displaying the graphs of value from sensors in a chart, and creating a serial port component for the synchronous and event-driven I/O to access serial driver properties [73],[74],[75]. Additional blocks are commonly used to add labels and pictures for making the graphic on user interface. The user interface that we designed is shown in Figure 2-34.

The user can decide locomotion mode system by using the two buttons "WHEEL" and "TRACK". When we press the button, the relay controls the direction of EHA to extend or shorten the position of piston. When we press the "WHEEL" button, the EHA shortens until the zero position. When we press the "TRACK" button, the EHA extends until the maximum position. We use the image of the vehicle to confirm the locomotion system and the image can switch depend on operation mode. The "Stop" button must be pressed before switching the locomotion mode to ensure the vehicle is not moving. To control minimum and maximum possible extension of the EHA, we located two limit switches on the chassis. If EHA shorten or extend the length until contact the limit switch, EHA will stop. The user can decide the direction of vehicle’s movement by suing the four

arrows allow (UP, DOWN, LEFT, RIGHT). The user can rotate the traction by input velocity. A velocity input is sent to tracks and wheels when the back arrow and forward arrow is pressed. We can monitor the torque, angular velocity and slip of each running gear, and also we can adjust the velocity accordingly. The velocity can adjust by using the "Part Control. The "Part Control" is section for controlling each actuator and motor individually by selecting velocity and rotation. The direction of rotation is indicated by the rotation arrow buttons. Also, we can stop each actuator and motor individually by press the stop buttons. The user interface can display the angular velocity and the torque exerted by every single motor in real-time. In the case of Electro-Hydraulic Actuator (EHA), the user can decide the actuator's extension by press the "PULL" and "PUSH".

The level of soil moisture in the field can be monitored in the "Soil moisture" section. Only two soil moisture sensors are used in our preliminary tests.

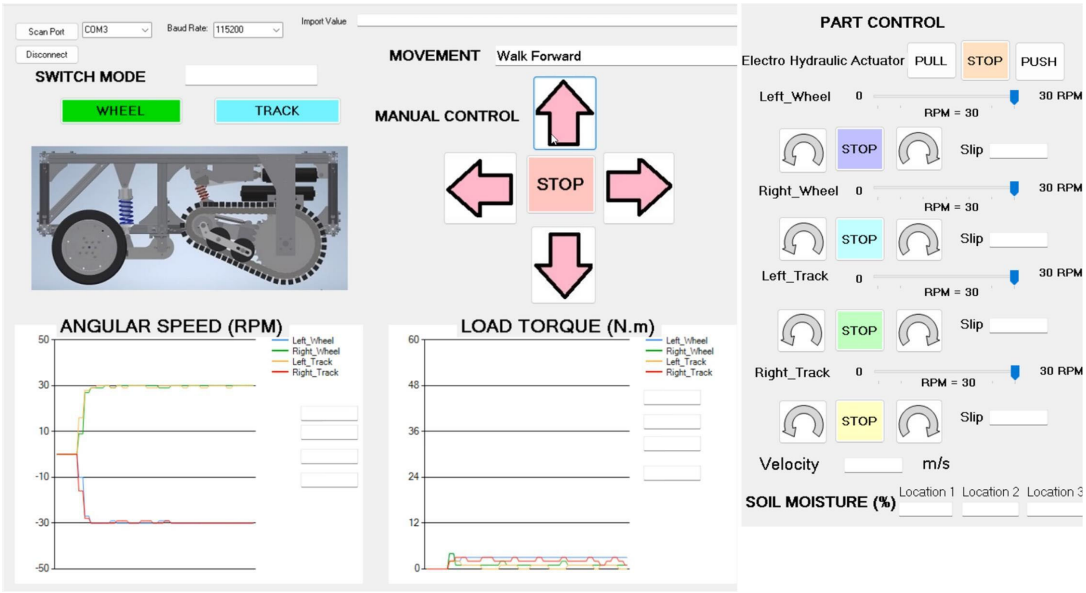

Figure 2-34 User interface

2.4 Summary

In this chapter, we presented our wheel/track reconfigurable vehicle, Hadrian. This vehicle can adjust its contact area by partially lifting and pushing the front tracks through a Scott-Russel mechanism driven by an electro-hydraulic actuator. We described the mechanical solution, the system architecture, and the user interface that is developed for easy remote control and autonomous control of the vehicle. The purpose of this vehicle is to transport the grape in the vineyard during harvesting while minimizing soil damage and adapting vehicle's performance based on the need.

The user interface allows the control of every motor and actuator while user is monitoring the, the rotational velocity, the torque, and slip. The graphical user interface is a tool for user-friendly vehicle control.

The next step is to test a wheel/track reconfigurable vehicle in the field and measure the performance and soil damage in several soil conditions. The experimental data will be used for controlling to make autonomous the selection of the best locomotion switching mode based on the field sensors data and onboard sensors data. This controller can improve the behavior of the vehicle and it can be the helpful and important tool in the agricultural field.

Chapter 3
Basic performance

Chapter 3. Basic performance

3.1. Soil properties

Compactness and soil moisture can be used to classify agricultural soil conditions. There are three classes of soil: 1) firm soil, 2) soft soil, and 3) wet saturated soil. Wet saturated soil is soil that has all pore spaces filled with water and devoid of air. It mean: 1) it is highly deformable.2) The deformation occurs only for distortion. The cone index (CI) is used to classify firm soil and soft soil. The firm soil has about 1000 kPa of the CI. The medium and soft soil has about 500 kPa and 250 kPa respectively.

The cohesion and angle of shearing resistance can be used to classify soil types. For soft soil, this soil has lower cohesion that make it easy to compact. The traction force of vehicle depends on angle of shearing resistance. For firm soil condition, soil strength is high and depends on both cohesion and angle shearing resistance. Finally, wet is incompressible soil, and has high deformation by distortion. Strength depends only on cohesion. Soil structure of three example is shown in Figure 3-1.

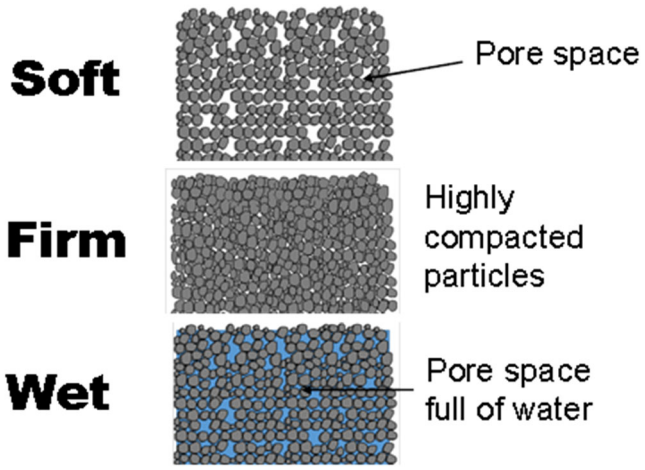

Figure 3-1 Soil structure of three soil conditions [1]

3.2. Field preparation

We prepared the soil conditions, which are firm soil, soft soil, and wet soil. Firm soil is the usual condition of the soil. Soft soil is the soil condition after plowing. Wet soil is soil condition after heavy rain. The soil is flattened to its original state with a compactor machine for firm soil preparation, as shown in Figure 3-2. We plow the soil by the tractor for the soft soil preparation as shown in Figure 3-3. We prepare wet soil using water from water tank as shown in Figure 3-4. Figure 3-5 shows the states of firm soil, soft soil, and wet soil. For the size of field experiment, the length of the field is 10 m and the width of the area is 1.5 m as shown in Figure 3-6. We test for 3 lanes, the total length is 30 m.

Figure 3-2 Compactor machine for firm soil preparation [1]

Figure 3-3 Tractor for soft soil preparation

Figure 3-4 Water tank for wet soil preparation

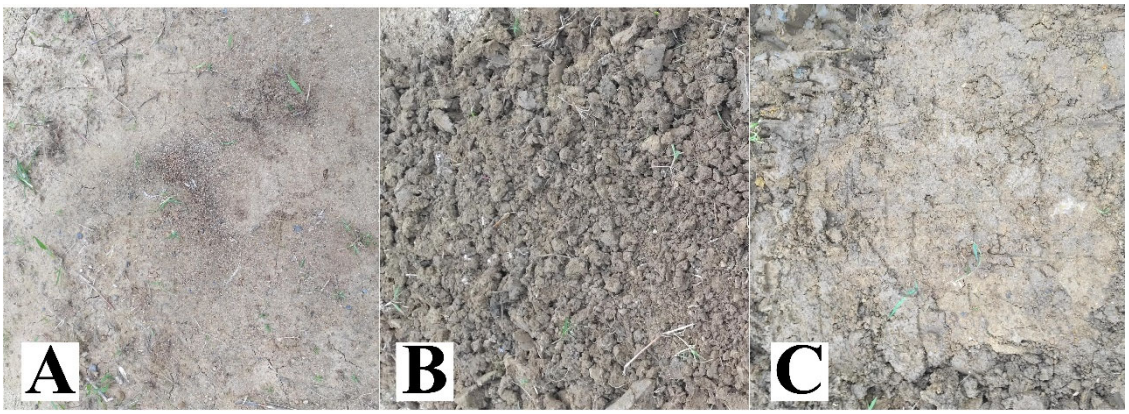

Figure 3-5 Soil conditions A) Firm (Original soil state) B) Soft (After plowing) C) Wet (After heavy rain)

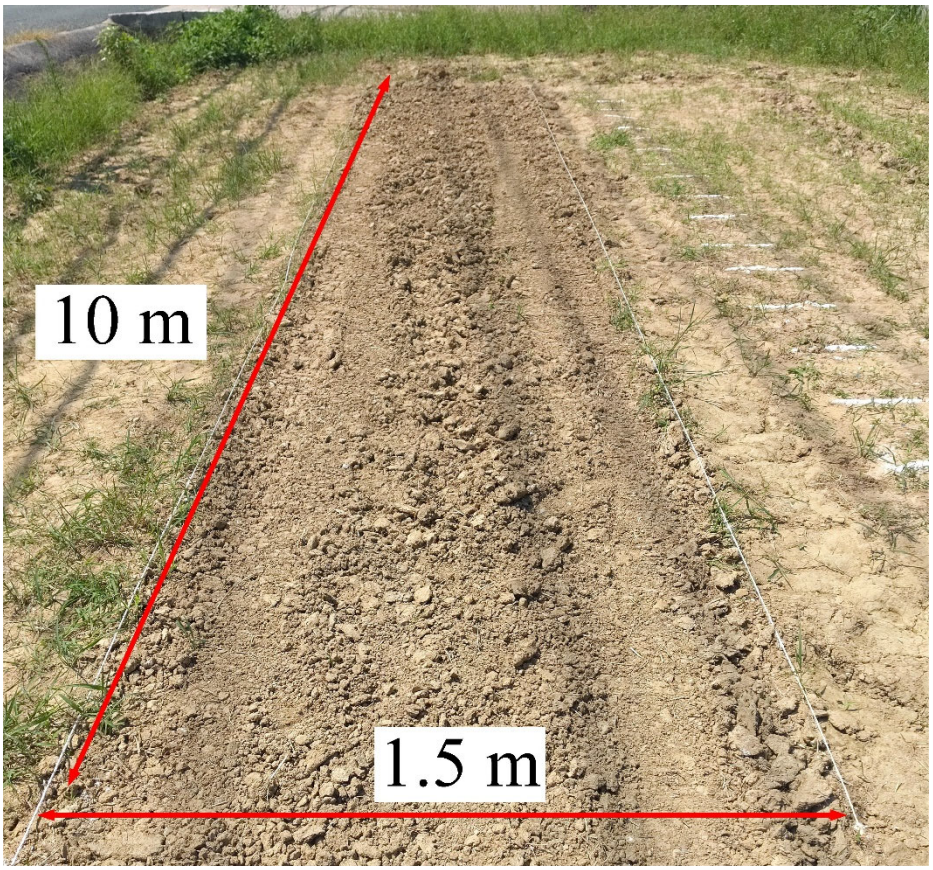

Figure 3-6 Size of field for 1 lane (Robot is tested for 3 lanes)

3.3. Soil Damage and Robot Performance

In this chapter, the robot is tested in each soil condition to collect data. The weight of the robot includes that without payload (total weight of 237 kg) and with payload (80 kg) (total weight of 317 kg). Four bags of 20 kg are put on the front and rear axles. The weight of the robot is shown in Figure 3-7. The robot is tested on three lanes, as shown in Figure 3-8. The robot uses wheel mode from 0 to 5 m, then switches to track mode and moves from 5 to 10 m. After the data is collected, we will decide which mode is preferable for each soil condition. Finally, we will implement a control strategy and show the results of the autonomous switching mechanism.

Figure 3-7 Weight conditions: without payload (left) and payload of 80 kg (right)

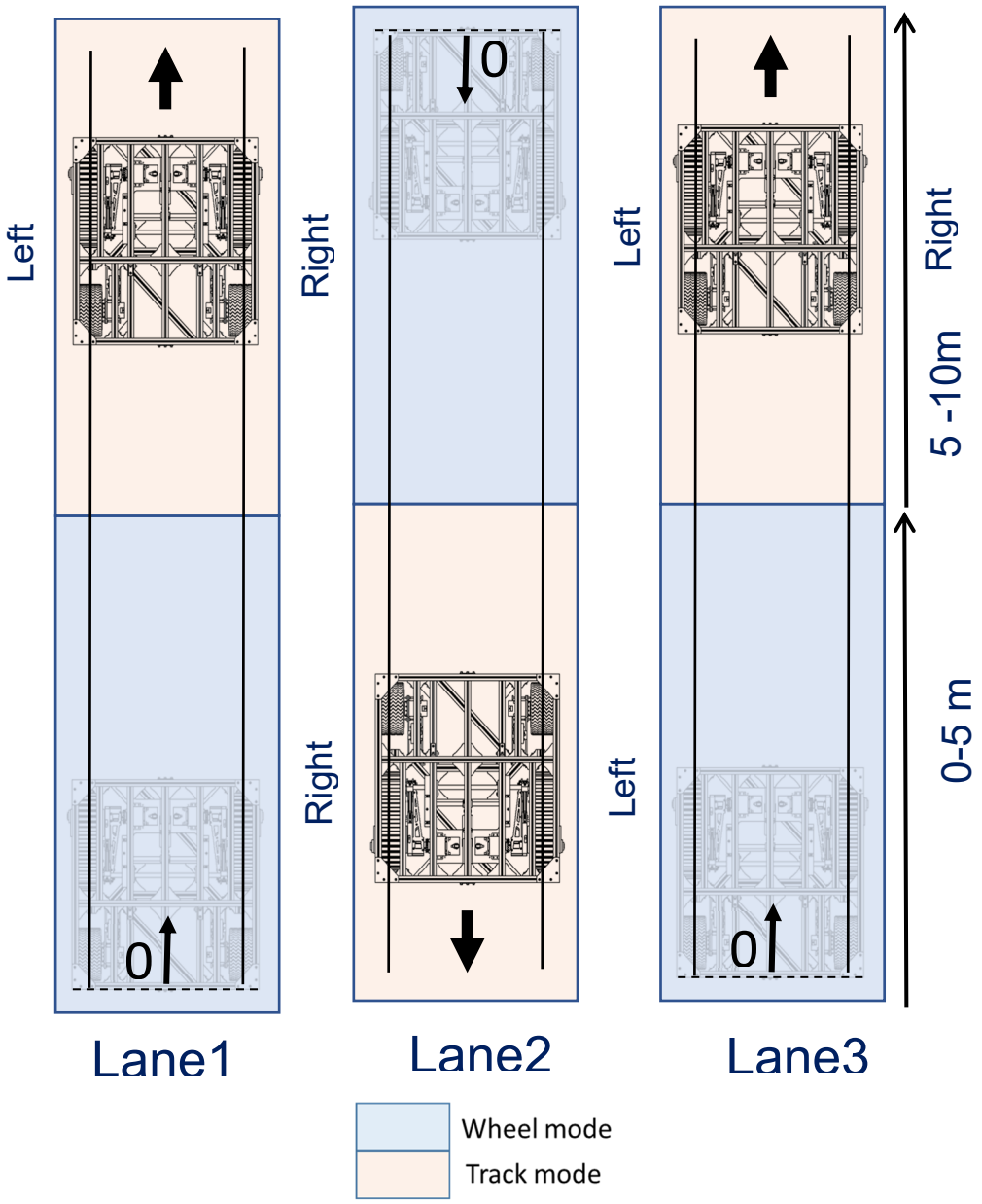

Figure 3-8 The robot is tested for 3 lanes. 1) wheel (0-5 m) and 2) track (5-10 m)

3.3.1 Soil compaction and Sinkage

The cone index (CI) is an empirical parameter that can be measured using a cone penetrometer. We use the cone index (CI) to estimate the soil compaction. The digital cone penetrometer SC900, developed by Spectrum Technology, Inc., is used to measure the cone index to estimate soil compaction. The digital cone penetrometer has an ultrasonic depth sensor to estimate the penetration depth. The digital cone penetrometer

SC900 can measure cone index in the depth of 0-45 cm and in the range of 0-7000 kPa. Figure 3–9 shows the digital cone penetrometer SC900. The CI measurement is shown in Figure 3–10. We measure every 50 cm before a vehicle passes and every 50 cm after a vehicle passes. The difference in distance between before and after the vehicle pass is 25 cm, as shown in Figure 3-11.

Figure 3-9 The digital cone penetrometer SC900

Figure 3-10 Cone Index (CI) measurement

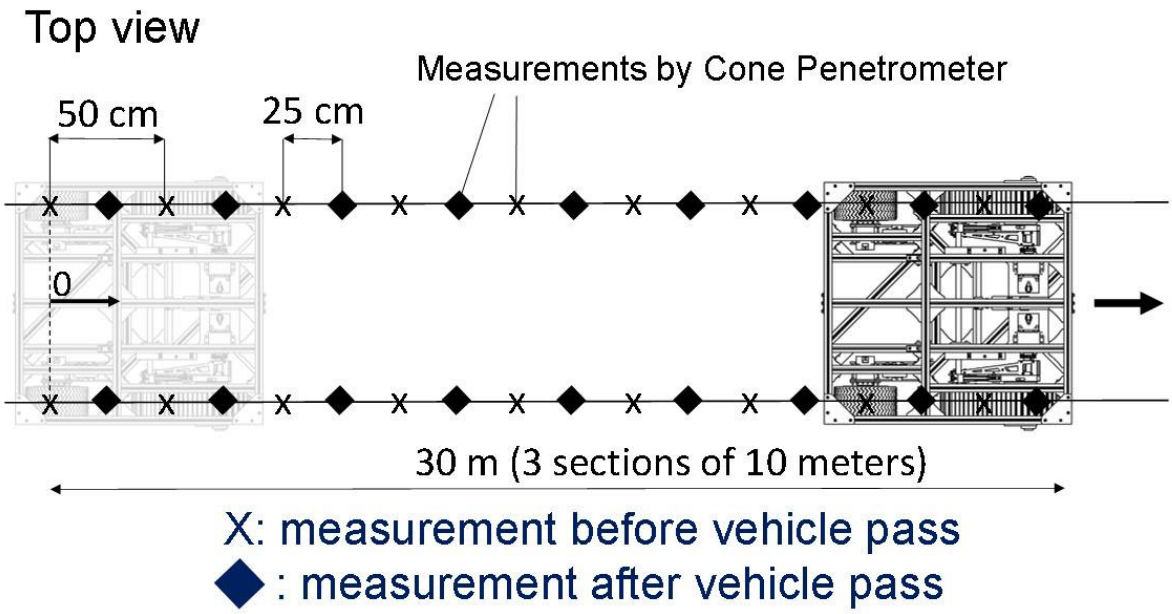

Figure 3-11 Cone Index (CI) measurement on field

For sinkage measurement, in the performance comparison based on the Bekker model [76], the wheel vehicle has higher rolling resistance because the wheel has greater sinkage than the track in soft soil conditions. On hard soil, track and wheel vehicles can cause similar sinkage that leads to similar rolling resistance. On cohesive soils like wet clay, the track system is preferable. On frictional soil, the area is not important; the wheel vehicle may outperform the track system because track cause higher soil distortion. The relative equation of sinkage and the contact area [76] is described below.

$$z = \left(\frac{p}{k_c / b + k_\phi} \right)^{1/n} = \left(\frac{W / bl}{k_c / b + k_\phi} \right)^{1/n} \tag{3.1}$$

where z, p, and W are the sinkage, pressure, and weight of the vehicle, respectively. b is the width, and l is the length of the running gear. k_Φ and k_c are the cohesive and frictional

moduli of soil deformation, and n is the exponent of soil deformation. This equation explains that a wheel has a smaller length (l), which leads to higher sinkage.

The rutting formation is the first sign of soil damage caused by the vehicle sinkage. We use the gauge caliper and a plate with holes to measure sinkage after the vehicle passes, as shown in Figure 3-12 and Figure 3-13. This method was adopted in [1] to measure the sinkage of a wheel and track tested in a soil bin facility. We measure every 50 cm for a total of 40 measurements for 1 lane (10 m), as shown in Figure 3-14. We have 3 lanes, and the total is 120 measurements.

Figure 3-12 Gauge caliper with the holes

Figure 3-13 Sinkage measurement

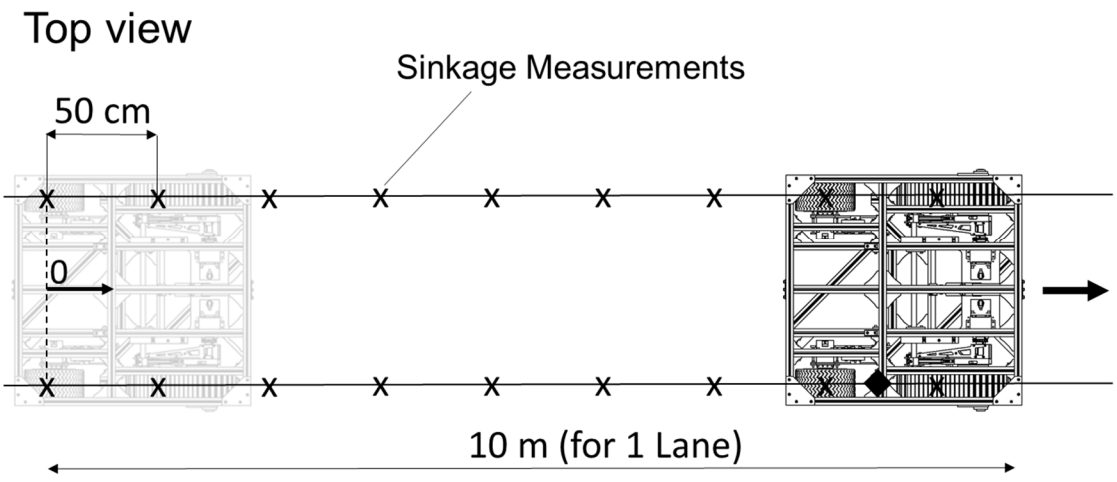

Figure 3-14 Sinkage measurement on field

Without payload conditions on firm soil, the results of CI and sinkage in three lanes are shown in Figures 3-15, 3-16, and 3-17. The results of wheel mode are shown at a distance of 0–5 m, and the results of track mode are shown at a distance of 5.5–10 m. Table 8 shows the average (AVG) and standard deviation (STDev) of 3 lanes for CI and sinkage on firm soil (without payload). The sinkage of the wheel and track is small. The average sinkage in wheel mode and track mode is 3.7 mm and 2.7 mm, respectively. Also, the difference before and after CI is small. The average CI before and after robot pass in wheel mode is 970 kPa and 980 kPa, respectively. The average CI before and after the robot passes in track mode is 954 kPa and 961 kPa, respectively.

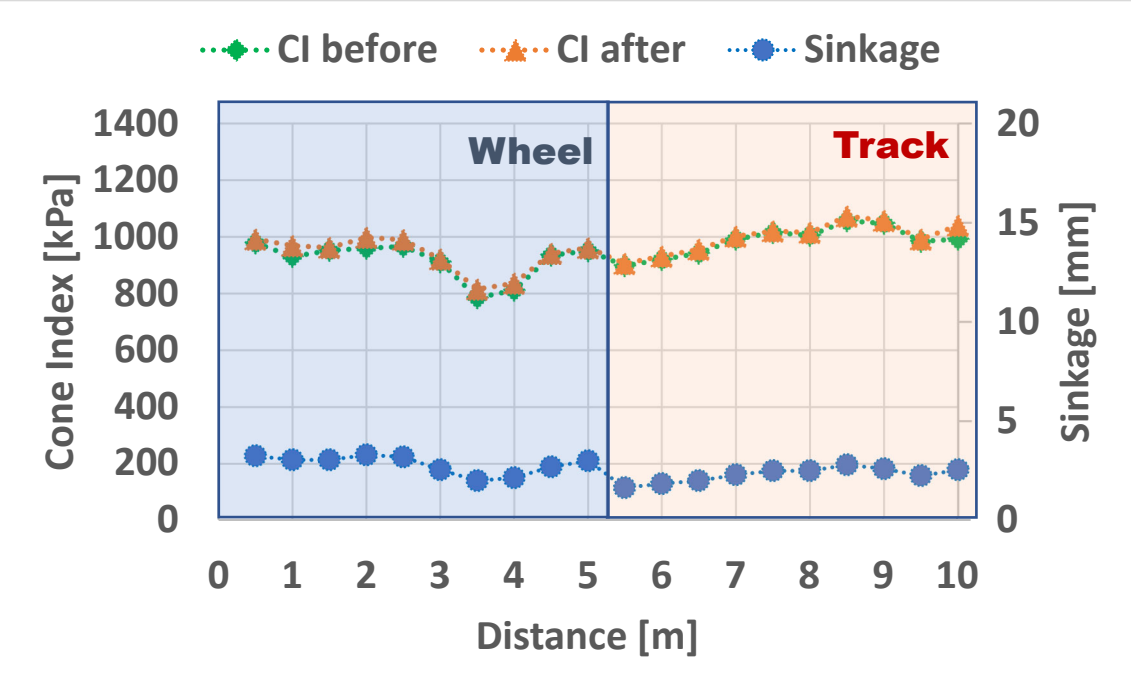

Figure 3-15 CI and Sinkage of lane 1 on firm soil (without payload)

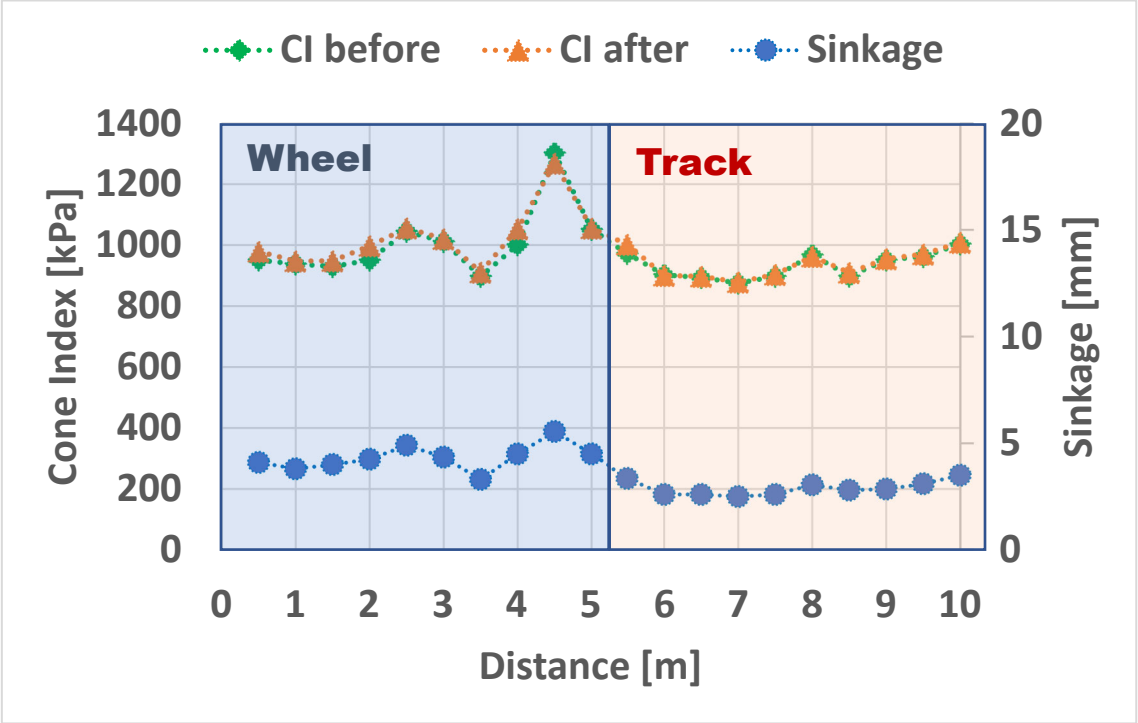

Figure 3-16 CI and Sinkage of lane 2 on firm soil (without payload)

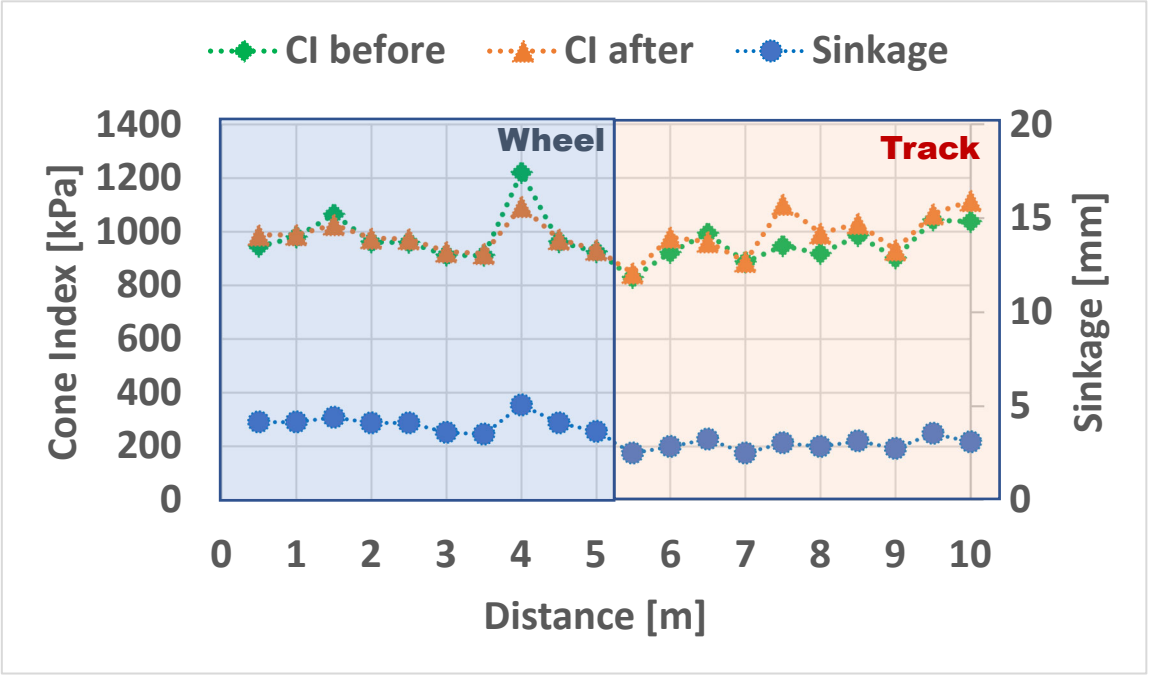

Figure 3-17 CI and Sinkage of lane 3 on firm soil (without payload)

Mode	CI before [kPa]	CI after [kPa]	Sinkage [mm]
Wheel	AVG: 970 STDev: 108	AVG: 980 STDev:133	AVG: 3.7 STDev:0.8
Track	AVG: 954 STDev: 85	AVG: 961 STDev:83	AVG: 2.7 STDev: 0.4

Table 8 Summary results of CI and sinkage on firm soil (without payload)

For payload conditions on firm soil, the results of CI and sinkage in 3 lanes are shown in Figures 3-18, 3-19, and 3-20. The results of wheel mode are shown at a distance of 0–5 m, and the results of track mode are shown at a distance of 5.5–10 m. Table 9 shows the average (AVG) and standard deviation (STDev) of 3 lanes for CI and sinkage on firm soil (payload). The average sinkage in wheel mode and track mode is 5 mm and 4.8 mm, respectively. The average CI before and after the robot pass in wheel mode is 960 kPa and 989 kPa, respectively. The average CI before and after the robot passes in track mode is 1057 kPa and 1084 kPa, respectively.

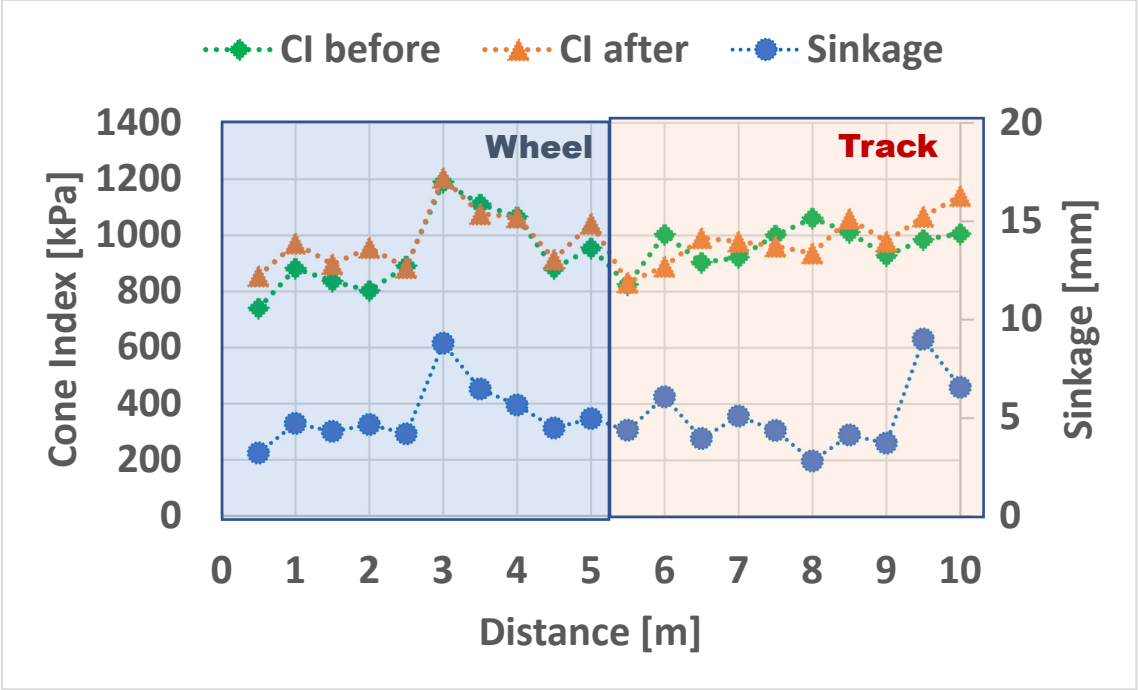

Figure 3-18 CI and Sinkage of lane 1 on firm soil (payload)

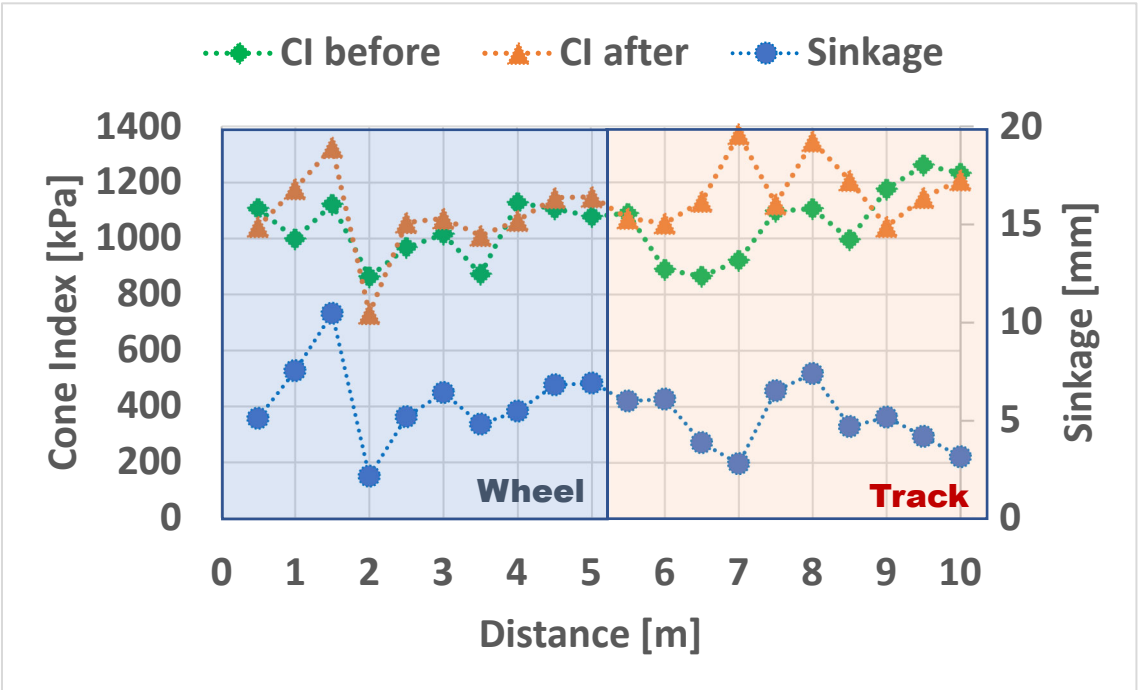

Figure 3-19 CI and Sinkage of lane 2 on firm soil (payload)

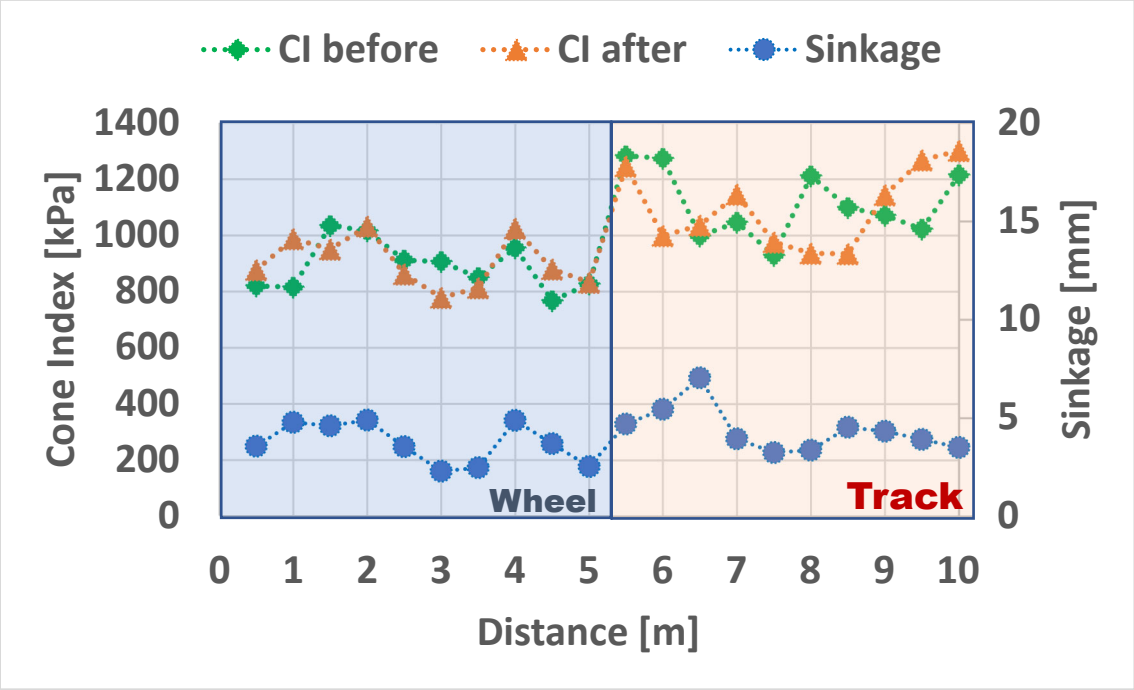

Figure 3-20 CI and Sinkage of lane 3 on firm soil (payload)

Mode	CI before [kPa]	CI after [kPa]	Sinkage [mm]
Wheel	AVG: 960 STDev123	AVG: 989 STDev:136	AVG: 5 STDev: 1.9
Track	AVG: 1057 STDev:128	AVG: 1084 STDev:137	AVG: 4.8 STDev: 1.5

Table 9 Summary results of CI and sinkage on firm soil (payload)

Without payload conditions on soft soil, the results of CI and sinkage in 3 lanes are shown in Figures 3-21, 3-22, and 3-23. The results of wheel mode are shown at a distance of 0–5 m, and the results of track mode are shown at a distance of 5.5–10 m. Table 10 shows the average (AVG) and standard deviation (STDev) of 3 lanes for CI and sinkage (without payload). On soft soil, the sinkage of the wheel is higher than that of the track

because the wheel has a small contact area, as described in Eq. (1.3). The average sinkage in wheel mode and track mode is 27 mm and 21 mm, respectively. The average CI before and after robot pass in wheel mode are 269 kPa and 361 kPa, respectively. The average CI before and after robot pass in track mode are 251 kPa and 300 kPa, respectively.

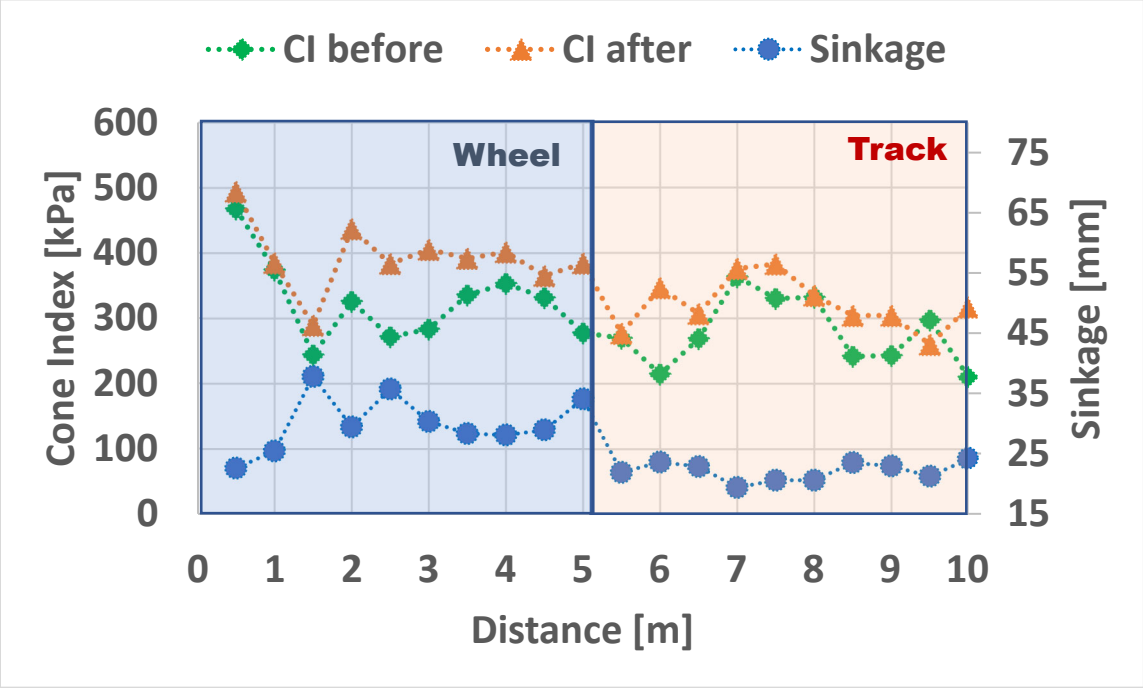

Figure 3-21 CI and Sinkage of lane 1 on soft soil (without payload)

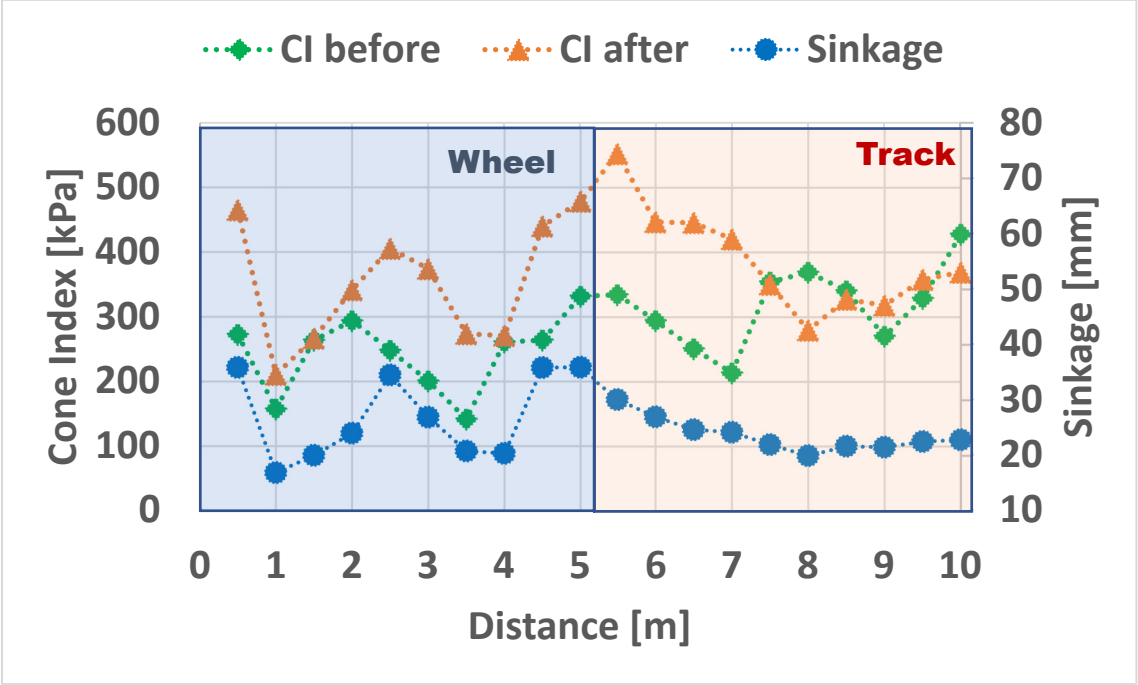

Figure 3-22 CI and Sinkage of lane 2 on soft soil (without payload)

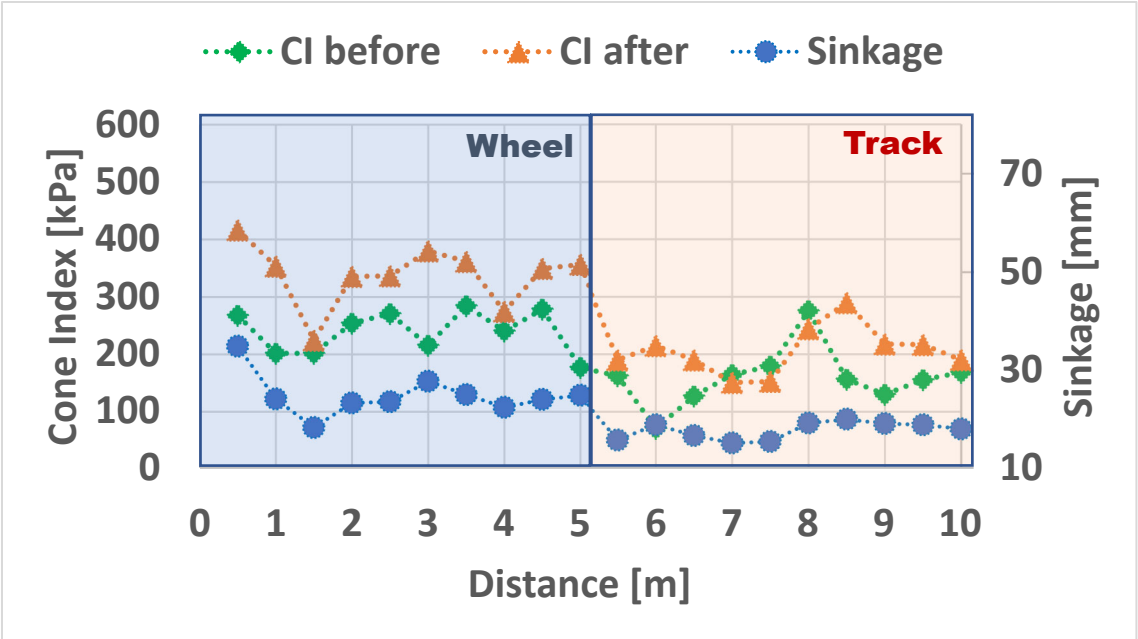

Figure 3-23 CI and Sinkage of lane 3 on soft soil (without payload)

Mode	CI before [kPa]	CI after [kPa]	Sinkage [mm]
Wheel	AVG: 269 STDev: 67	AVG: 361 STDev:71	AVG: 27 STDev:5.9
Track	AVG: 251 STDev: 84	AVG: 300 STDev:79	AVG: 21 STDev: 2.6

Table 10 Summary results of CI and sinkage on soft soil (without payload)

For payload conditions on soft soil, the results of CI and sinkage in 3 lanes are shown in Figures 3-24, 3-25, and 3-26. The results of wheel mode are shown at a distance of 0–5 m, and the results of track mode are shown at a distance of 5.5–10 m. Table 11 shows the average (AVG) and standard deviation (STDev) of 3 lanes for CI and sinkage (payload). The average sinkage in wheel mode and track mode is 49 mm and 40 mm, respectively. The sinkage in wheel mode is higher than in track mode. The average CI before and after robot pass in wheel mode are 186 kPa and 376 kPa, respectively. The average CI before and after the robot pass in track mode is 165 kPa and 320 kPa, respectively.

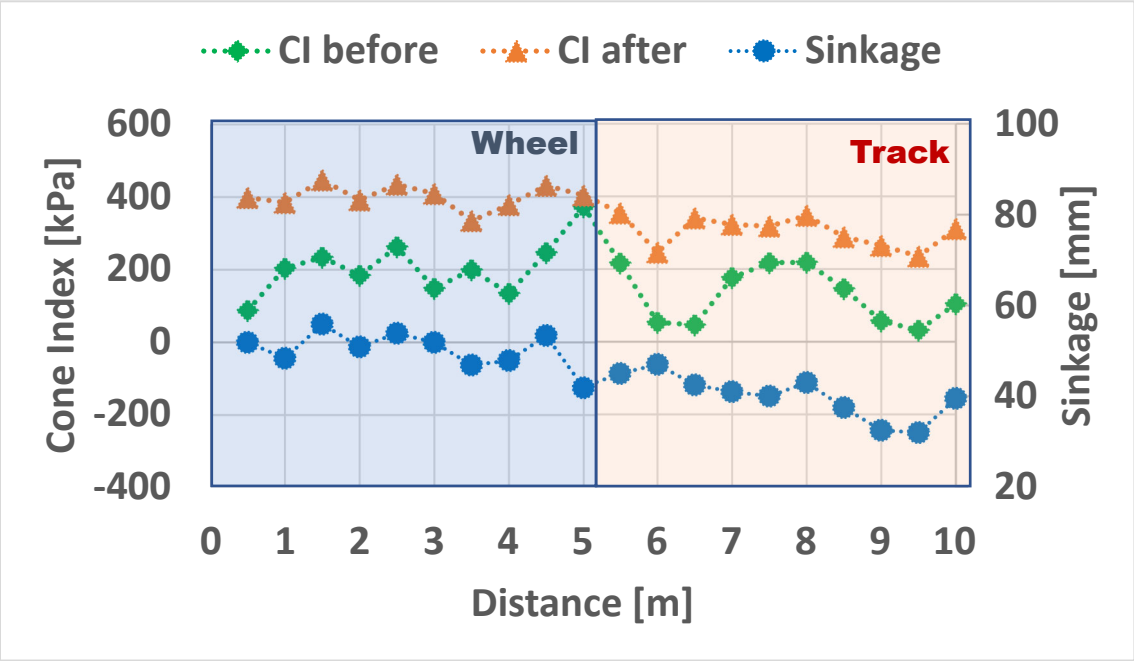

Figure 3-24 CI and Sinkage of lane 1 on soft soil (payload)

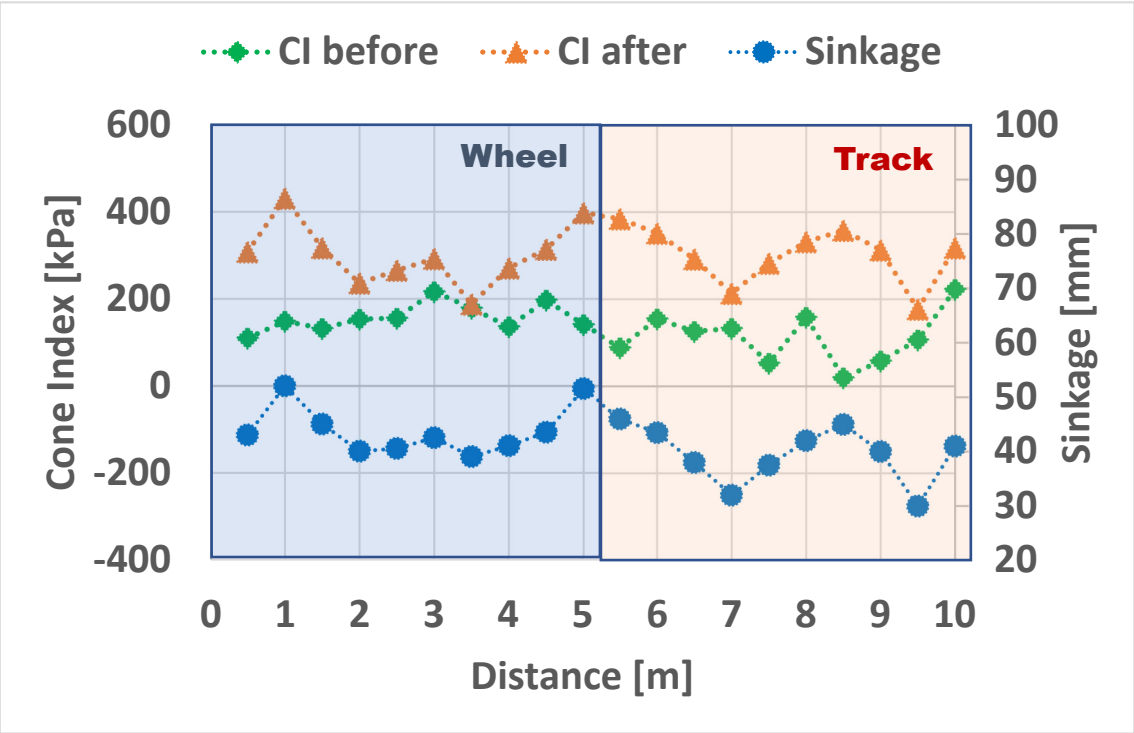

Figure 3-25 CI and Sinkage of lane 2 on soft soil (payload)

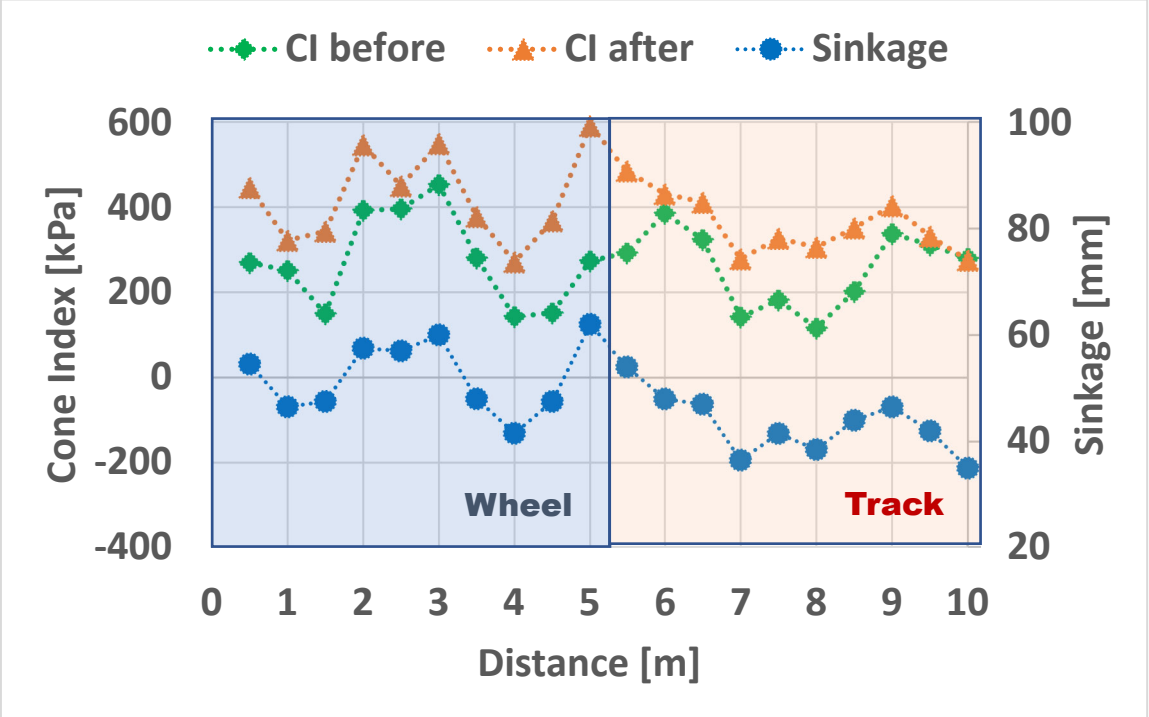

Figure 3-26 CI and Sinkage of lane 3 on soft soil (payload)

Mode	CI before [kPa]	CI After [kPa]	Sinkage [mm]
Wheel	AVG: 186 STDev: 92	AVG: 376 STDev:92	AVG: 49 STDev:6.2
Track	AVG: 165 STDev: 99	AVG: 320 STDev:64	AVG: 40 STDev: 5.5

Table 11 Summary results of CI and sinkage on soft soil (payload)

Without payload conditions on wet soil, the results of CI and sinkage in 3 lanes are shown in Figures 3-27, 3-28, and 3-29. The results of wheel mode are shown at a distance of 0–5 m, and the results of track mode are shown at a distance of 5.5–10 m. Table 12 shows the average (AVG) and standard deviation (STDev) of 3 lanes for CI and sinkage (without payload). The average sinkage in wheel mode and track mode is 21 mm and 18 mm, respectively. The average CI before and after robot pass in wheel mode are 310 kPa and 414 kPa, respectively. The average CI before and after robot pass in track mode are 303 kPa and 376 kPa, respectively.

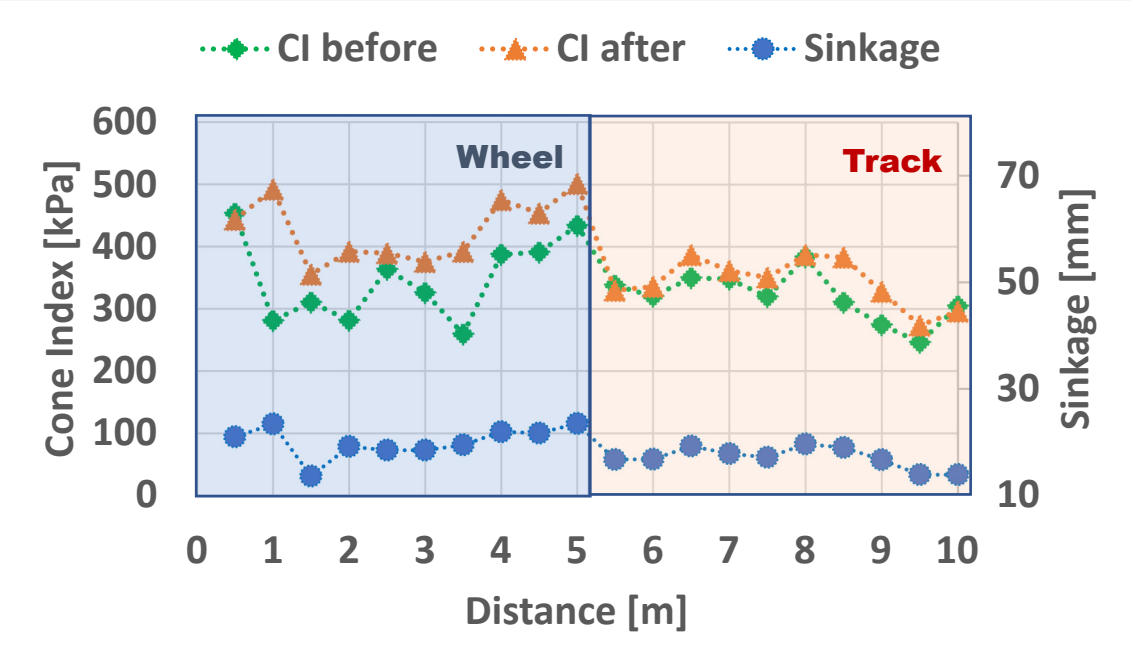

Figure 3-27 CI and Sinkage of lane 1 on soft soil (without payload)

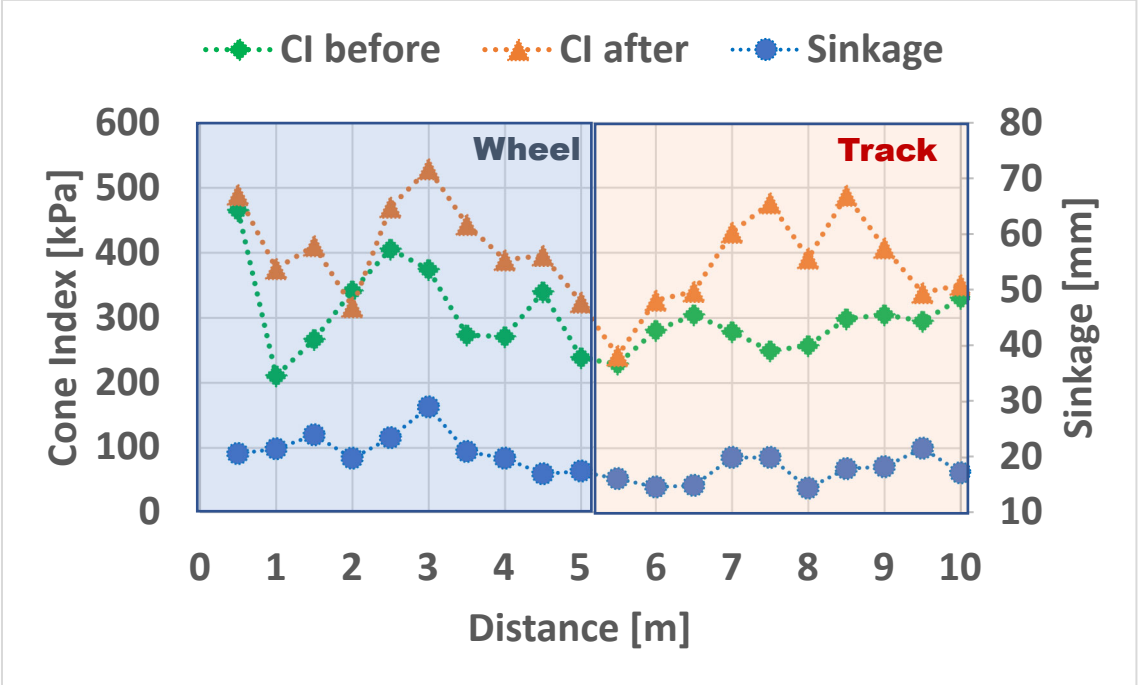

Figure 3-28 CI and Sinkage of lane 2 on soft soil (without payload)

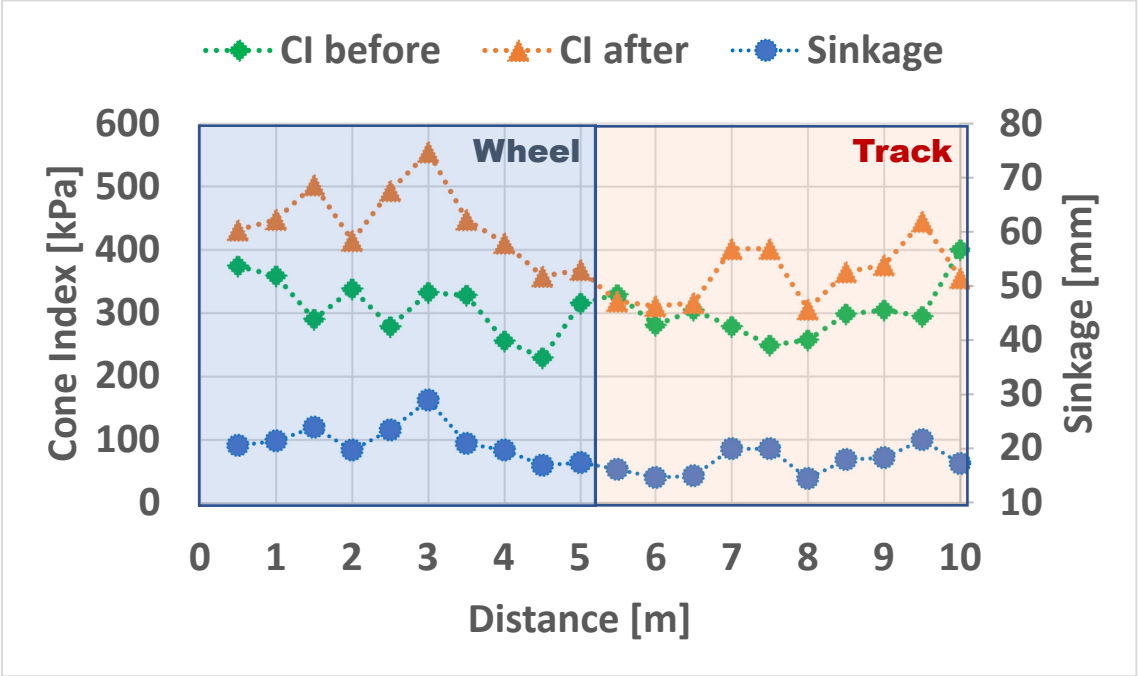

Figure 3-29 CI and Sinkage of lane 3 on soft soil (without payload)

Mode	CI before [kPa]	CI After [kPa]	Sinkage [mm]
Wheel	AVG: 310 STDev: 57	AVG: 414 STDev:66	AVG: 22 STDev:3.4
Track	AVG: 303 STDev: 45	AVG: 376 STDev:71	AVG: 18 STDev: 2.9

Table 12 Summary results of CI and sinkage on wet soil (without payload)

For payload conditions on wet soil, the results of CI and sinkage in 3 lanes are shown in Figures 3-30, 3-31, and 3-32. The results of wheel mode are shown at a distance of 0–5 m, and the results of track mode are shown at a distance of 5.5–10 m. Table 13 shows the average (AVG) and standard deviation (STDev) of 3 lanes for CI and sinkage (payload). The average sinkage in wheel mode and track mode is 29 mm and 23 mm, respectively. The sinkage in wheel mode is higher than in track mode. The average CI before and after robot pass in wheel mode are 348 kPa and 526 kPa, respectively. The average CI before and after robot pass in track mode are 330 kPa and 484 kPa, respectively.

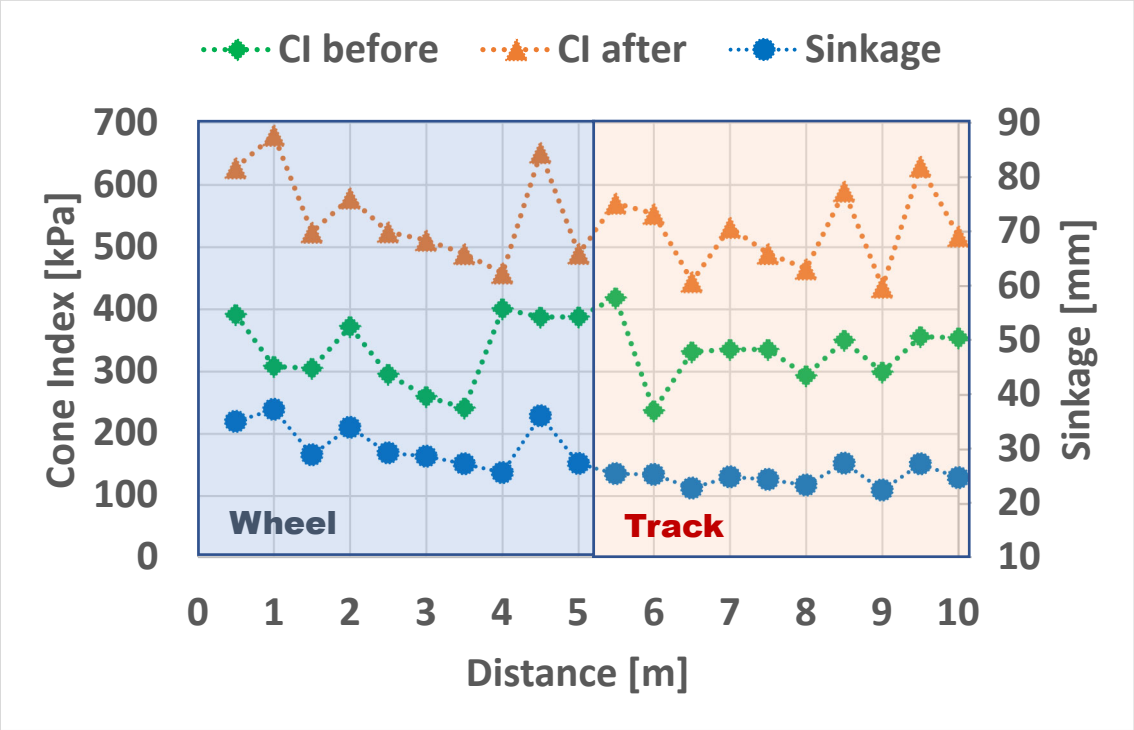

Figure 3-30 CI and Sinkage of lane 1 on wet soil (payload)

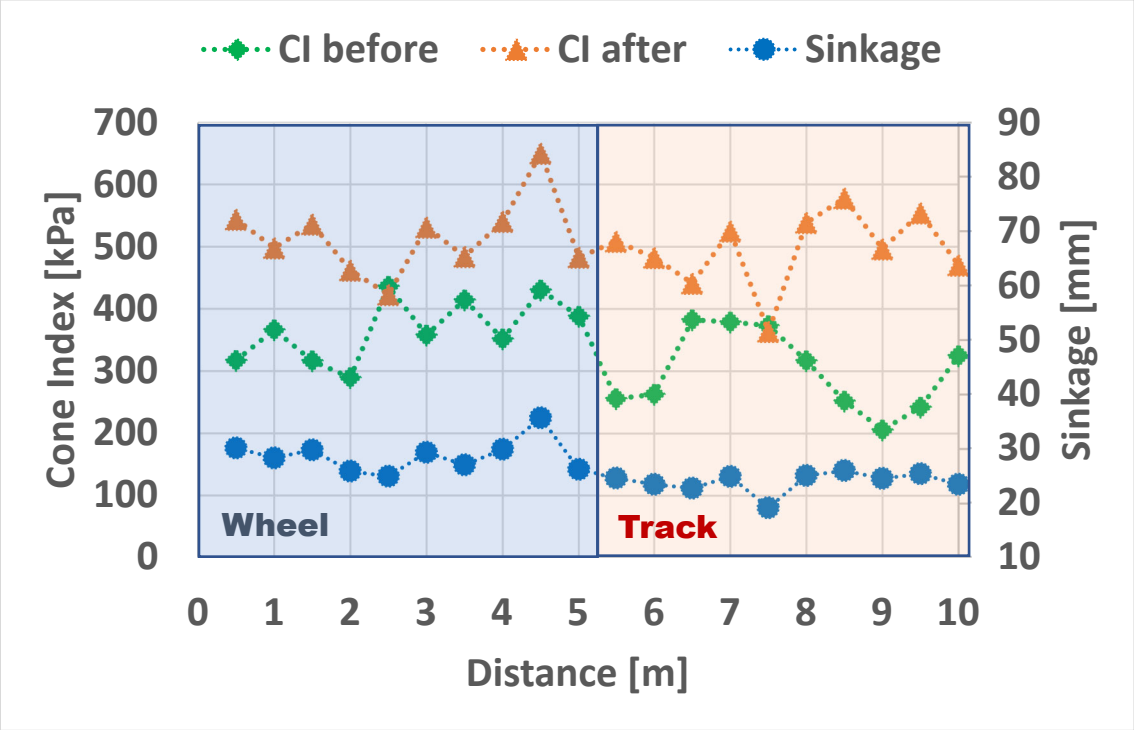

Figure 3-31 CI and Sinkage of lane 2 on wet soil (payload)

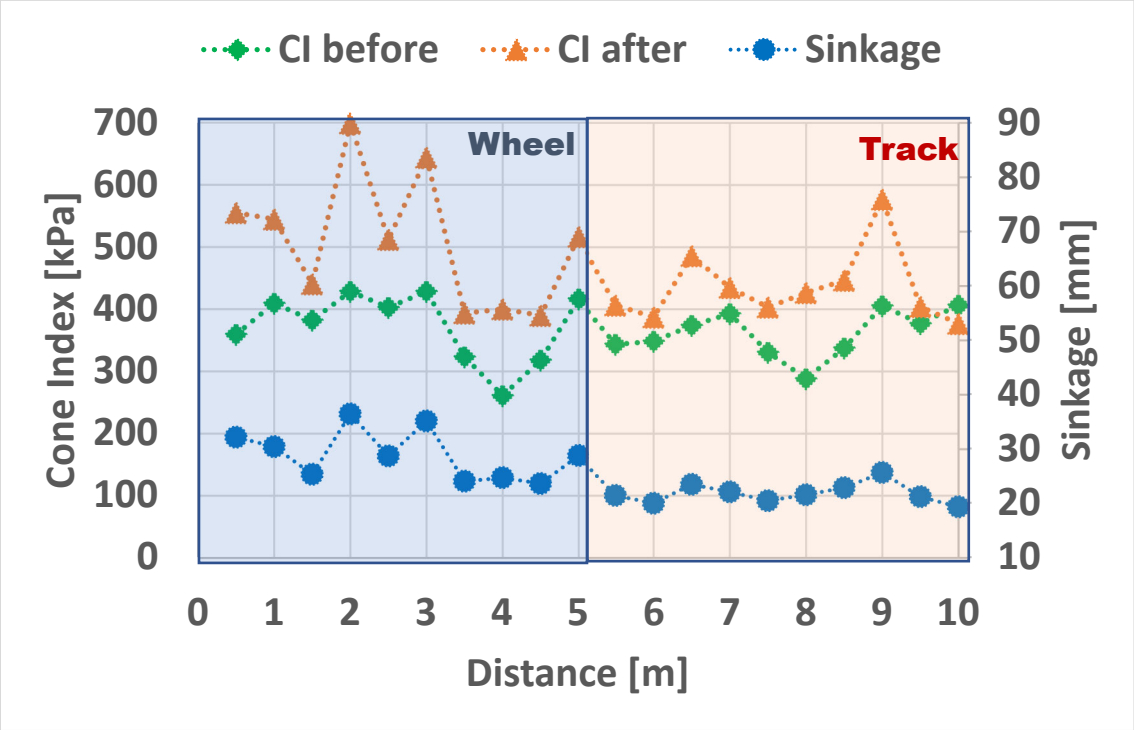

Figure 3-32 CI and Sinkage of lane 3 on wet soil (payload)

Mode	CI before [kPa]	CI after [kPa]	Sinkage [mm]
Wheel	AVG: 348 STDev: 56	AVG: 526 STDev:82	AVG: 29 STDev:4
Track	AVG: 330 STDev: 55	AVG: 484 STDev:70	AVG: 23 STDev: 2

Table 13 Summary results of CI and sinkage on wet soil (payload)

Without payload conditions on soft wet soil, the results of CI and sinkage in 3 lanes are shown in Figures 3-33. The results of wheel mode are shown at a distance of 0–5 m, and the results of track mode are shown at a distance of 5.5–10 m. Table 14 shows the average (AVG) and standard deviation (STDev) of 3 lanes for CI and sinkage (without payload). The average sinkage in wheel mode and track mode is 66 mm and 54 mm, respectively. The average CI before and after robot pass in wheel mode are 70 kPa and

164 kPa, respectively. The average CI before and after robot pass in track mode are 83 kPa and 131 kPa, respectively.

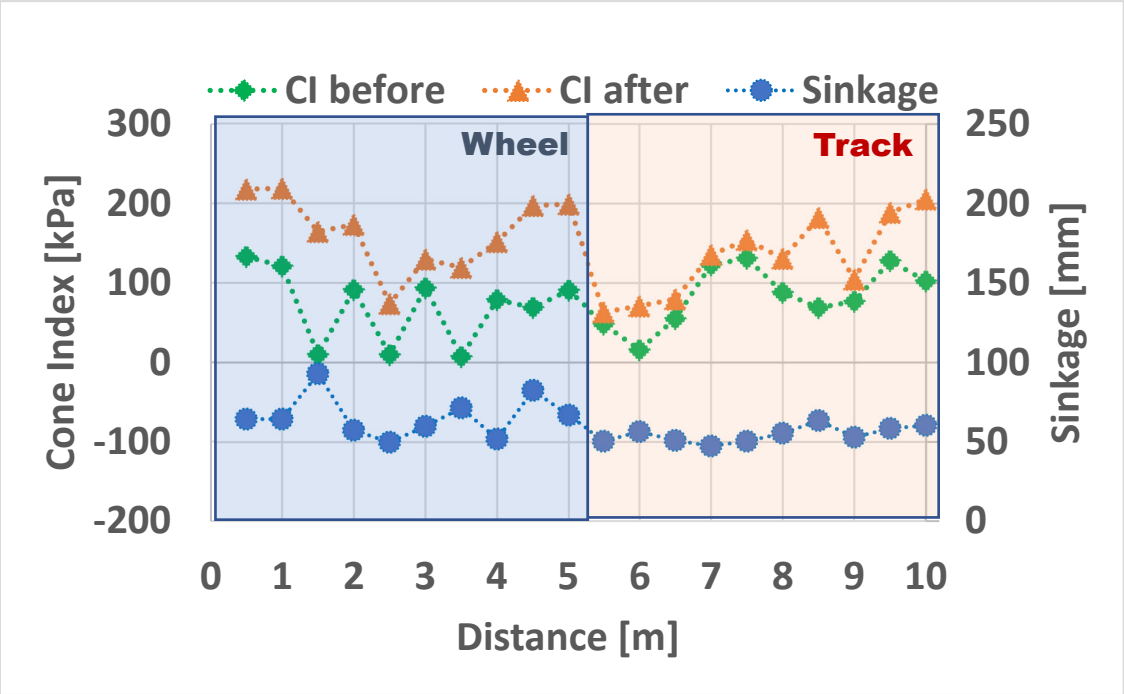

Figure 3-33 CI and Sinkage of 1 lane on soft wet soil (without payload)

Mode	CI before [kPa]	CI After [kPa]	Sinkage [mm]
Wheel	AVG: 70 STDev: 46	AVG: 164 STDev:46	AVG: 66 STDev:13
Track	AVG: 83 STDev: 38	AVG: 131 STDev:51	AVG: 54 STDev: 5

Table 14 Summary results of CI and sinkage on soft wet soil (without payload)

3.3.2 Soil distortion

For soil distortion measurement, we use shear displacement to estimate the soil distortion. The shear displacement is measured after the vehicle passes and is given by the chalk displacement. We put the chalk every 50 cm. The chalk displacement method is the origin of this research. Figure 3-34 shows shear displacement by chalk on the field. The comparison of chalk displacement between before and after the robot pass is shown in Figure 3-35. We use MATLAB software and "spatial_calibration_demo.m" to calibrate chalk displacement from the pixels to mm in the photo. The "spatial_calibration_demo.m" was developed by Alex Perrakis [77]. The instructions for calibration are shown in Figure 3-36, Figure 3-37 and 3-38. First, we upload an image of chalk displacement as shown in Figure 3-36. Next, we calibrate using the ruler in the photo, as shown in Figure 3-37. Finally, we make the line to refer and measure chalk displacement as shown in Figure 3-38. We measure 2 times and calculate the average. This software has higher accuracy than looking at pictures directly. The shear displacement and chalk displacement are related to slip and contact area, as described in Eq. (1.2).

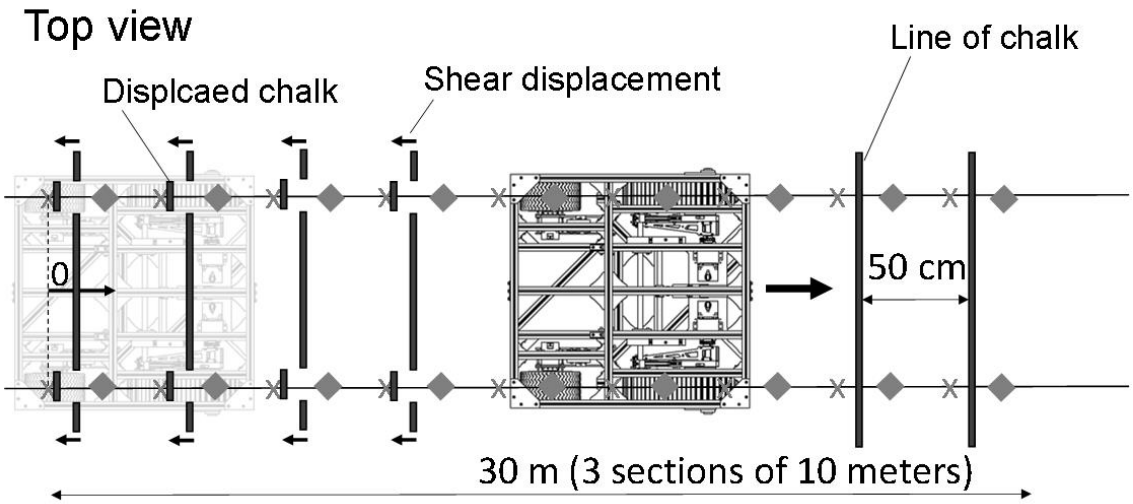

Figure 3-34 The chalk displacement measurement on field

Figure 3-35 The chalk displacement before (left) and after (right) robot pass.

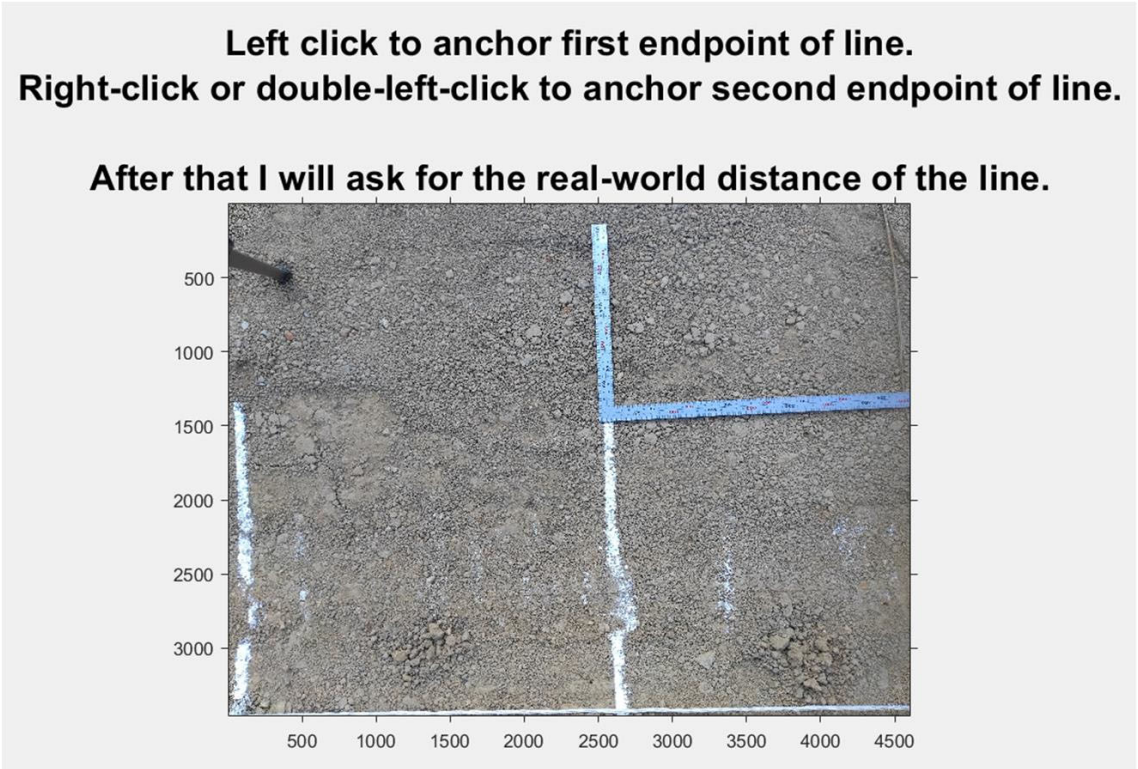

Figure 3-36 Upload picture to measurement software.

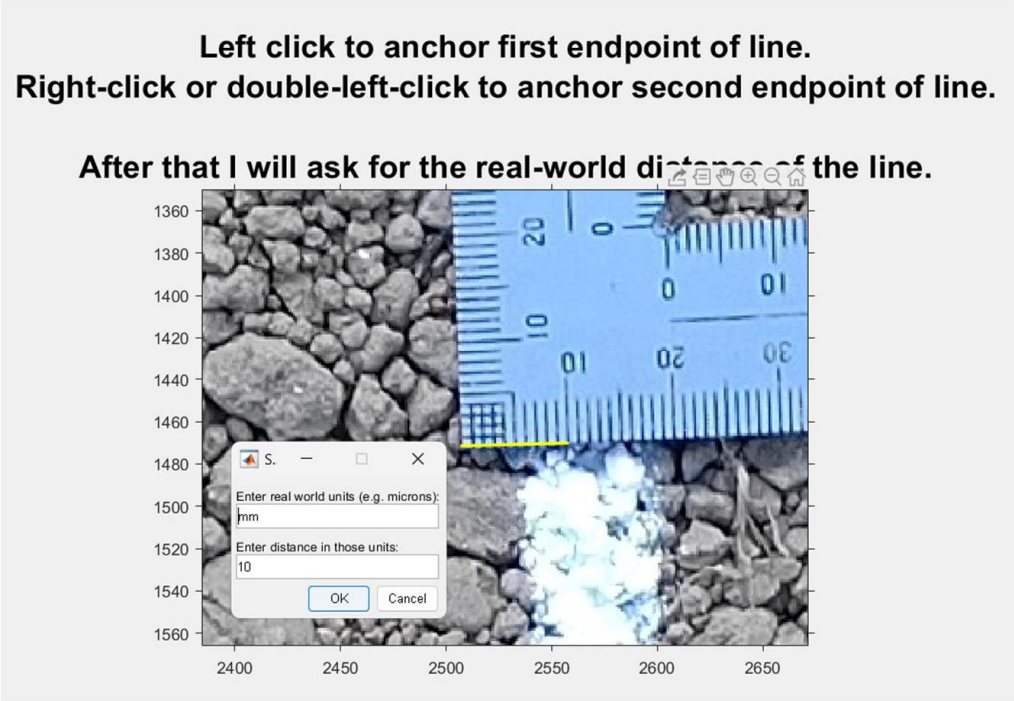

Figure 3-37 Calibrate pixel to mm by referring the ruler

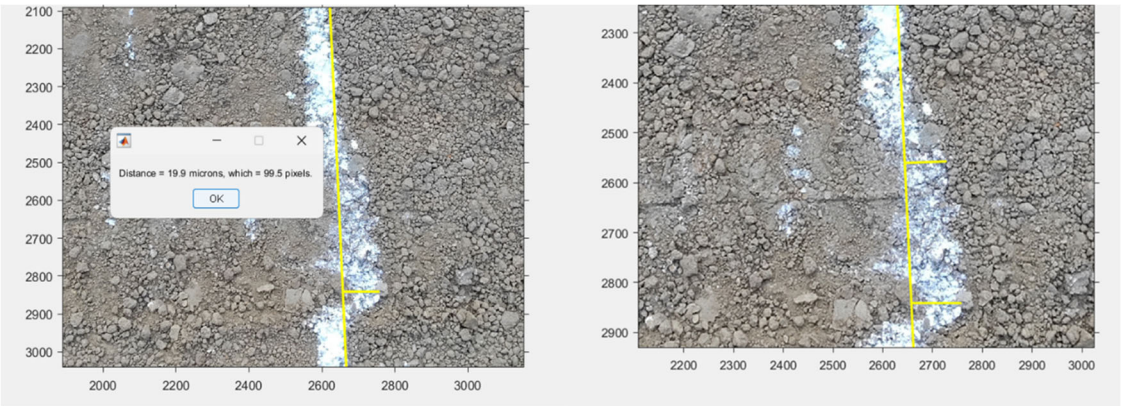

Figure 3-38 Make the reference line and measure chalk displacement

Without payload conditions on firm soil, the results of shear displacement in three lanes are shown in Figures 3-39, 3-40, and 3-41. The results of wheel mode are shown at a distance of 0–5 m, and the results of track mode are shown at a distance of 5.5–10 m. Table 15 shows a summary of the results of the shear displacement of 3 lanes (without payload). The average shear displacement in wheel mode and track mode is 7.5 mm and

20.5 mm, respectively. Tracks cause higher shear displacement because they have a longer contact area, as described in Eq. (1.2).

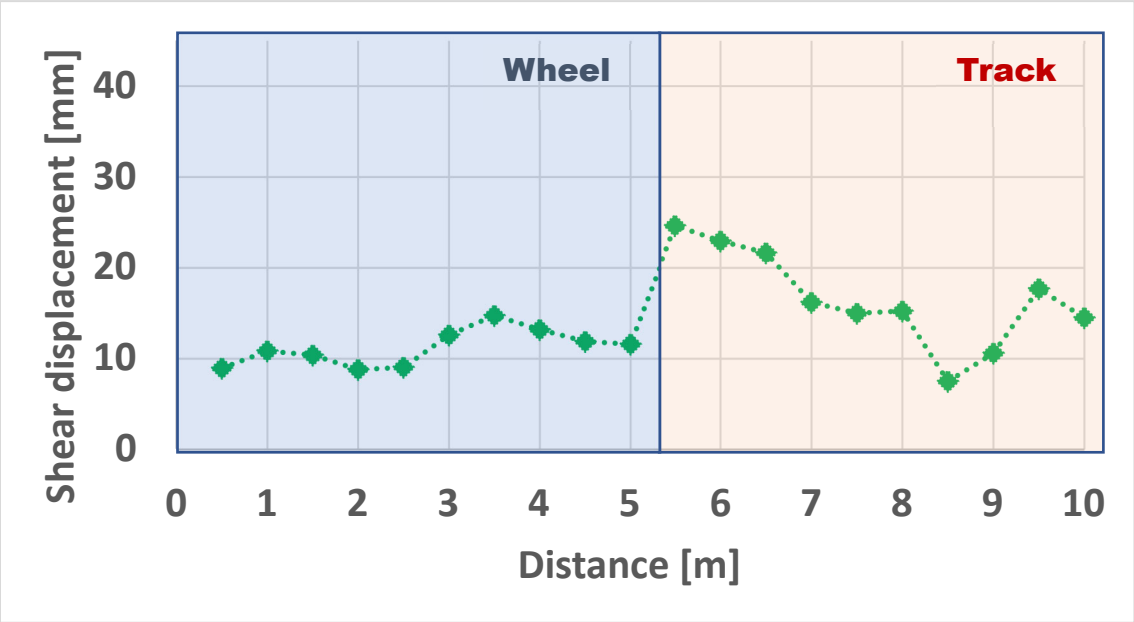

Figure 3-39 Shear displacement of lane 1 on firm soil (without payload)

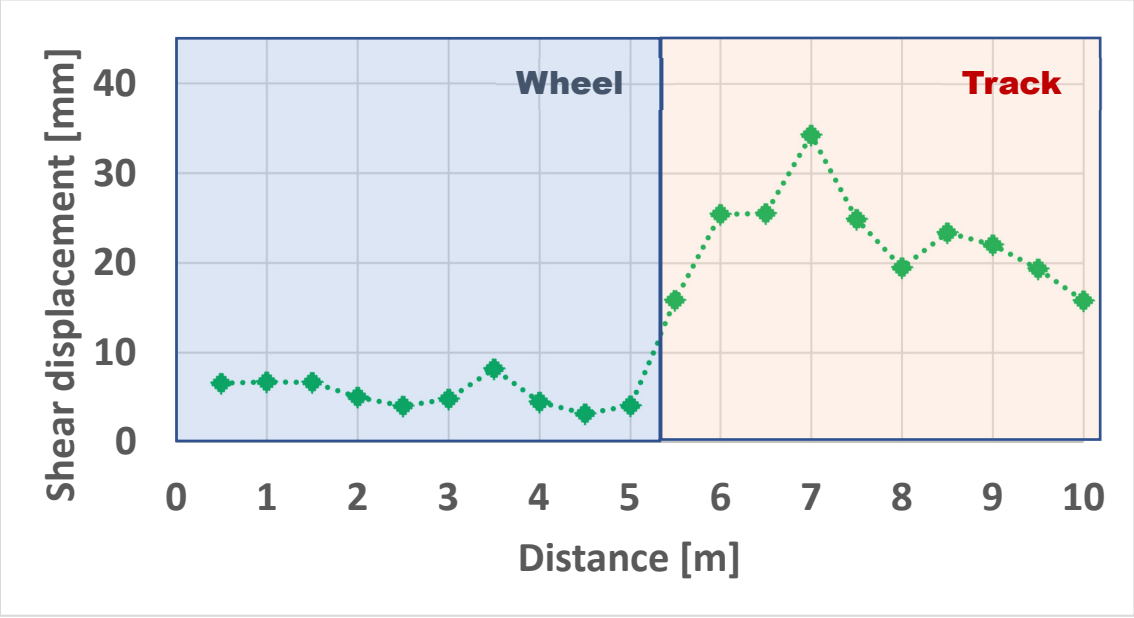

Figure 3-40 Shear displacement of lane 2 on firm soil (without payload)

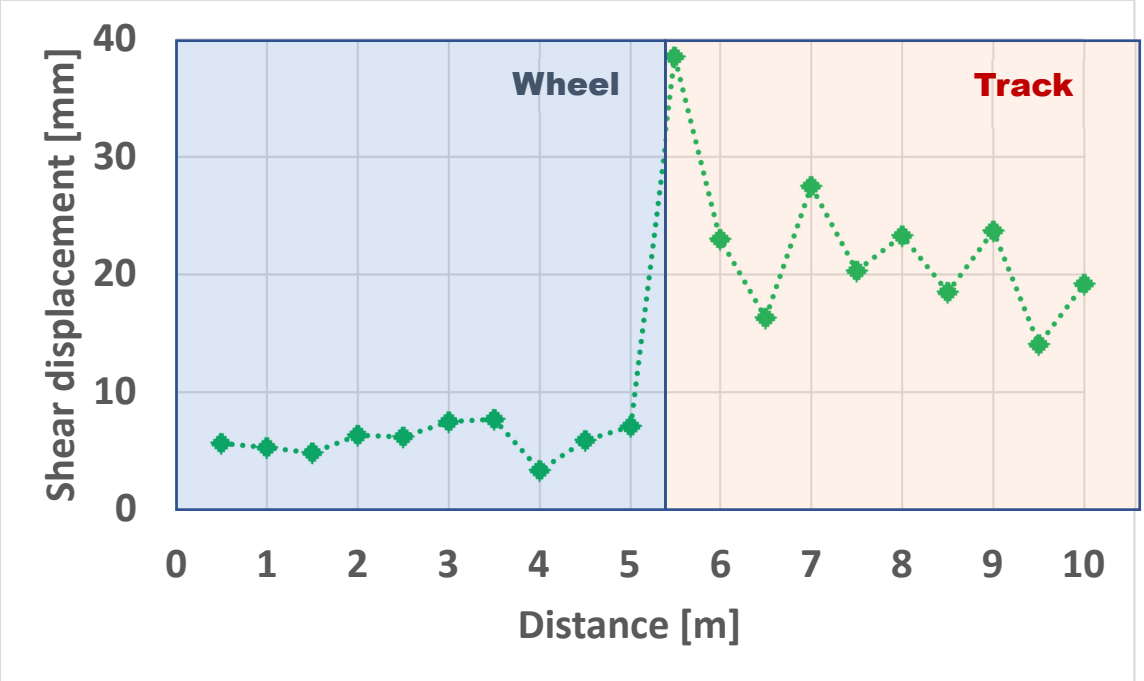

Figure 3-41 Shear displacement of lane 3 on firm soil (without payload)

Mode	**Chalk displacement** [mm]
Wheel	Average: 7.5 Standard deviation: 3
Track	Average: 20.5 Standard deviation: 6.4

Table 15 Summary results of shear displacement on firm soil (without payload)

For payload conditions on firm soil, the results of shear displacement of 3 lanes are shown in Figures 3-42, 3-43, and 3-44. The results of wheel mode are shown at a distance of 0–5 m, and the results of track mode are shown at a distance of 5.5–10 m. Table 16 shows a summary of the results of the shear displacement of 3 lanes (payload). The average shear displacement in wheel mode and track mode is 7 mm and 20 mm, respectively.

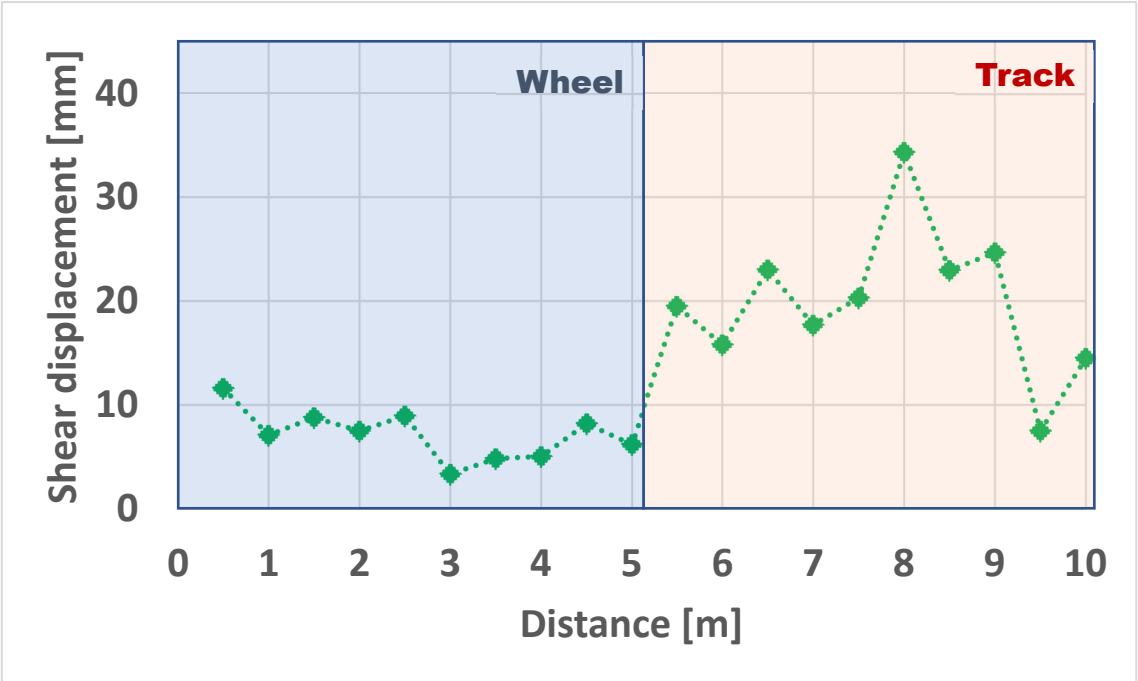

Figure 3-42 Shear displacement of lane 1 on firm soil (payload)

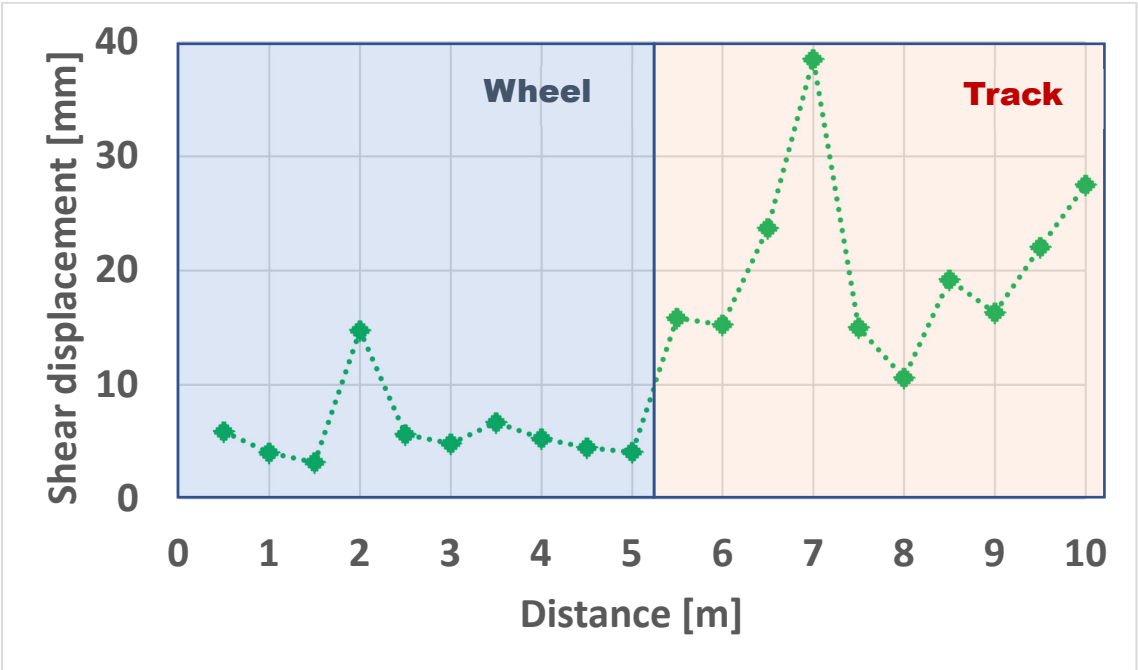

Figure 3-43 Shear displacement of lane 2 on firm soil (payload)

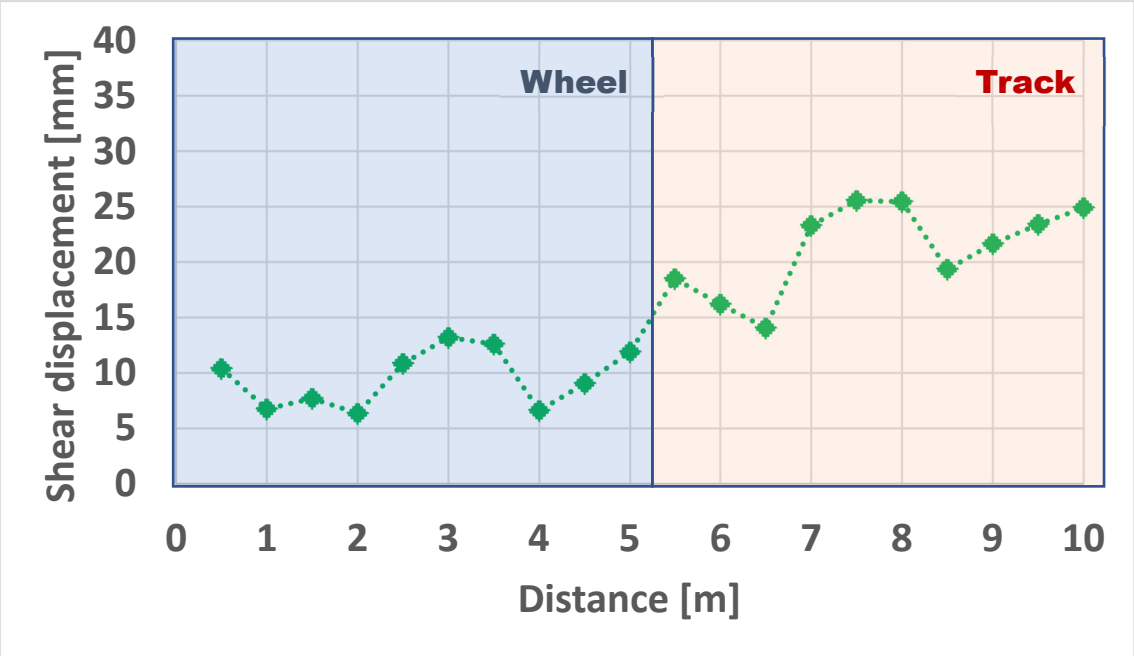

Figure 3-44 Shear displacement of lane 3 on firm soil (payload)

Mode	**Shear displacement** [mm]
Wheel	Average: 7 Standard deviation: 3
Track	Average: 20 Standard deviation: 6.4

Table 16 Summary results of shear displacement on firm soil (payload)

Without payload conditions on soft soil, the results of shear displacement of 3 lanes on soft soil are shown in Figures 3-45, 3-46, and 3-47. The results of wheel mode are shown at a distance of 0–5 m, and the results of track mode are shown at a distance of 5.5–10 m. Table 17 shows a summary of the results of the shear displacement of 3 lanes on soft soil (without payload). The average shear displacement in wheel mode and track mode is 6.7 mm and 14.9 mm, respectively. Tracks cause higher shear displacement because they have a longer contact area, as described in Eq. (1.2).

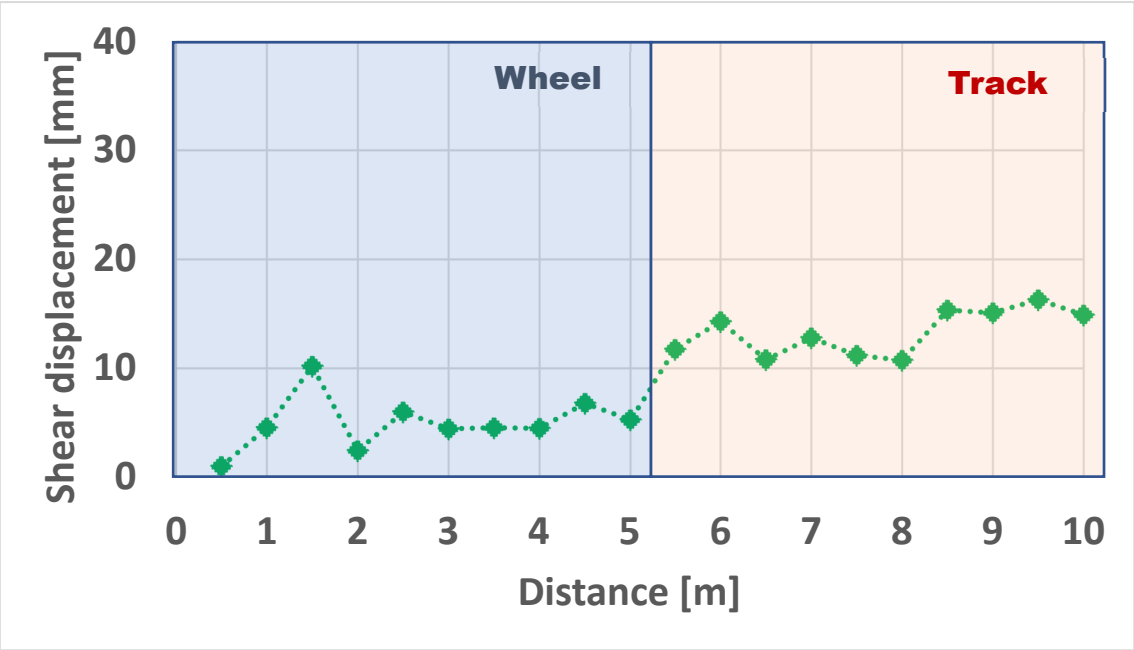

Figure 3-45 Shear displacement of lane 1 on soft soil (without payload)

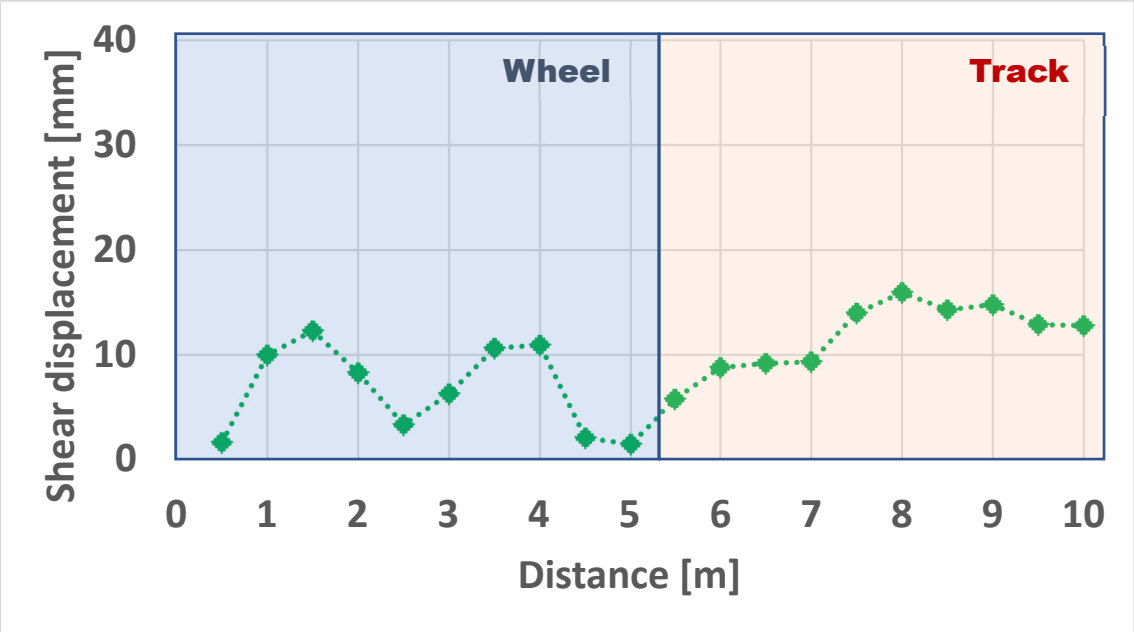

Figure 3-46 Shear displacement of lane 2 on soft soil (without payload)

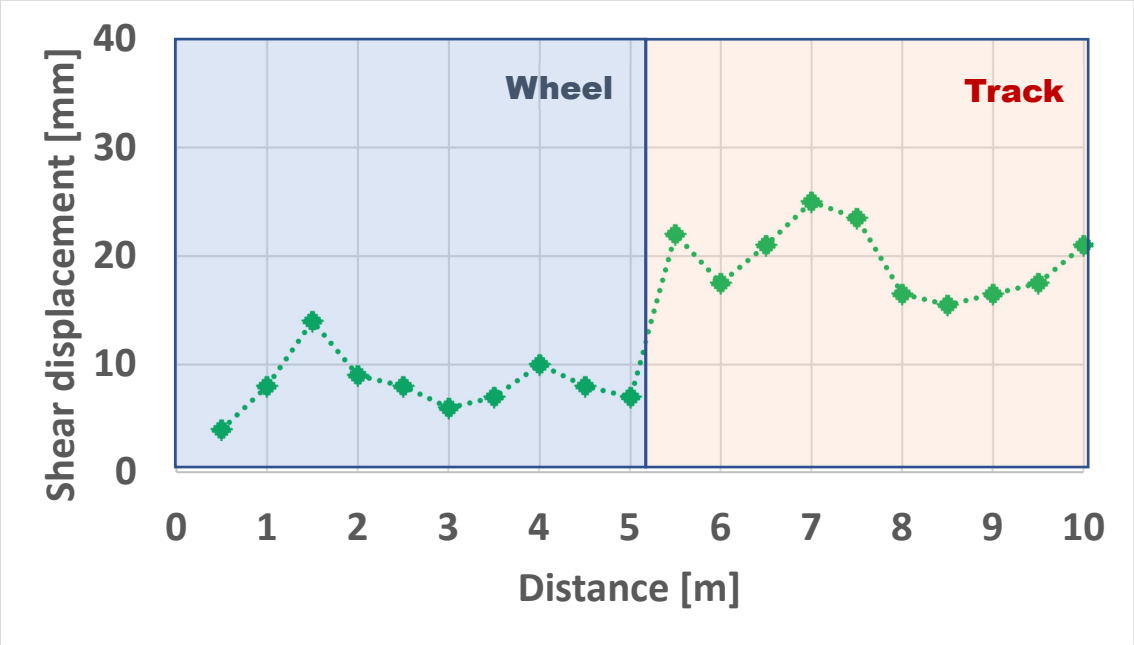

Figure 3-47 Shear displacement of lane 3 on soft soil (without payload)

Mode	**Chalk displacement** [mm]
Wheel	Average: 6.7 Standard deviation: 3
Track	Average: 14.9 Standard deviation: 4

Table 17 Summary results of shear displacement on soft soil (without payload)

For payload conditions on soft soil, the results of shear displacement of 3 lanes are shown in Figures 3-48, 3-49, and 3-50. The results of wheel mode are shown at a distance of 0–5 m, and the results of track mode are shown at a distance of 5.5–10 m. Table 18 shows a summary of the results of the shear displacement of three lanes on soft soil (payload). The average shear displacement in wheel mode and track mode is 3.6 mm and 13 mm, respectively.

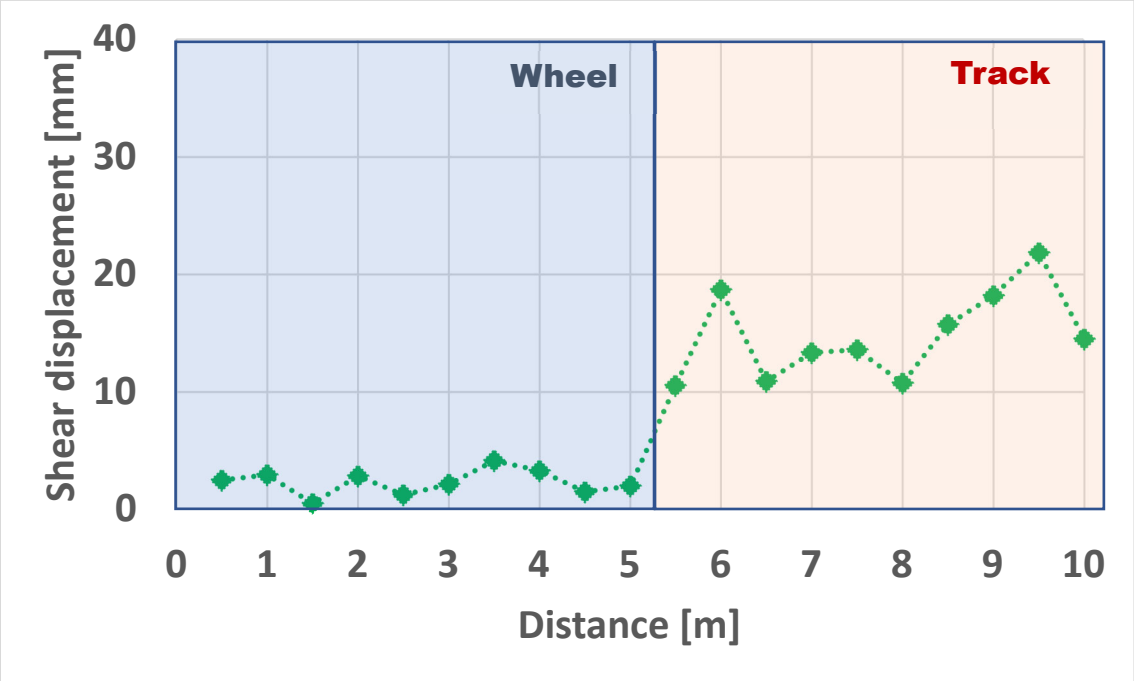

Figure 3-48 Shear displacement of lane 1 on soft soil (payload)

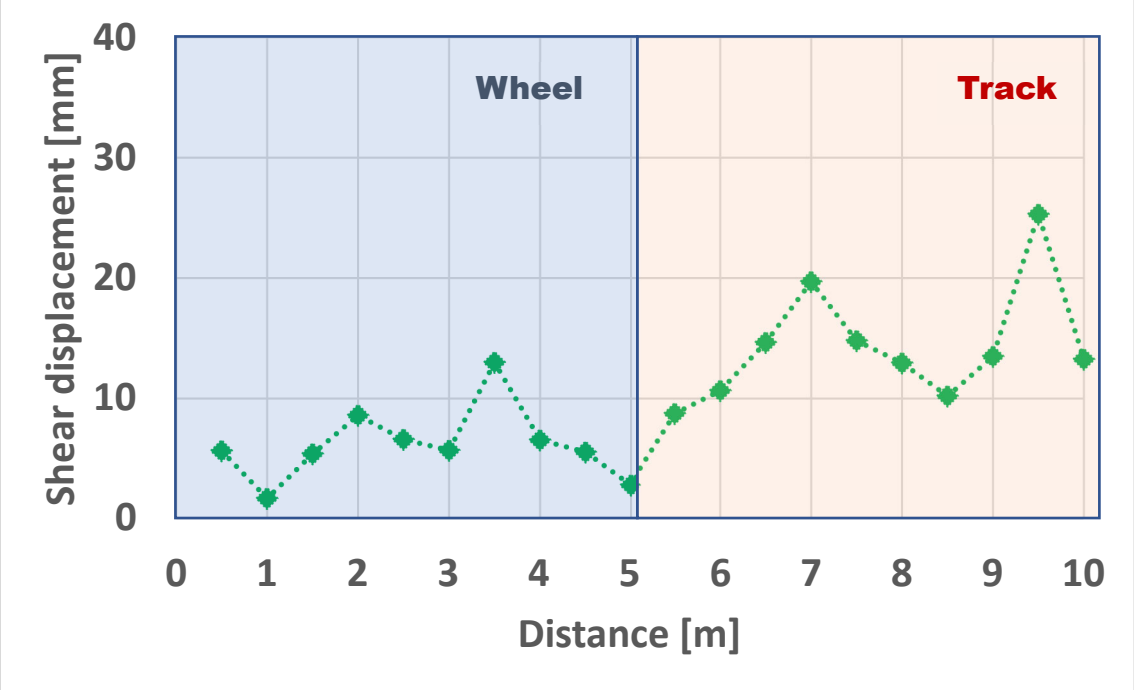

Figure 3-49 Shear displacement of lane 2 on soft soil (payload)

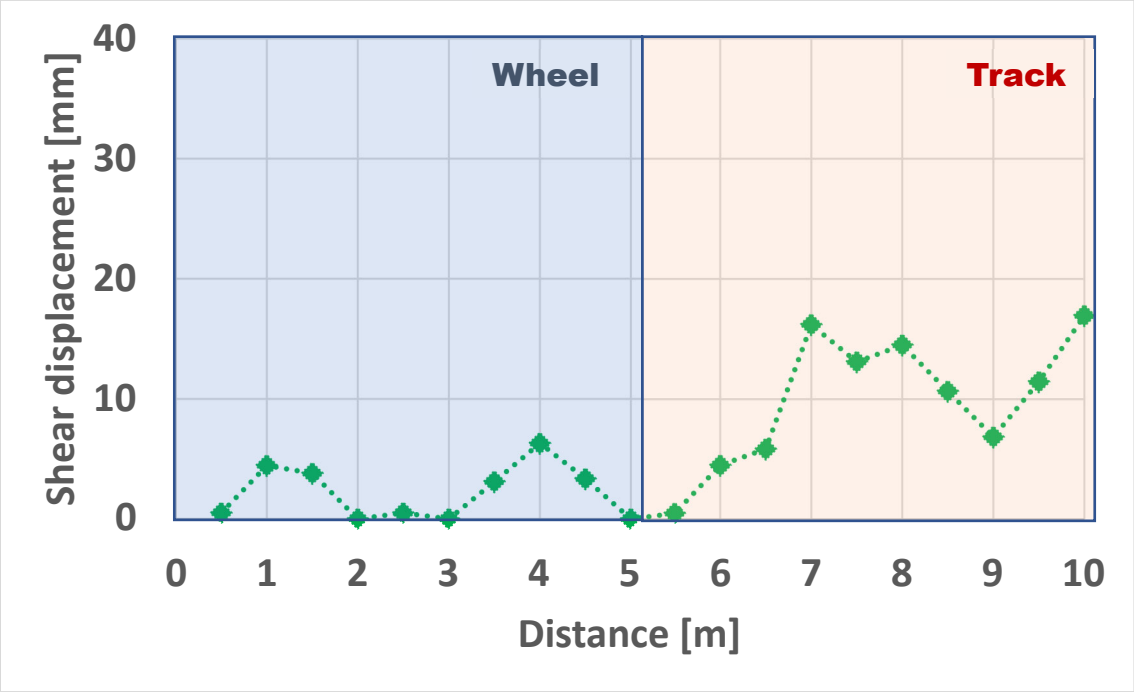

Figure 3-50 Shear displacement of lane 3 on soft soil (payload)

Mode	**Chalk displacement** [mm]
Wheel	Average: 3.6 Standard deviation: 2.8
Track	Average: 13 Standard deviation: 5

Table 18 Summary results of shear displacement on soft soil (without payload)

Without payload conditions on wet soil, the results of the shear displacement of 3 lanes are shown in Figures 3–51, 3–52, and 3–53. The results of wheel mode are shown at a distance of 0–5 m, and the results of track mode are shown at a distance of 5.5–10 m. Table 19 shows a summary of the results of the shear displacement of 3 lanes (without payload). The average shear displacement in wheel mode and track mode is 11 mm and

22 mm, respectively. Tracks cause higher shear displacement because they have a longer contact area.

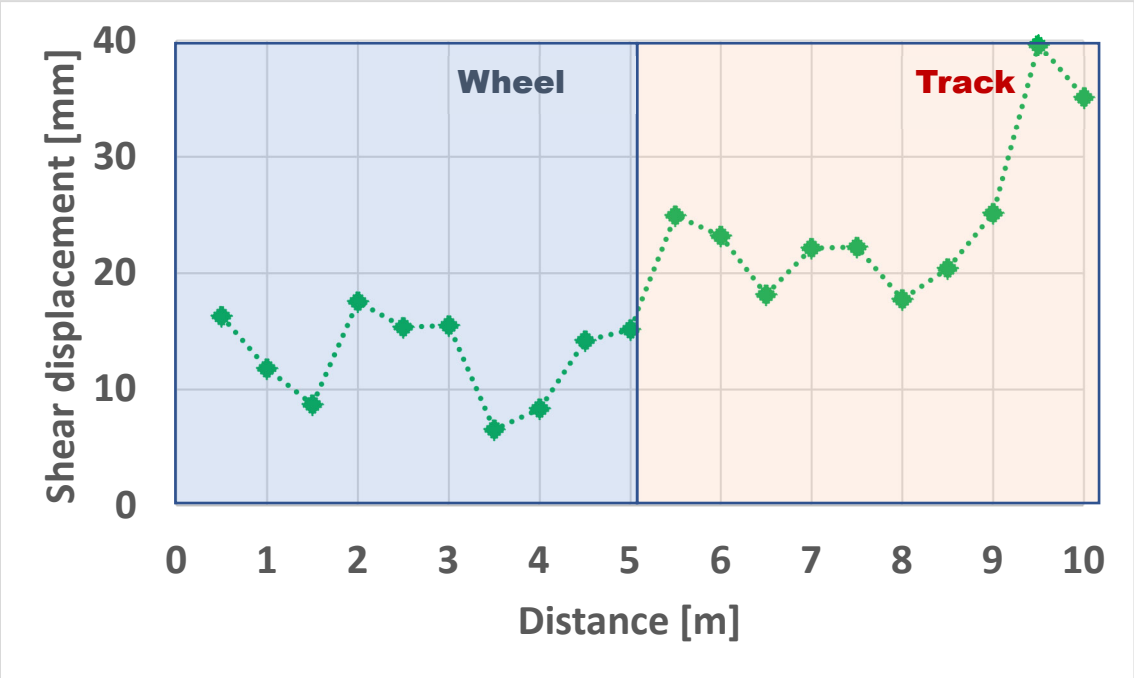

Figure 3-51 Shear displacement of lane 1 on wet soil (without payload)

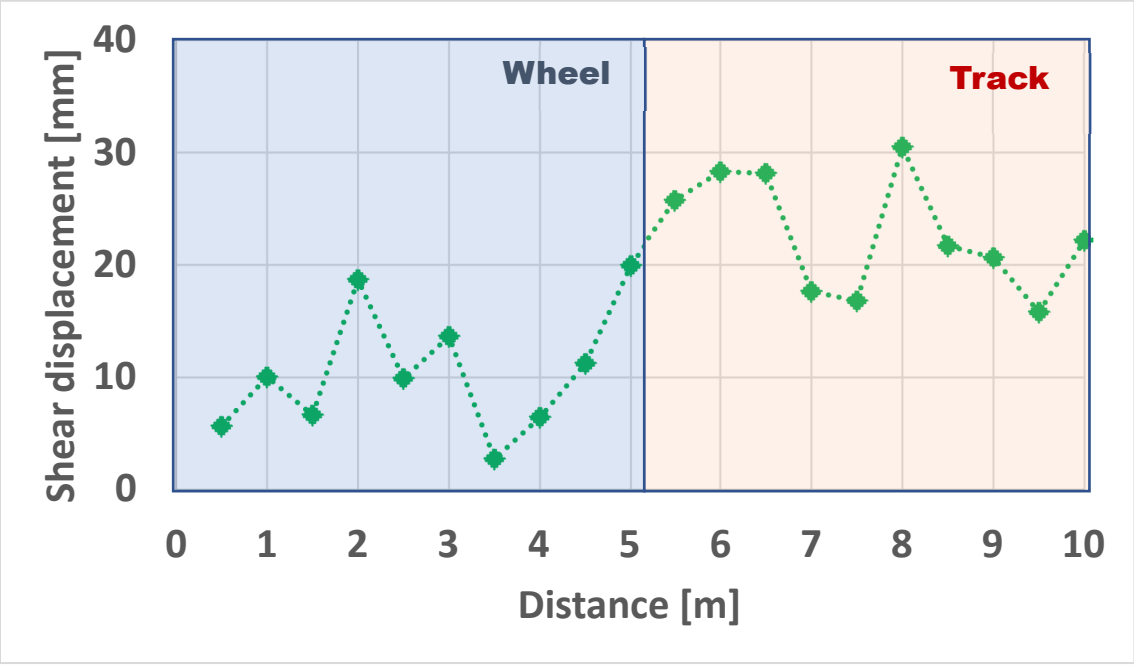

Figure 3-52 Shear displacement of lane 2 on wet soil (without payload)

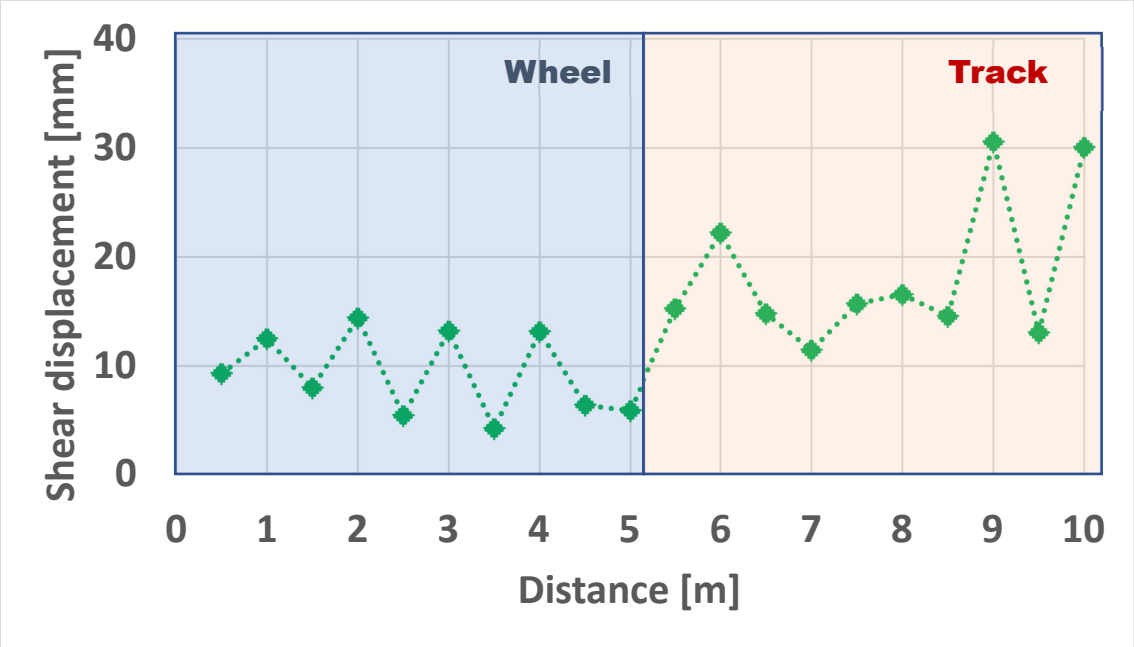

Figure 3-53 Shear displacement of lane 3 on wet soil (without payload)

Mode	**Chalk displacement** [mm]
Wheel	Average: 11 Standard deviation: 4.6
Track	Average: 22 Standard deviation: 6.7

Table 19 Summary results of shear displacement on wet soil (without payload)

For payload conditions on wet soil, the results of shear displacement of 3 lanes are shown in Figures 3–54, 3–55, and 3–56. The results of wheel mode are shown at a distance of 0–5 m, and the results of track mode are shown at a distance of 5.5–10 m. Table 20 shows a summary of the results of the shear displacement of three lanes on soft soil (payload). The average shear displacement of wheel mode and track mode is 10.5 mm and 21.3 mm, respectively.

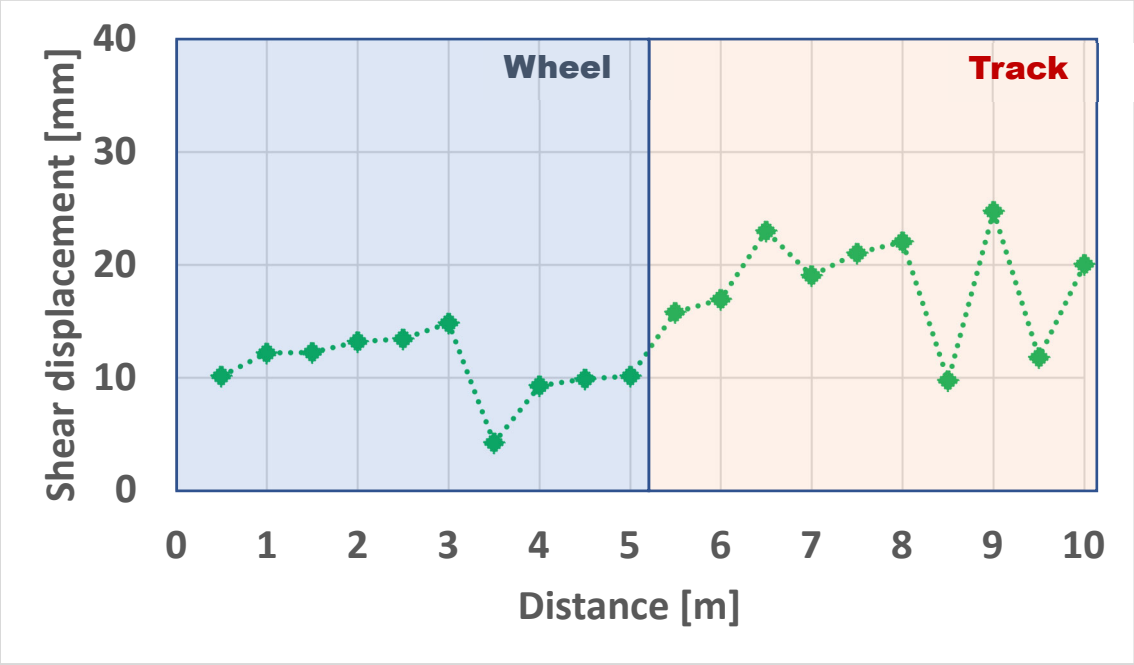

Figure 3-54 Shear displacement of lane 1 on wet soil (payload)

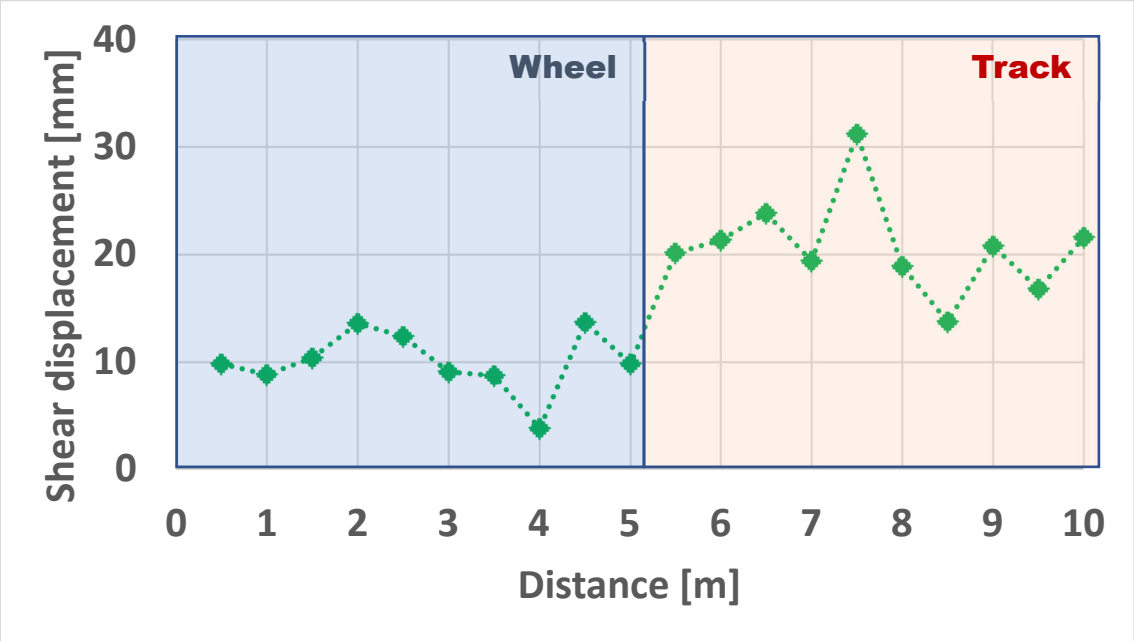

Figure 3-55 Shear displacement of lane 2 on wet soil (payload)

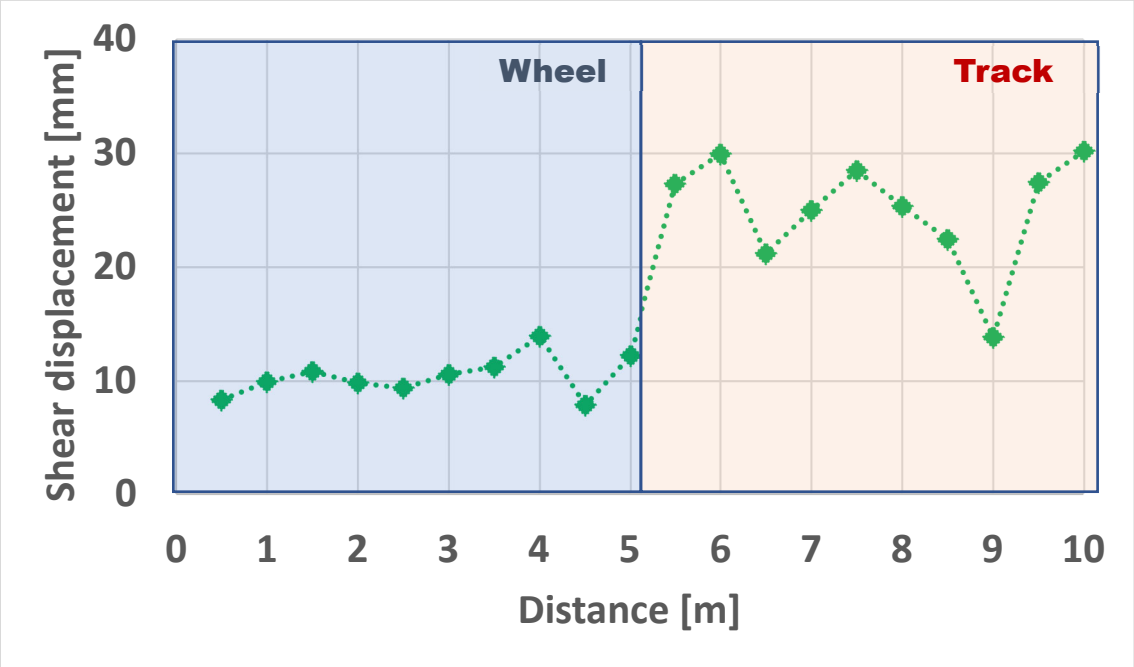

Figure 3-56 Shear displacement of lane 3 on wet soil (payload)

Mode	**Chalk displacement** [mm]
Wheel	Average: 10.5 Standard deviation: 2.5
Track	Average: 21.3 Standard deviation: 5.4

Table 20 Summary results of shear displacement on wet soil (payload)

Without payload conditions on soft wet soil, the results of the shear displacement of 3 lanes are shown in Figures 3–57. The results of wheel mode are shown at a distance of 0–5 m, and the results of track mode are shown at a distance of 5.5–10 m. Table 21 shows a summary of the results of the shear displacement of 3 lanes (without payload). The average shear displacement in wheel mode and track mode is 12 mm and 23 mm, respectively. Tracks cause higher shear displacement because they have a longer contact area.

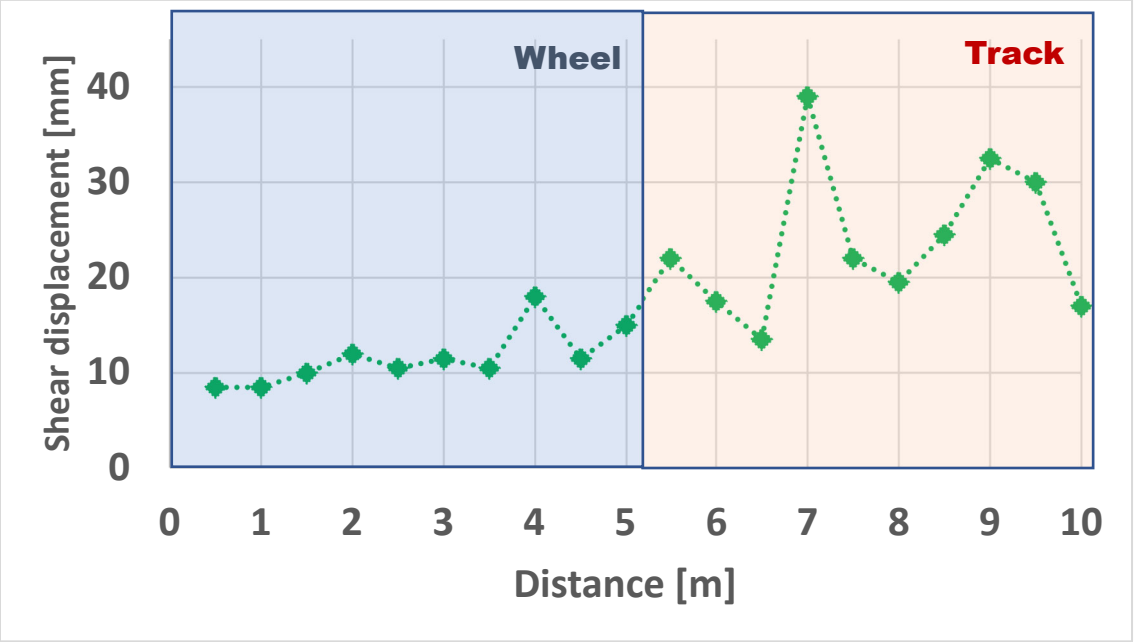

Figure 3-57 Shear displacement of 1 lane on soft wet soil (without payload)

Mode	Chalk displacement [mm]
Wheel	Average: 12 Standard deviation: 4.3
Track	Average: 23 Standard deviation: 10.1

Table 21 Summary results of shear displacement on soft wet soil (without payload)

3.3.3 Power

In the performance comparison based on the Bekker model [76], the wheel vehicle has higher rolling resistance because the wheel has greater sinkage than the track in soft soil conditions. On hard soil, track and wheel vehicles can cause similar sinkage. The relative equation of rolling resistance and sinkage [76] is described below.

$$R = b(k_c / b + k_\phi)\left[\frac{z^{n+1}}{n+1}\right] \tag{3.2}$$

where R is rolling resistance. b is the width, and l is the length of the running gear. k_Φ and k_c are the cohesive and frictional modulus of soil deformation, and n is the exponent of soil deformation. z is the sinkage. This equation explains that rolling resistance is high if sinkage is high. Wheels cause higher sinkage, which leads to higher rolling resistance. However, the wheel has high mobility on hard soil if compared with a track. In our previous research [1], we compared rolling resistance between the track and the wheel. The rolling resistance of the wheel and track are similar on firm soil because the sinkage is similar. Conversely, the rolling resistance of the wheel is higher than the track in soft soil and wet soil because the sinkage of the wheel is higher than the track. The rolling resistance is considered the power consumption of motors. We calculate power consumption using this equation.

$$P = \tau\omega \tag{3.3}$$

where P is power (W), τ is torque (N.m.), and ω is angular speed (rad/s). We can get data on torque and angular speed from the motor. We use the total power of four motors to estimate the power consumption of the robot.

Without payload conditions on firm soil, the results of the power of 3 lanes are shown in Figures 3-58, 3-59, and 3-60. Table 22 shows a summary of the results of the power of 3 lanes (without payload). The average power of the rear axle and front axle in wheel mode is 9 W and 68 W, respectively. The average power of the rear axle and front axle in track mode is 22 W and 53 W, respectively. The power of the front axle is higher than that of the rear axle because the front running gears are compacting the soil and making the conditions more favorable than the rear running gears, as described in Chapter 2.1.1. The total power of wheel mode and track mode is 77 W and 75 W, respectively.

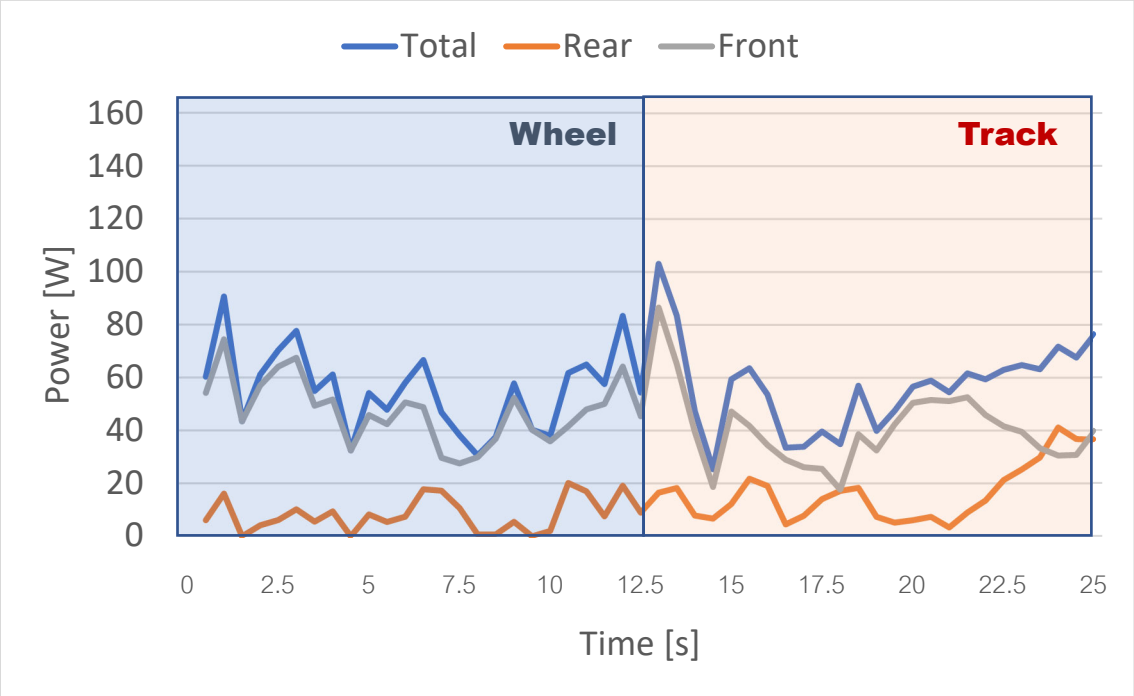

Figure 3-58 power of lane 1 on firm soil (without payload)

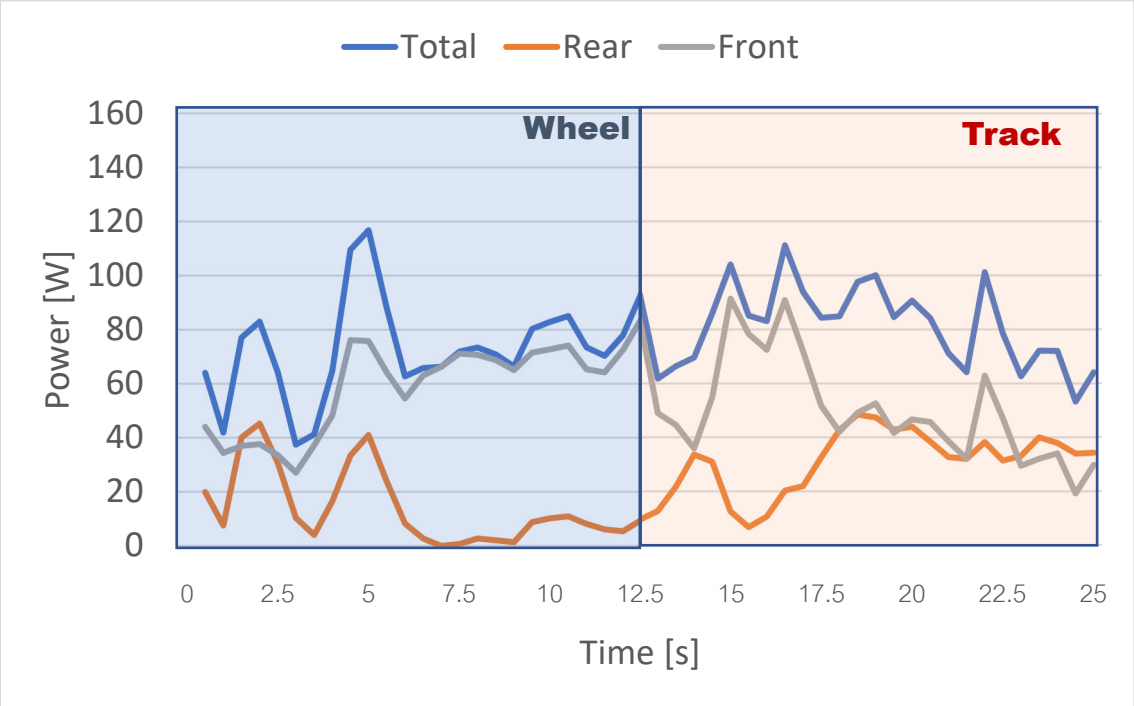

Figure 3-59 power of lane 2 on firm soil (without payload)

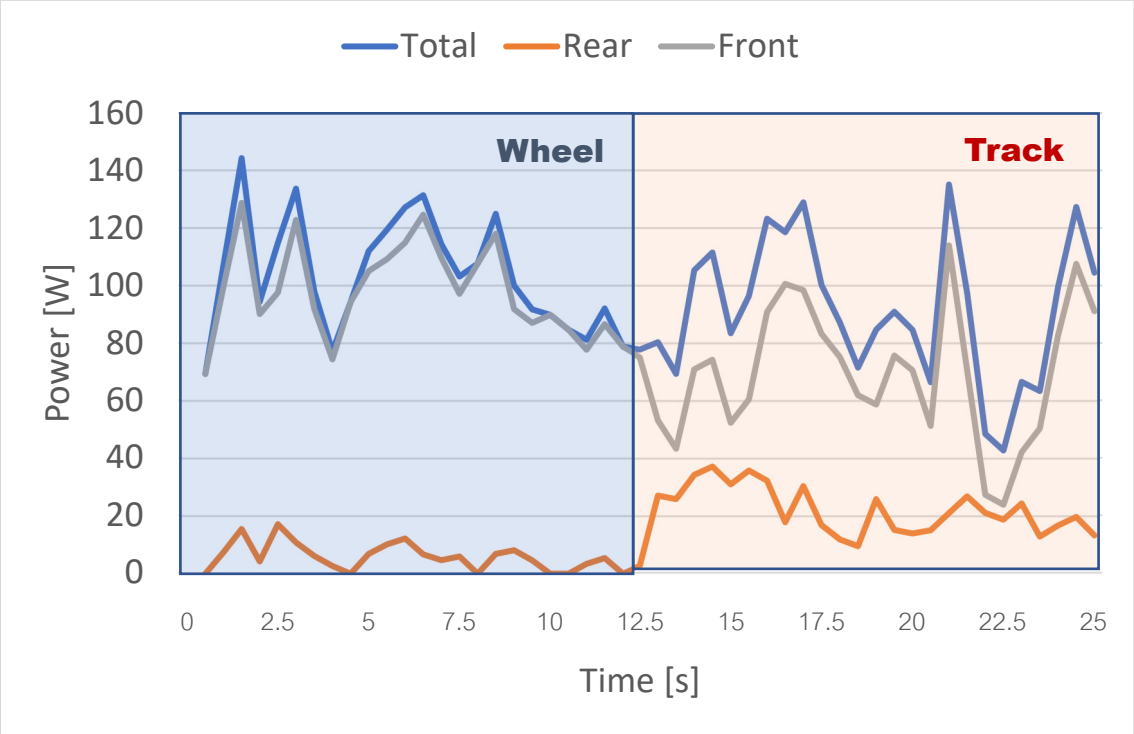

Figure 3-60 power of lane 3 on firm soil (without payload)

Mode	Rear (W)	Front (W)	Total (W)
Wheel	AVG: 9 STDev: 10	AVG: 68 STDev: 26	AVG:77 STDev:26
Track	AVG: 22 STDev:12	AVG: 53 STDev: 22	AVG:75 STDev:24

Table 22 Summary results of power on firm soil (without payload)

For payload conditions on firm soil, the results of the power of 3 lanes are shown in Figures 3-61, 3-62, and 3-63. Table 23 shows a summary of the results of the power of 3 lanes on firm soil (payload). The average power of the rear axle and front axle in wheel mode is 10 W and 95 W, respectively. The average power of the rear axle and front axle in track mode is 28 W and 77 W, respectively. The power of the front axle is higher than that of the rear axle because the front running gears are compacting the soil and making

the conditions more favorable than the rear running gears, as described in Chapter 2.1.1. The total power of wheel mode and track mode is 105 W and 105 W, respectively.

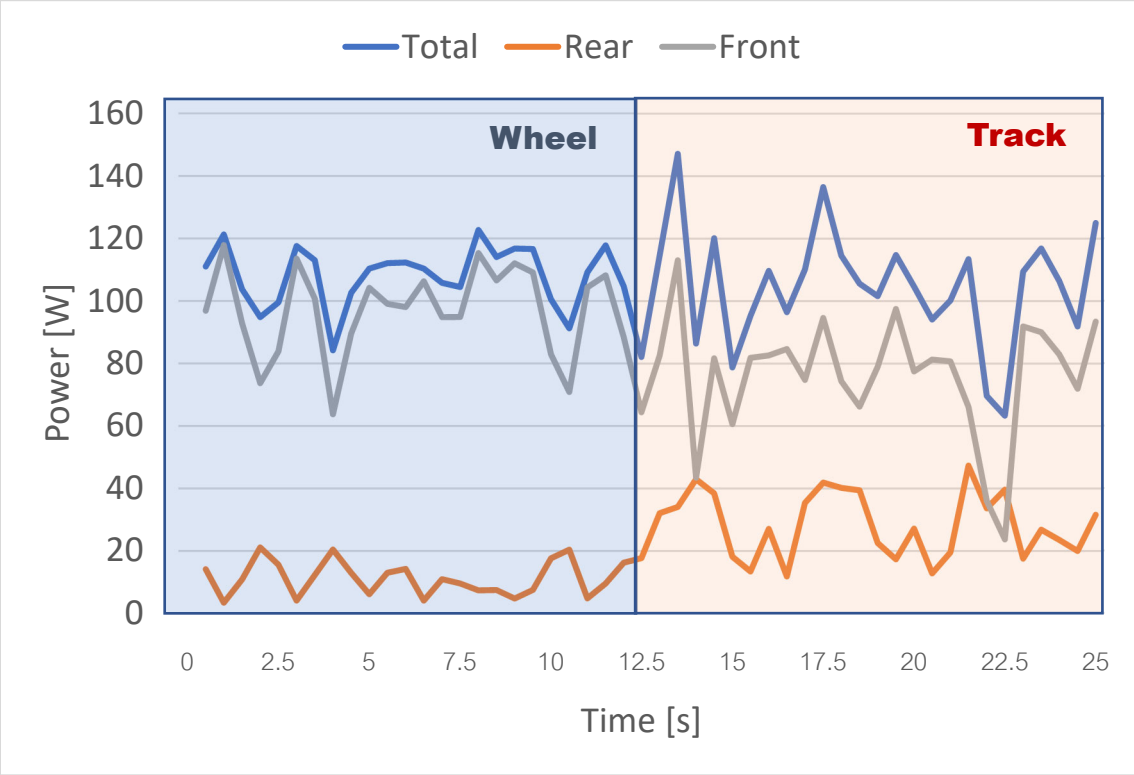

Figure 3-61 power of lane 1 on firm soil (payload)

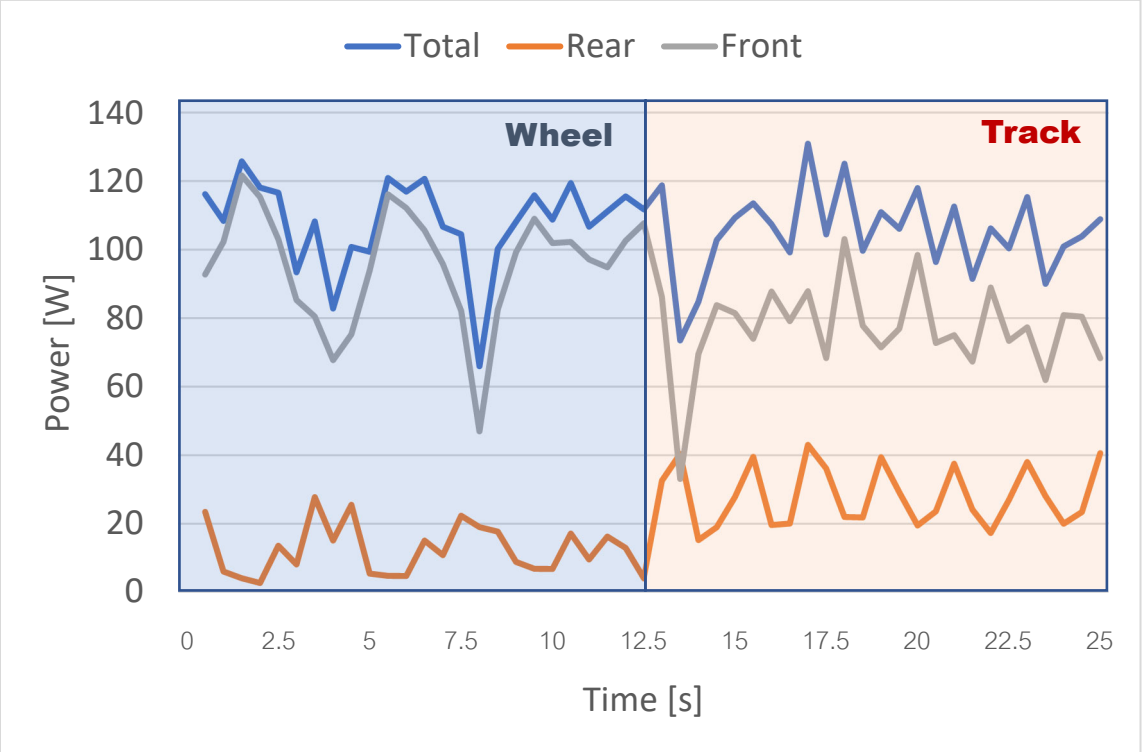

Figure 3-62 power of lane 2 on firm soil (payload)

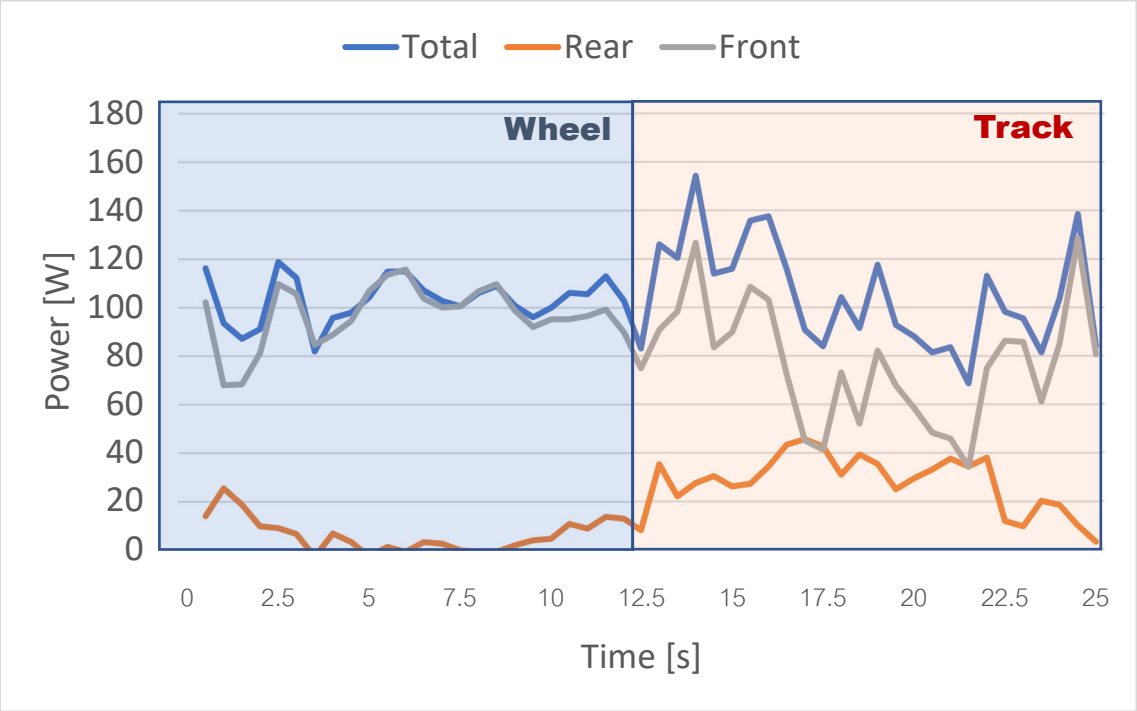

Figure 3-63 power of lane 3 on firm soil (payload)

Mode	Rear (W)	Front (W)	Total (W)
Wheel	AVG: 10 STDev: 7	AVG: 95 STDev: 15	AVG:105 STDev:11
Track	AVG: 28 STDev:10	AVG: 77 STDev: 20	AVG:105 STDev:18

Table 23 Summary results of power on firm soil (payload)

Without payload conditions, the results of the power of 3 lanes are shown in Figures 3-64, 3-65, and 3-66. Table 24 shows a summary of the results of the power of 3 lanes (without payload). The average power of the rear axle and front axle in wheel mode is 40 W and 108 W, respectively. The average power of the rear axle and front axle in track mode is 42 W and 69 W, respectively. The power of the front axle is higher than that of the rear axle because the front running gears are compacting the soil and making the conditions more favorable than the rear running gears, as described in Chapter 2.2.1. The total power of wheel mode and track mode is 148 W and 111 W, respectively.

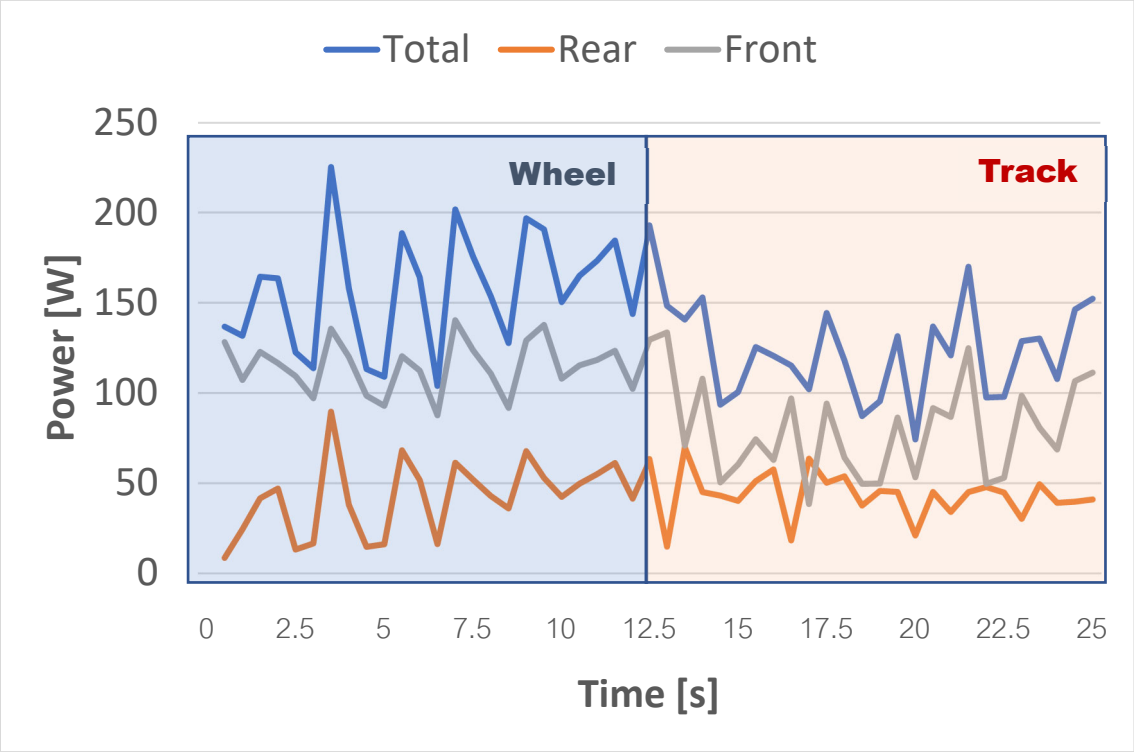

Figure 3-64 power of lane 1 on soft soil (without paylo

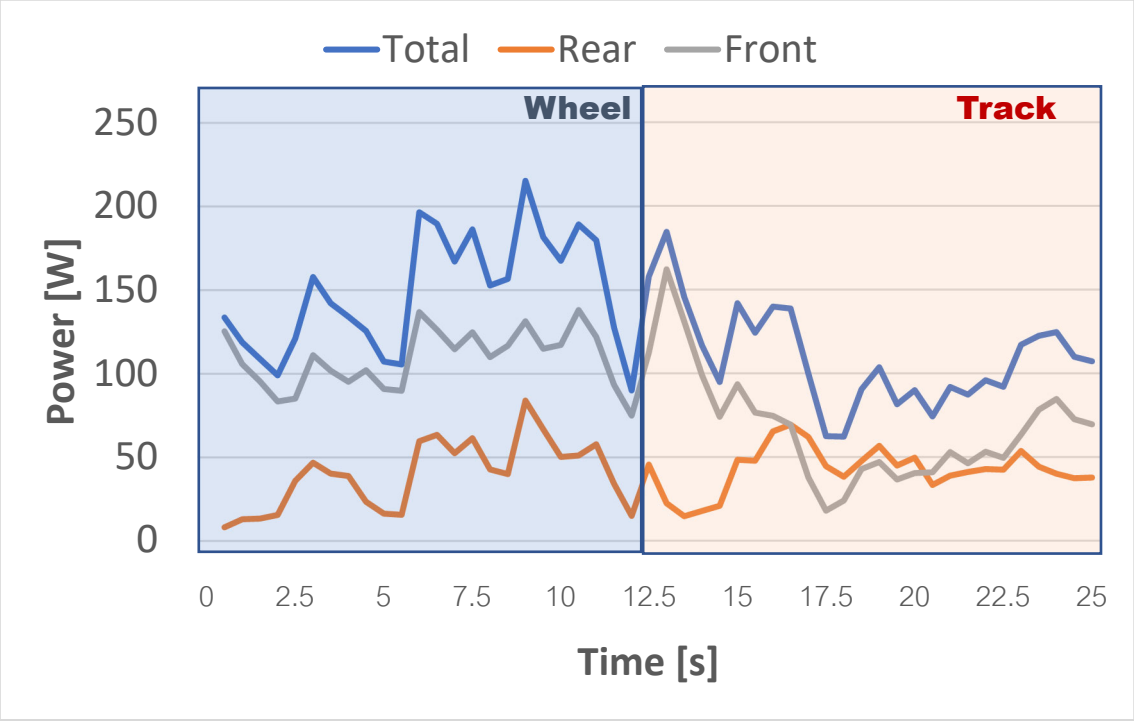

Figure 3-65 power of lane 2 on soft soil (without payload)

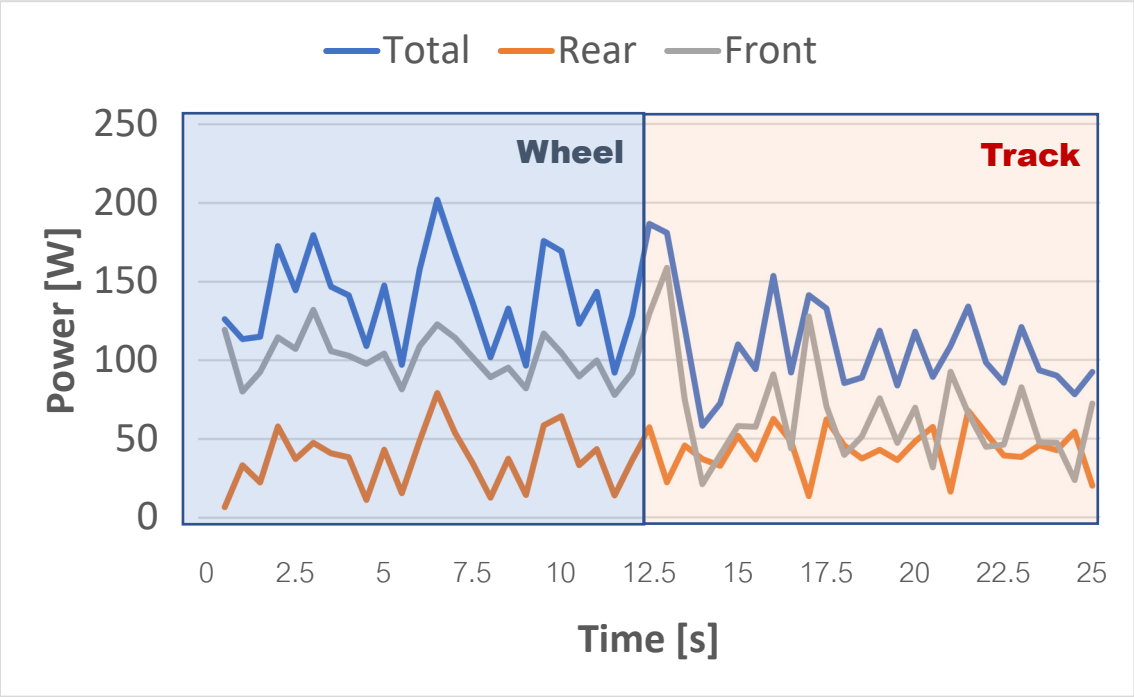

Figure 3-66 power of lane 3 on soft soil (without payload)

Mode	Rear (W)	Front (W)	Total (W)
Wheel	AVG: 40 STDev: 20	AVG: 108 STDev: 16	AVG:148 STDev:32
Track	AVG: 42 STDev:13	AVG: 69 STDev: 30	AVG:111 STDev:27

Table 24 Summary results of power on soft soil (without payload)

For payload conditions, the results of the power of 3 lanes are shown in Figures 3-67, 3-68, and 3-69. Table 25 shows a summary of the results of the power of 3 lanes (payload). The average power of the rear axle and front axle in wheel mode is 79 W and 180 W, respectively. The average power of the rear axle and front axle in track mode is 50 W and 116 W, respectively. The power of the front axle is higher than that of the rear axle because the front running gears are compacting the soil and making the conditions more

favorable than the rear running gears, as described in Chapter 2. 1.1. The total power of wheel mode and track mode is 259 W and 166 W, respectively.

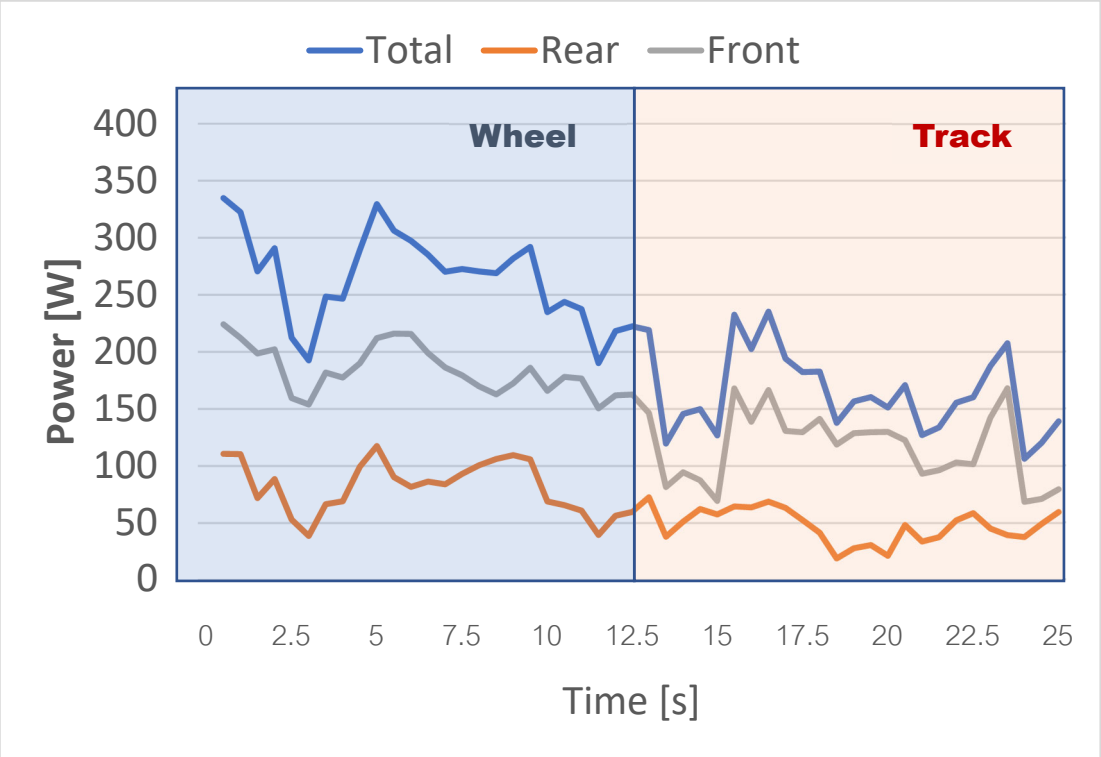

Figure 3-67 power of lane 1 on soft soil (payload)

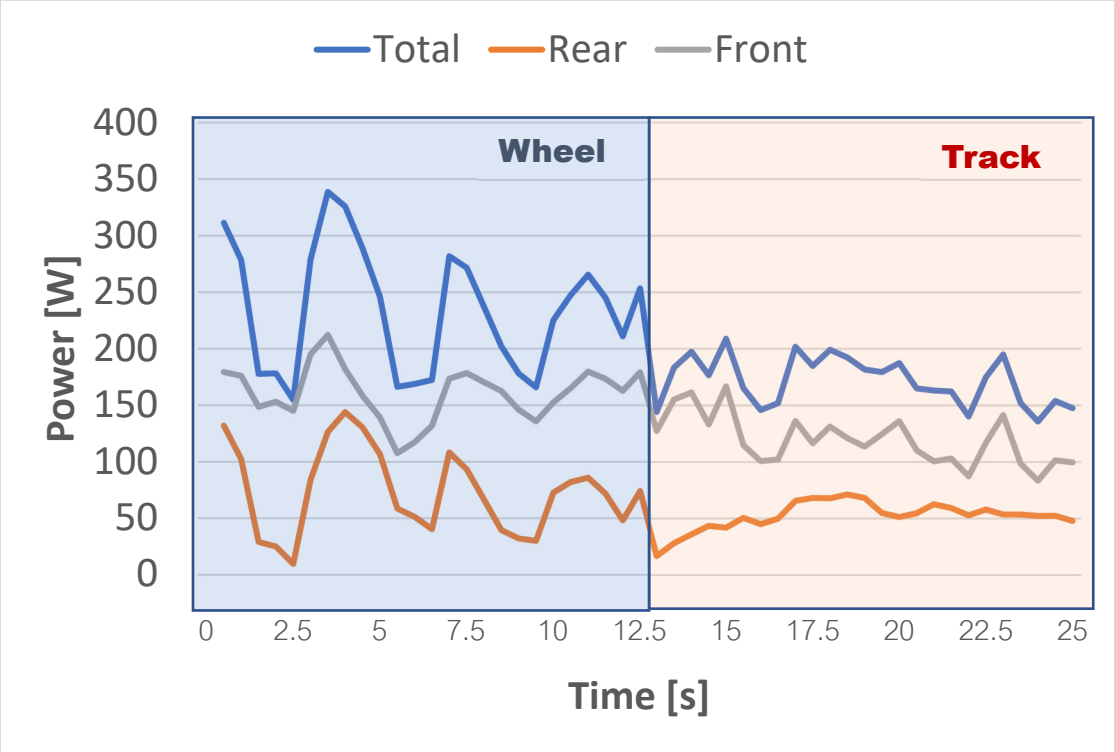

Figure 3-68 power of lane 2 on soft soil (payload)

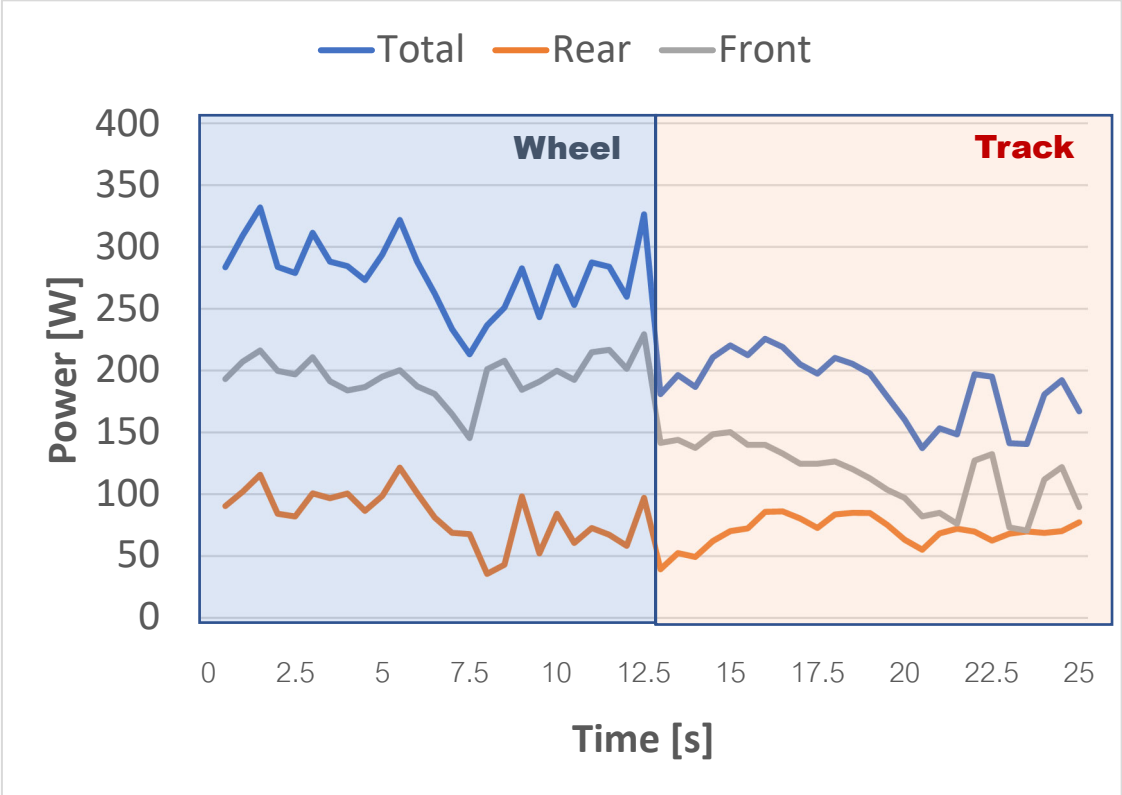

Figure 3-69 power of lane 3 on soft soil (payload)

Mode	Rear (W)	Front (W)	Total (W)
Wheel	AVG: 79 STDev: 28	AVG: 180 STDev: 25	AVG:259 STDev:46
Track	AVG: 50 STDev:15	AVG: 116 STDev: 30	AVG:166 STDev:35

Table 25 Summary results of power on soft soil (payload)

Without payload conditions, the results of the power of 3 lanes are shown in Figures 3-70, 3-71, and 3-72. Table 26 shows a summary of the results of the power of 3 lanes (without payload). The average power of the rear axle and front axle in wheel mode is 47 W and 88 W, respectively. The average power of the rear axle and front axle in track mode is 33 W and 75 W, respectively. The power of the front axle is higher than that of the rear axle because the front running gears are compacting the soil and making the conditions more favorable than the rear running gears, as described in Chapter 2. 1.1. The total power of wheel mode and track mode is 135 W and 108 W, respectively.

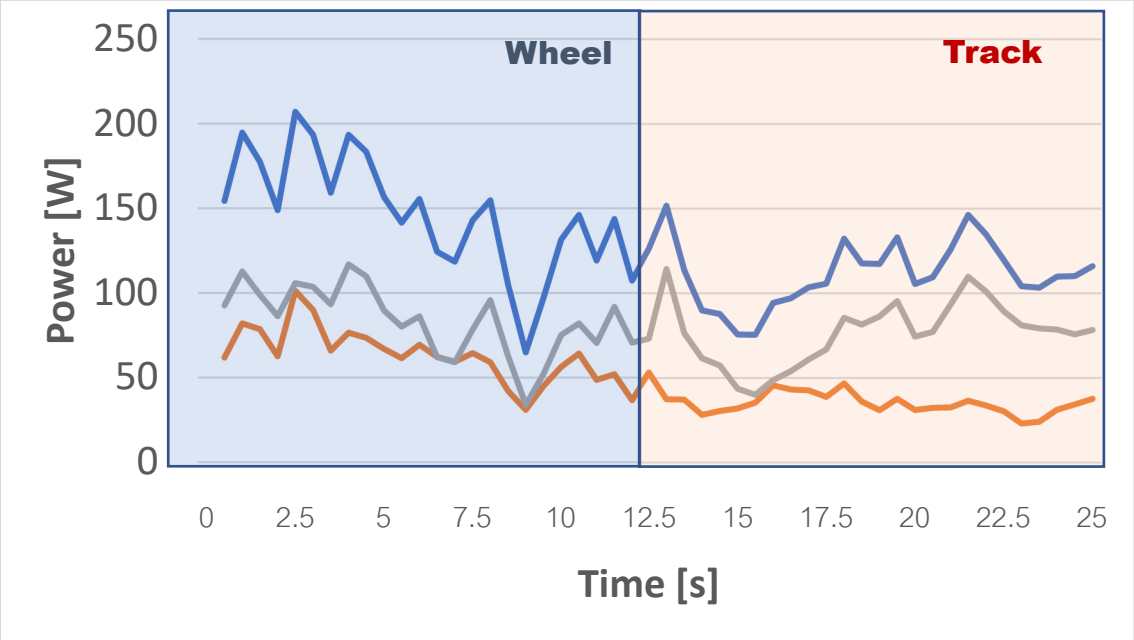

Figure 3-70 power of lane 1 on wet soil (without payload)

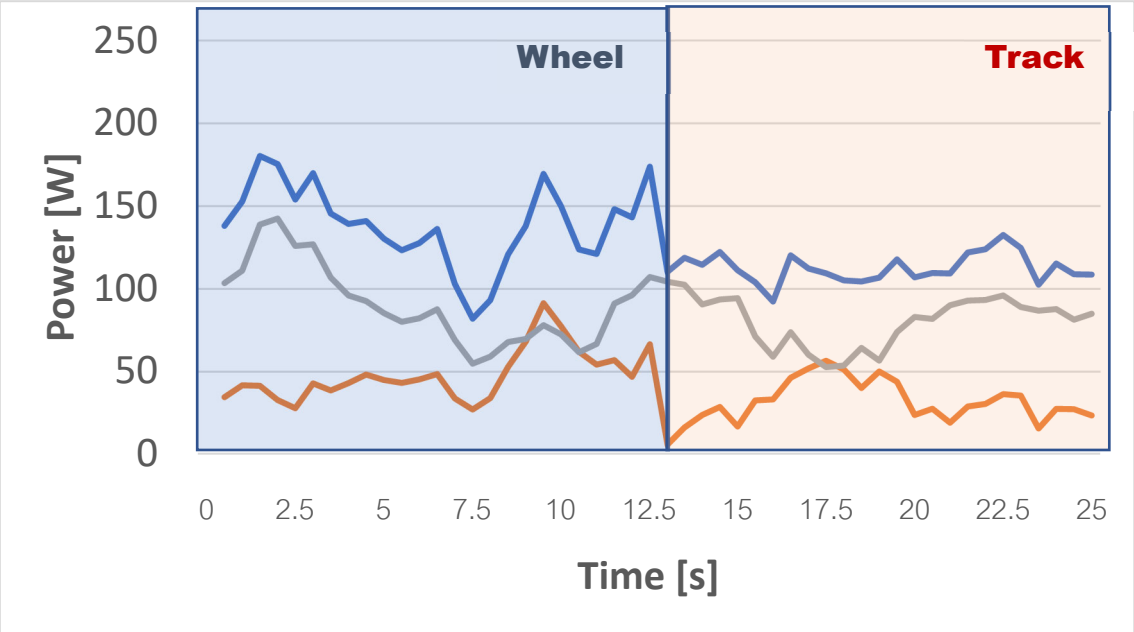

Figure 3-71 power of lane 2 on wet soil (without payload

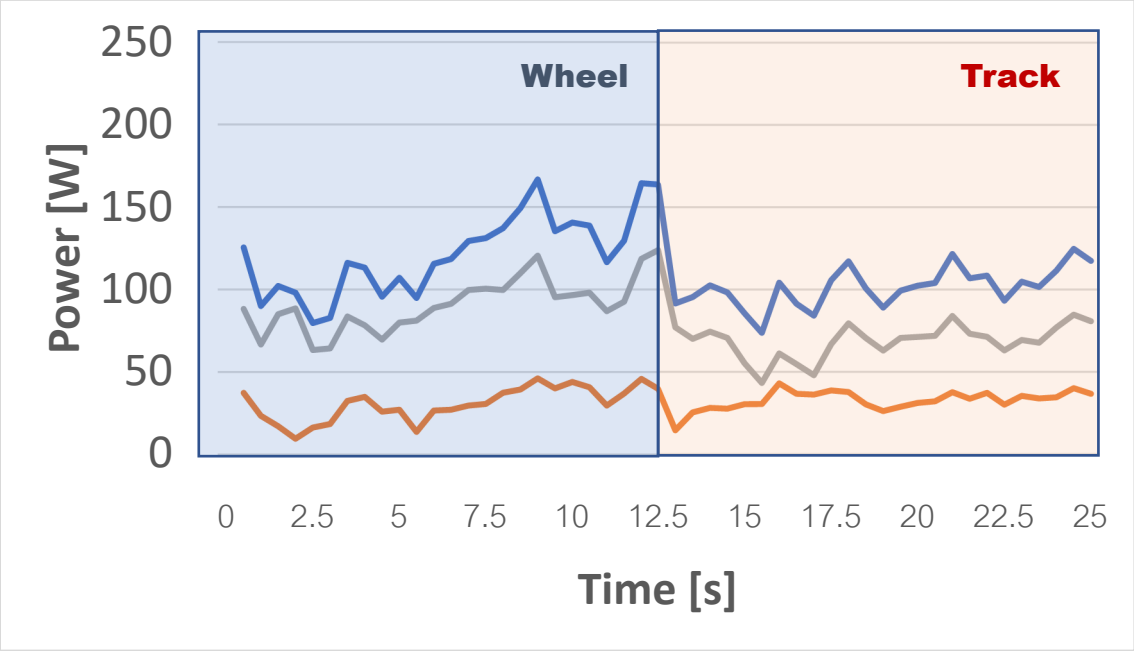

Figure 3-72 power of lane 3 on wet soil (without payload)

Mode	Rear (W)	Front (W)	Total (W)
Wheel	AVG: 47 STDev: 19	AVG: 88 STDev: 20	AVG:135 STDev:30
Track	AVG: 33 STDev:8	AVG: 75 STDev: 15	AVG:108 STDev:14

Table 26 Summary results of power on wet soil (without payload)

For payload conditions, the results of the power of 3 lanes are shown in Figures 3-73, 3-74, and 3-75. Table 27 shows a summary of the results of the power of 3 lanes (payload). The average power of the rear axle and front axle in wheel mode is 58 W and 124 W, respectively. The average power of the rear axle and front axle in track mode is 48 W and 97 W, respectively. The power of the front axle is higher than that of the rear axle because the front running gears are compacting the soil and making the conditions more favorable

than the rear running gears, as described in Chapter 2.1.1. The total power of wheel mode and track mode is 182 W and 145 W, respectively.

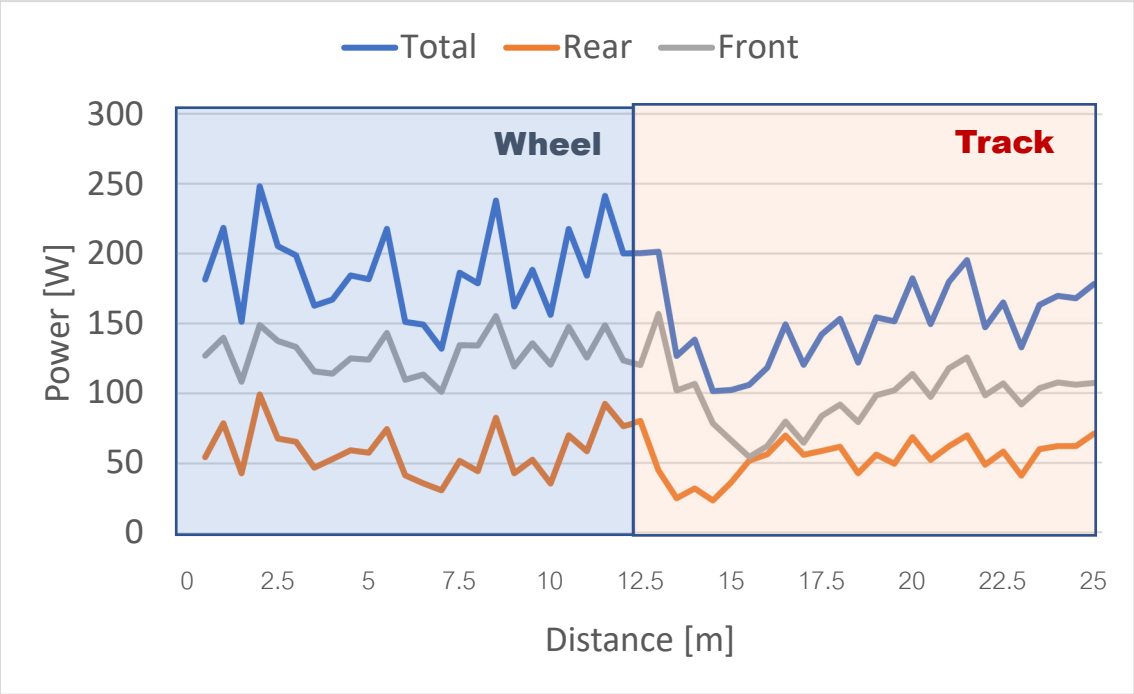

Figure 3-73 power of lane 1 on wet soil (payload)

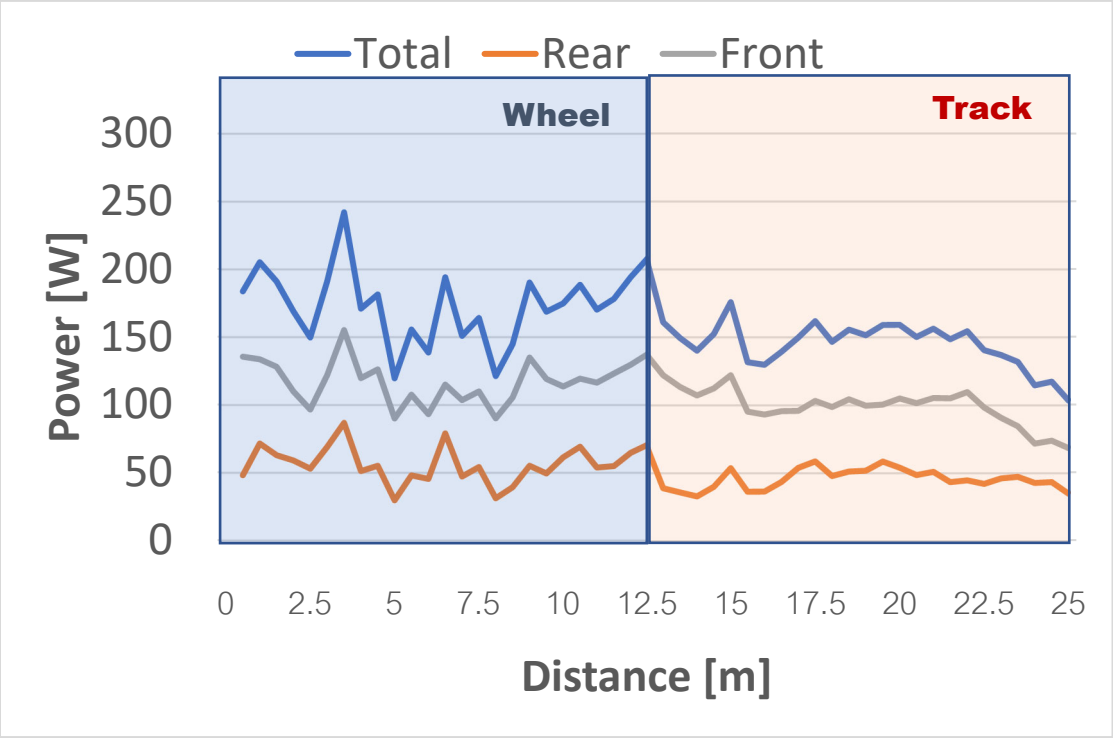

Figure 3-74 power of lane 2 on wet soil (payload)

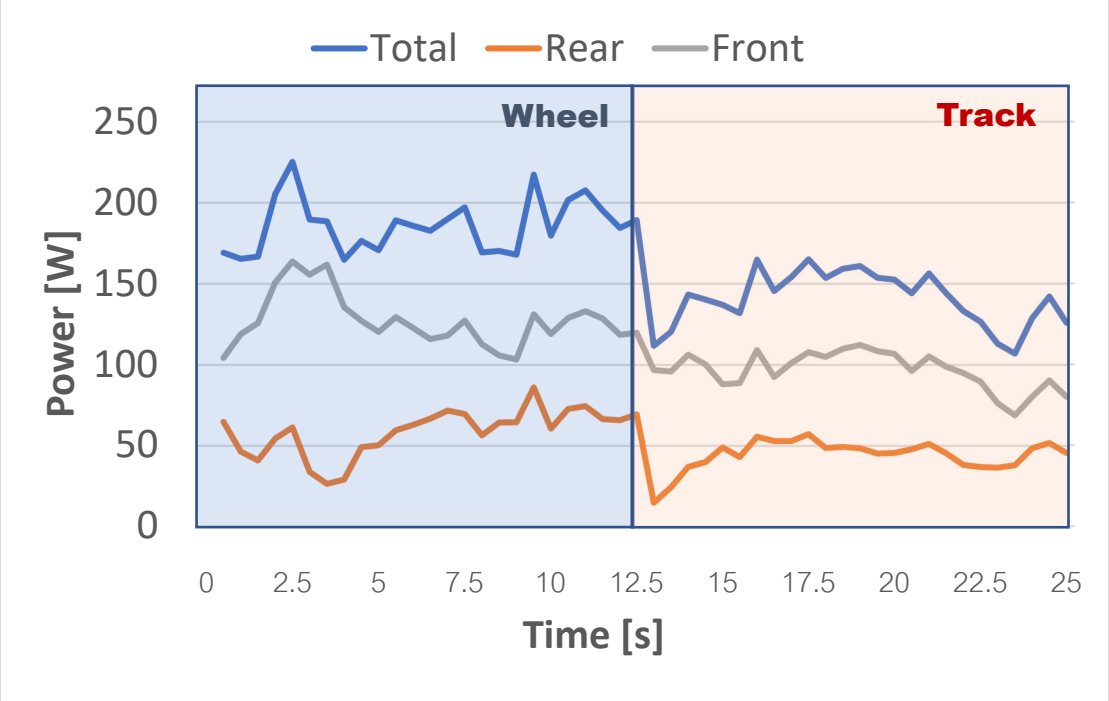

Figure 3-75 power of lane 3 on wet soil (payload)

Mode	Rear (W)	Front (W)	Total (W)
Wheel	AVG: 58 STDev: 15	AVG: 124 STDev: 16	AVG:182 STDev:26
Track	AVG: 48 STDev:11	AVG: 97 STDev: 16	AVG:145 STDev:21

Table 27 Summary results of power on wet soil (payload)

Without payload soft wet soil condition, the results of the power of soft wet soil condition are shown in Figures 3-76. Table 28 shows a summary of the power of 1 lane on soft wet soil condition. (without payload). The average power of the rear axle and front axle in wheel mode is 114 W and 160 W, respectively. The average power of the rear axle and front axle in track mode is 51 W and 141 W, respectively. The power of the front axle is higher than that of the rear axle because the front running gears are compacting the soil and making the conditions more favorable than the rear running gears, as described in Chapter 2.2.1. The total power of wheel mode and track mode is 274 W and 192 W, respectively.

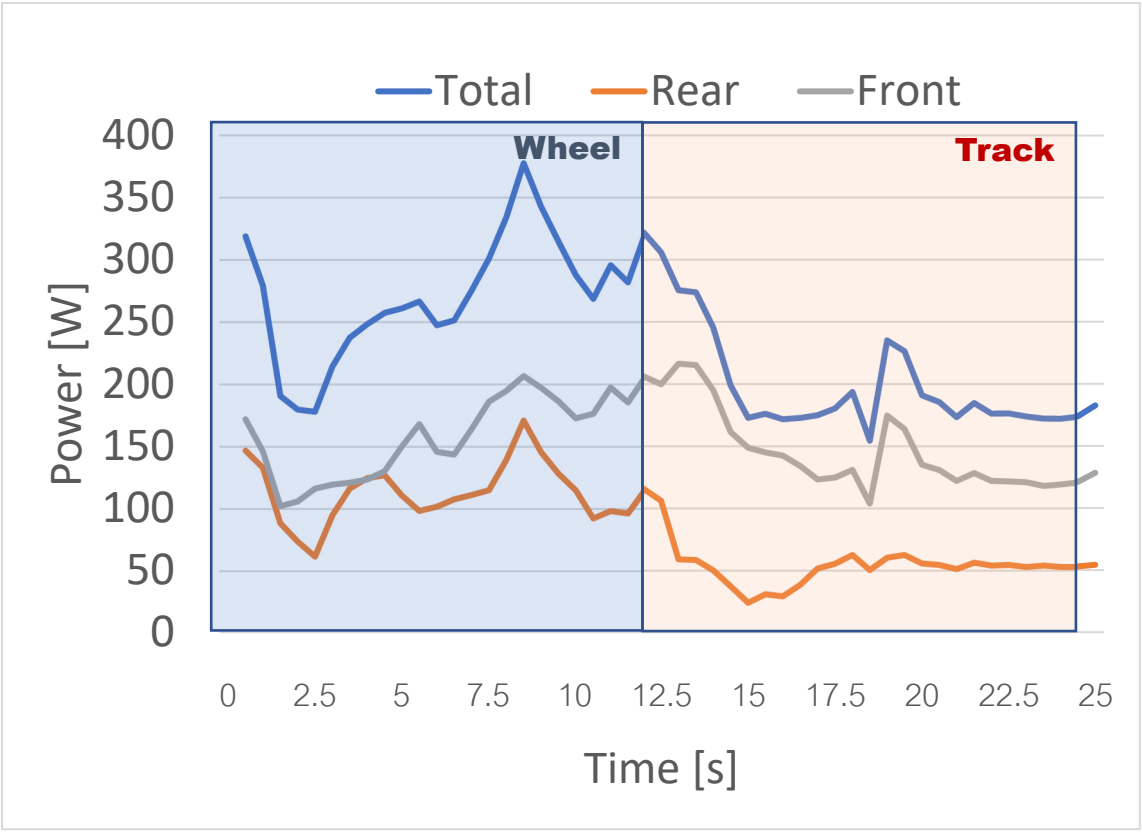

Figure 3-76 power on soft wet soil of 1 lane (without payload)

Mode	Rear (W)	Front (W)	Total (W)
Wheel	AVG: 114 STDev: 23	AVG: 160 STDev: 33	AVG:274 STDev:50
Track	AVG: 51 STDev:10	AVG: 141 STDev: 30	AVG:192 STDev:32

Table 28 Summary results of power on soft wet soil (without payload)

3.3.4 Slip

In our preliminary tests, the vehicle moves on straight lanes, and the slip of running gear is evaluated using a laser distance sensor (LDS). The laser distance sensor is located

at the end of the lane, and the sensor points to a flat black panel that is mounted on the front of Hadrian, as shown in Figure 3-77. We measure the position of the vehicle, and we can estimate the velocity of movement using a laser distance sensor (LDS). Then, we can evaluate slip *i* as below:

$$i = \frac{\omega r - V}{\omega r} \tag{3.4}$$

where ω is the angular speed of the motor, r is the radius of the running gear, and V is the estimated vehicle moving velocity.

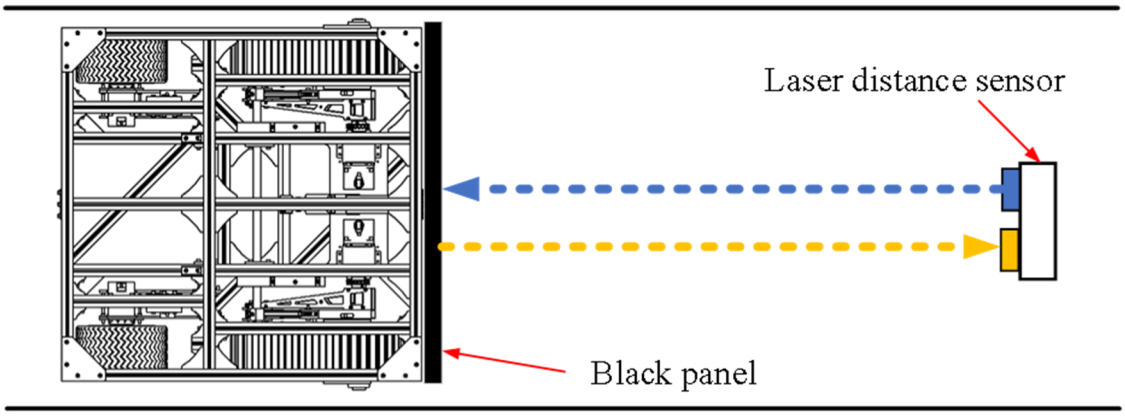

Figure 3-77 Velocity measurement using laser distance sensor

3.3.5 Soil moisture

The soil moisture sensor that is used in this research is the Analog Waterproof Capacitive Soil Moisture Sensor (SEN0308 DFRobot), as we described in Chapter 2. Soil moisture is the water content of the soil, and it can be expressed in terms of volume. Soil moisture in wet soil is higher if compared with firm and soft soil because it has more water. The soil moisture measurement is shown in Figure 3–78.

Figure 3-78 Soil moisture measurement

The average soil moisture of firm soil, soft soil, wet soil and soft wet soil are 20%, 35%, 70% and 73% respectively.

3.4. Discussion

Tables 29 and 30 show summaries of results for three soil conditions: without payload and with payload, respectively. The power consumption of the payload condition is higher than without the payload condition because of the weight, as described in Eq. (1.4). The wheel/track reconfigurable vehicle is designed to switch modes based on the soil conditions to minimize 1) soil compaction, 2) soil distortion, and 3) power consumption. For soil compaction, the difference between CI before and robot pass of wheel mode is higher than track mode in soft and wet soil. Wheel mode cause higher soil compaction. So, track mode is better to reduce soil compaction on soft soil and wet soil. For soil distortion, track mode causes higher shear displacement in three soil conditions because

track has a longer contact area. Shear displacement is related to slip. Shear displacement on firm soil and wet soil is higher because it has a higher slip. The slip of soft soil is low because it has a higher grip. The difference in shear displacement between wheel mode and track mode is considered to determine which mode is better for each soil condition. On firm soil, the difference in shear displacement between wheel mode and track mode is 13 (without payload and payload conditions). On soft soil, the difference in shear displacement between wheel mode and track mode is 8.2 (without payload) and 9.5 (with payload). On wet soil, the difference in shear displacement between wheel mode and track mode is 11 (without payload) and 10.8 (with payload). The difference in shear displacement between wheel mode and track mode on firm soil is the highest. The power consumption of wheel mode and track mode is similar on firm soil. On soft soil and wet soil, the power consumption of wheel mode is higher because wheel mode causes higher sinkage. For power consumption, power is an indirect measure of the rolling resistance, sinkage, and soil compaction on dry soil. The power of wheel mode and track mode are similar because the power consumption depends on rubber deformation, internal friction of the robot and the elastic deformation of the soil, it does not depend on the sinkage. On soft soil, the power consumption of wheel mode is higher because sinkage is higher. On we saturated soil, power is still function of sinkage. there is no compaction, only distortion is considered. In case of saturated soil, the soil damage is almost unavoidable, so we can expect to use tracks and restrict the soil damage by avoiding the sinkage as much as possible. but only soil distortion is considered. The soil damage of wet saturated soil, the power is also a function of the payload.

After the results are obtained, we can consider which locomotion mode is better for each soil condition. On firm soil, wheel mode is preferable because wheel mode causes lower soil distortion if compared with track mode (the difference in shear displacement is 13 mm, which is the highest). Also, the power consumption of wheel and track modes is similar on firm soil. On soft soil and wet soil, track mode is preferable because track mode uses less power compared with wheel mode. After we decide which mode is better for each soil condition, we will design the control strategy to switch modes autonomously using the cost function.

Soil Types	**Mode**	**Sinkage [mm]**	**Power [W]**	**Slip rear [%]**	**Slip front [%]**	**Moisture [%]**	**CI before [kPa]**	**CI after [kPa]**	**Shear displace-ment [mm]**
Firm	Wheel	3.7	77	11.4	12.3	20	970	980	7.5
	Track	2.7	75	11.5	10.8		954	961	20.5
Soft	Wheel	27	148	10.9	11.3	35	269	361	6.7
	Track	21	111	10.7	9.9		251	300	14.9
Firm	Wheel	22	135	13.2	14.1	70	310	414	11
Wet	Track	18	108	13.3	12.2		303	376	22
Soft	Wheel	66	274	15.1	16.3	73	70	164	12
Wet	Track	54	192	14	13.3		83	131	23

Table 29 Summary results on three soil condition (without payload)

Soil Types	Mode	Sinkage [mm]	Power [W]	Slip rear [%]	Slip front [%]	Moisture [%]	CI before [kPa]	CI after [kPa]	Shear displace-ment [mm]
Firm	Wheel	5	105	11.4	12.3	20	960	989	7
	Track	4.8	105	11.1	10.5		1057	1084	20
Soft	Wheel	49	259	10.4	11.3	35	186	376	3.6
	Track	40	166	10.2	9.7		165	320	13.1
Wet	Wheel	29	182	13.1	14.1	70	348	526	10.5
	Track	23	145	13.4	12.7		330	484	21.3

Table 30 Summary results on three soil condition (payload)

The relation between shear displacement and slip is expressed in Figure 3-79. If slip is high, the shear displacement is high as described in Eq.(1.2). Shear displacement is related to contact length. The contact length of track and wheel are 160 and 65 mm respectively. The contact length of track mode is higher than wheel mode, so track cause higher slip.

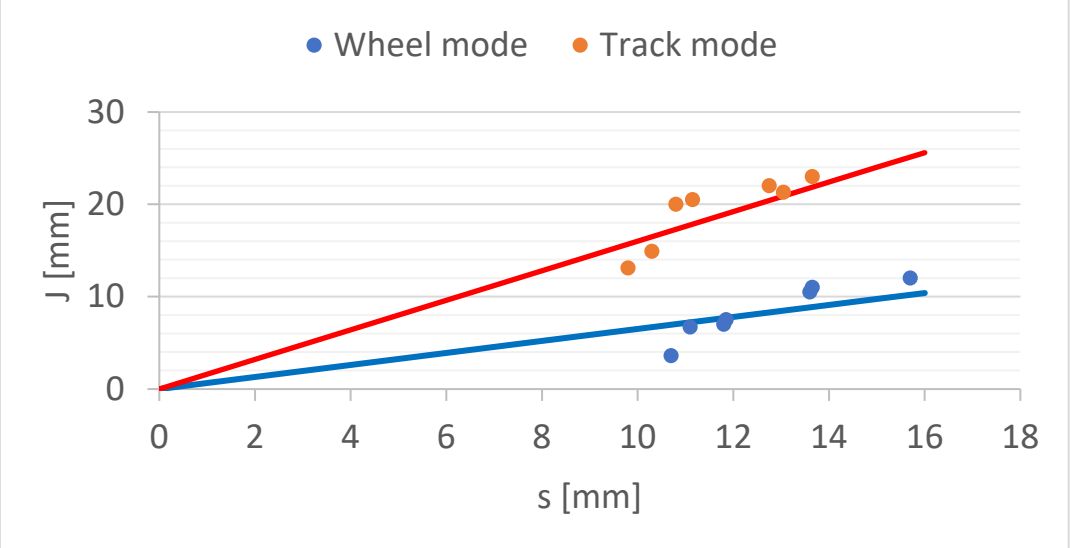

Figure 3-79 Relation between shear displacement and slip

The relation between power and sinkage is expressed in Figure 3-80. If sinkage is high, the power is high as described in Eq.(1.3).

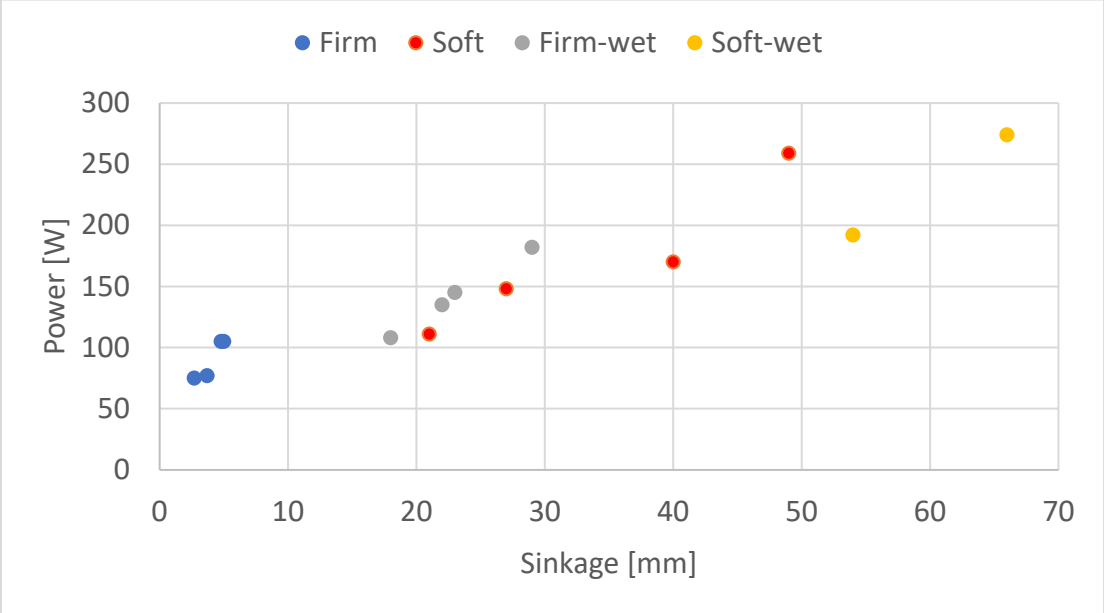

Figure 3-80 Relation between power and sinkage

The relation between cone index (CI) and power is expressed in Figure 3-81. If cone index is low power is high. The relation equation of CI and power [78] is defined as below.

$$P = \frac{k_1}{CI} + k_2 \tag{3.5}$$

where P is power. CI is Cone Index and k_1 and k_2 is constant value. The k_1 and k_2 can be obtained by using MATLAB after we input the data that we obtained from experiment.

Wheel mode (CI before): $$P = \frac{2.9\times10^4}{C_I} + 8.6\times10^1 \tag{3.6}$$

Wheel mode (CI after): $$P = \frac{8.7\times10^4}{C_I} + 1.0\times10^1 \tag{3.7}$$

Track mode (CI before): $$P = \frac{9.3\times10^3}{C_I} + 1.0\times10^2 \tag{3.8}$$

Track mode (CI after): $$P = \frac{2.6\times10^{4}}{C_I} + 7.5\times10^{1} \quad (3.9)$$

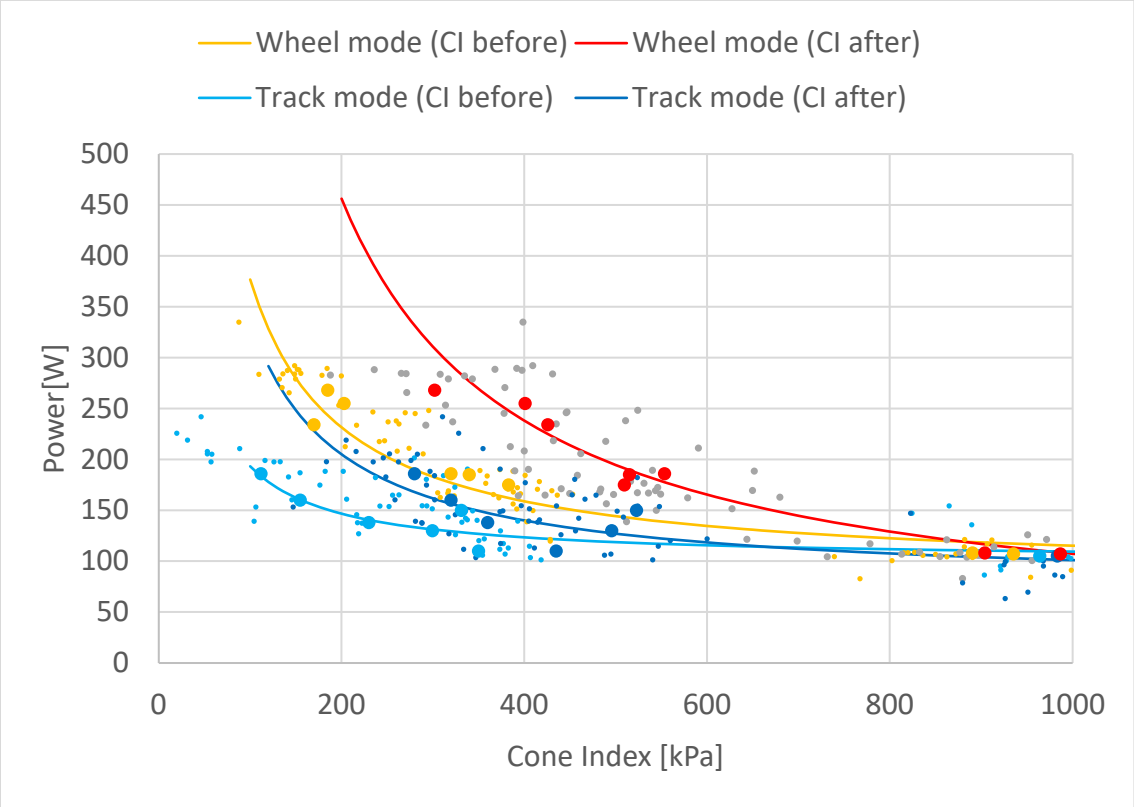

Figure 3-81 Relation between power and cone index

Chapter 4
Locomotion Switching

Chapter 4. Locomotion Switching

4.1. Algorithm of Locomotion Switching

After the results of firm, soft, and wet soil are obtained, we will implement an autonomous switching mode using cost function. This robot is built to minimize power and soil damage. On firm soil, track mode causes higher soil distortion, but the power consumption is similar to wheeled mode, so wheel mode is preferable. On soft soil and wet soil, wheel mode causes higher power consumption, so tracked mode is preferable.

Since wheel mode and track mode use different power on soft soil and wet soil, the sensor to define the current mode is very important. Two limit switches are located in the robot to define the current mode (wheel or track), as shown in Figure 4-1. If the limit switch (A) contacts the shaft when the electro-hydraulic actuator (EHA) extends the length, the current mode is wheel mode. On the other hand, if the limit switch (B) contacts the shaft when EHA shortens the length, the current mode is track mode.

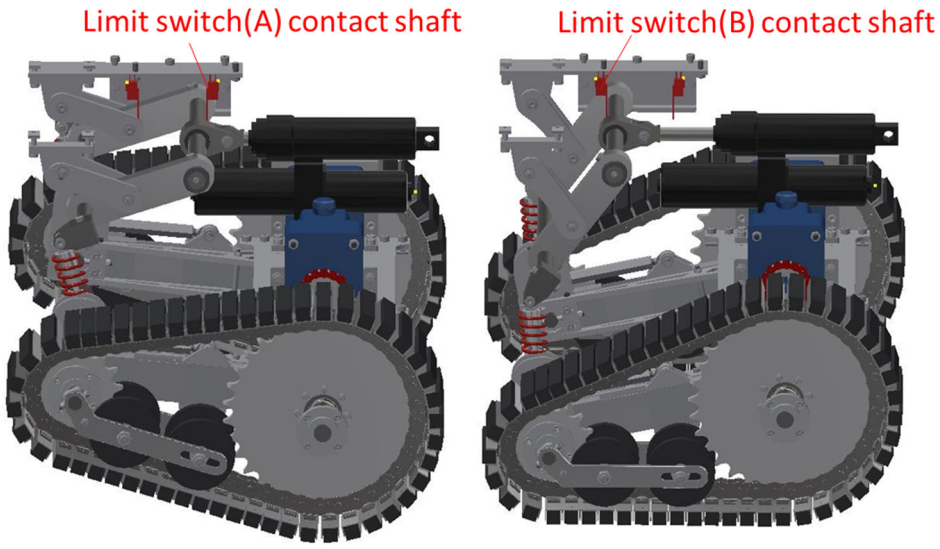

Figure 4-1 Limit switch wheel mode (left) track mode (right)

We use information from Figure 3-81 to find the relationship between power and cone index. Figure 4-2 shows the relation between power and cone index (CI) before and after a robot pass. The CI from 0–500 kPa is soft soil, and the CI from 500–1000 kPa is firm soil. For example, the current mode of the robot is wheel mode. P_{wheel} is the power of robot in wheel mode that can be measured from sensor. At power P_{wheel} = 260 W of wheel mode, we can calculate CI using Eq. (3.6). The CI of P_{wheel} = 260 W is 166 kPa. We can estimate the power of track mode using the same cone index as Eq. (3.8). In figure, if the power of wheel mode is 260 W, CI_{before} = 166 kPa. The power of track mode is 156 W. $\Delta P_{estimate} = P_{wheel}\ (CI_{before}) - P_{track}\ (CI_{before}) =$ 260 - 156 = 104 W. $\Delta P_{estimate}$ is used to switch modes. If the robot changes from wheel mode to track mode, it can reduce power and soil compaction.

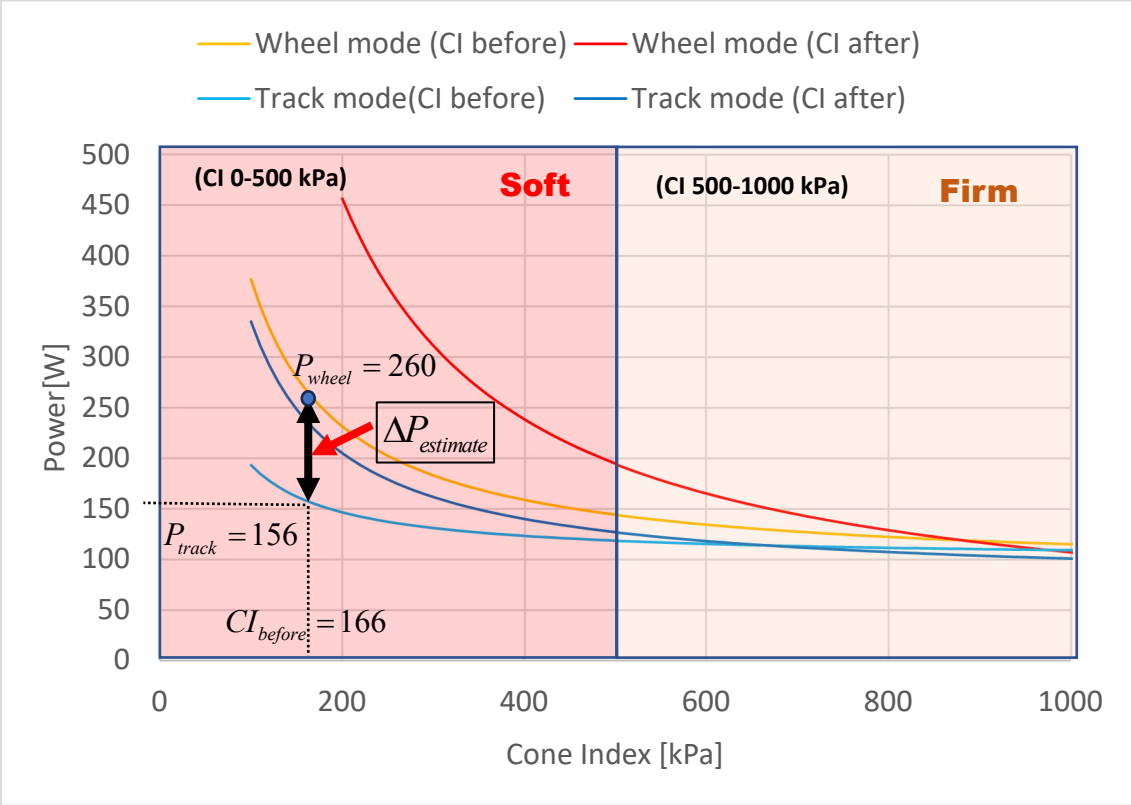

Figure 4-2 Power estimation between wheel mode and track mode.

The moving average is used to avoid variation in input data. Figures 4-3 and 4-4 show the results of power, moving average, average, and standard deviation of wheel mode and track mode on firm soil. Figures 4-5 and 4-6 show the results of power, moving average, average, and standard deviation of wheel mode and track mode on soft soil. We try to increase the number of data points for moving averages step by step. At number of data = 7, the moving average data is inside the standard deviation. So, we select a number of data points of 7 for the moving average in our experiment. A moving average of 7 data points (3.5 second) can reduce the amount of variation.

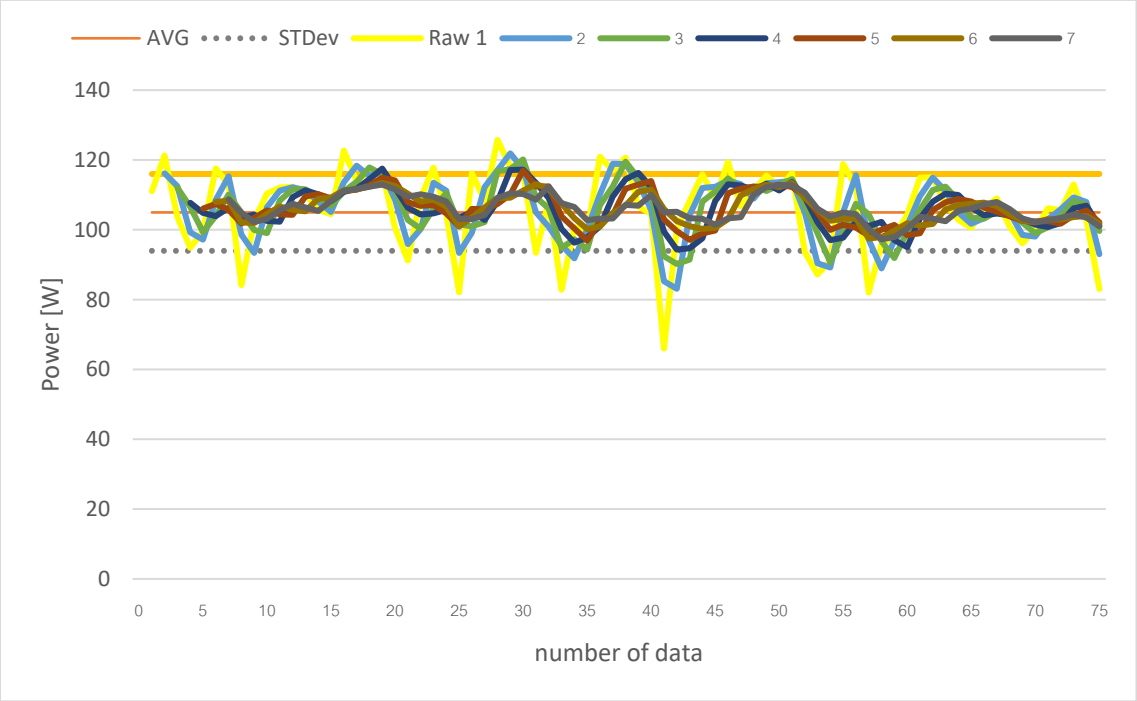

Figure 4-3 Moving average of wheel mode on firm soil

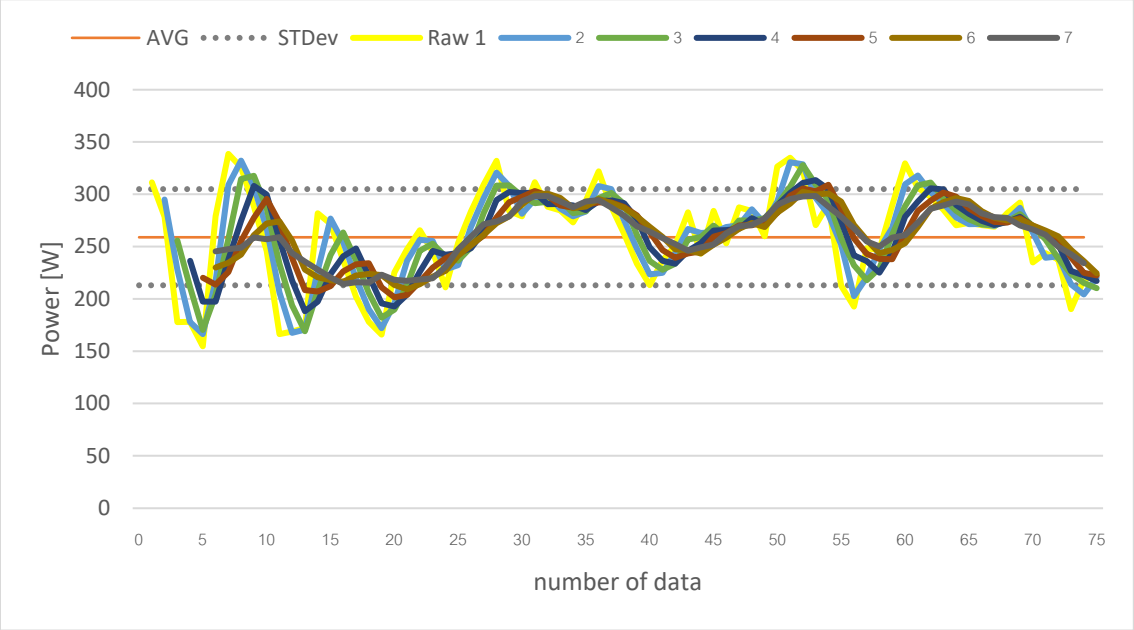

Figure 4-4 Moving average of track mode on firm soil

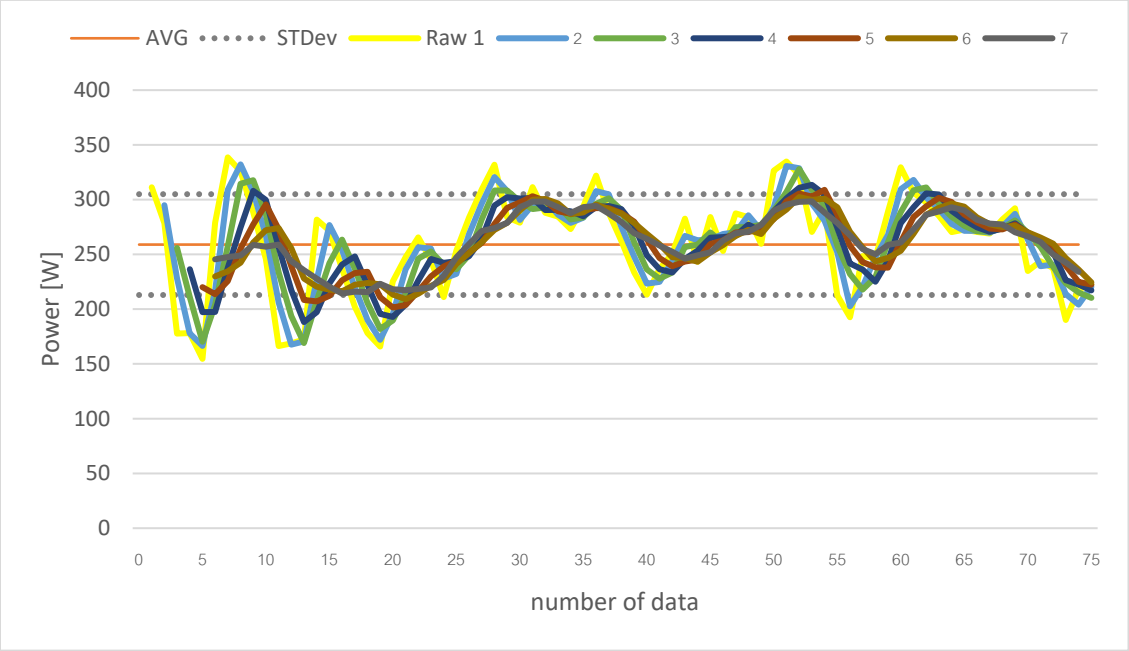

Figure 4-5 Moving average of wheel mode on soft soil.

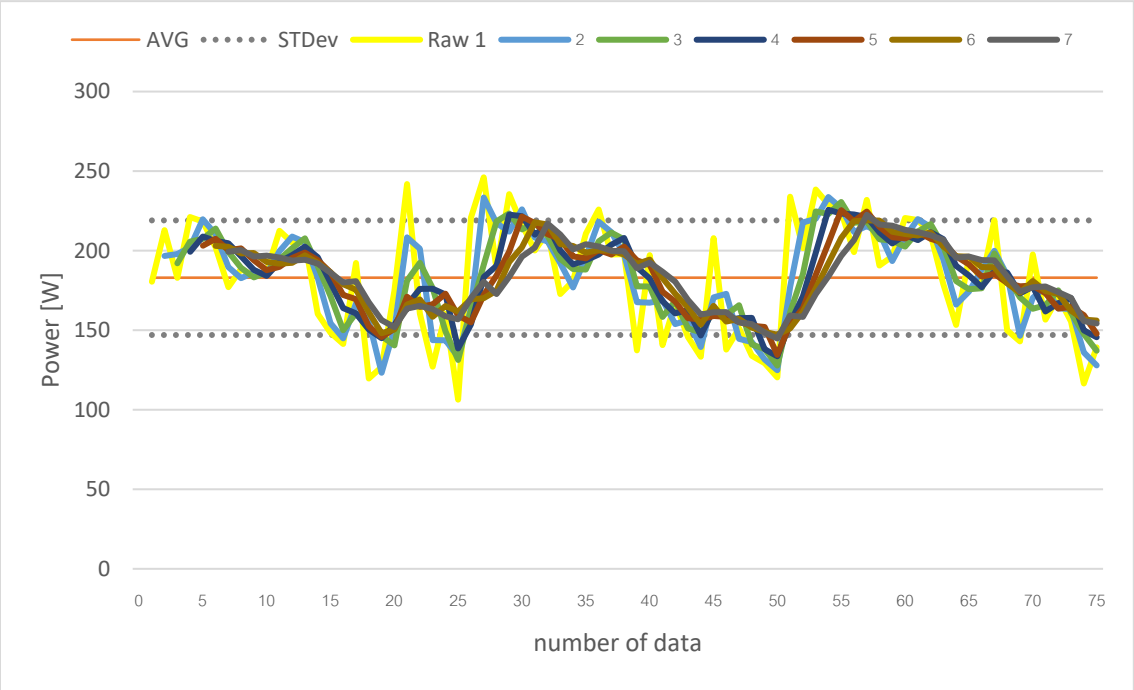

Figure 4-6 Moving average of track mode on soft soil.

The cost function is used in this research to switch modes. Cost function(C) is function of soil compaction and soil distortion Cost function is the tradeoff between soil compaction and soil distortion, as shown in Eq (4.1). The soil damage includes sinkage and soil distortion. The power is an indirect measure of sinkage, and the slip is an indirect measure of soil distortion.

$$C = \Delta P_{estimate} - wS \tag{4.1}$$

where $\Delta P_{estimate}$ is estimate power and indirect measure of soil compaction and S is is slip and indirect measure of soil distortion and shear displacement. w is the weight to adjust the ratio.

Normalization of P and S is used to calculate the cost function. The data from tables 30 and 31 are used to normalize $\Delta P_{estimate}$ and S. For P, we normalize to 0 for 0 W and 1 for 500 W. For S, we normalize to 0 for 0% and 1 for 100%. Next, we define a threshold for the cost function. We define that if the cost function is plus (+), use track mode, and if the cost function is minus (-), use wheel mode to understand easier. Next, we define the weight of the cost function. The cost function should classify soft soil and firm soil. The weight is selected using information from Figure 4-7. Figure 4-7 show the cost function every cone index. The weight should classify soft and firm soil. In this experiment, w is 0.5. The weight of 0.5 can classify soft soil and firm soil as shown in Figure 4-7.

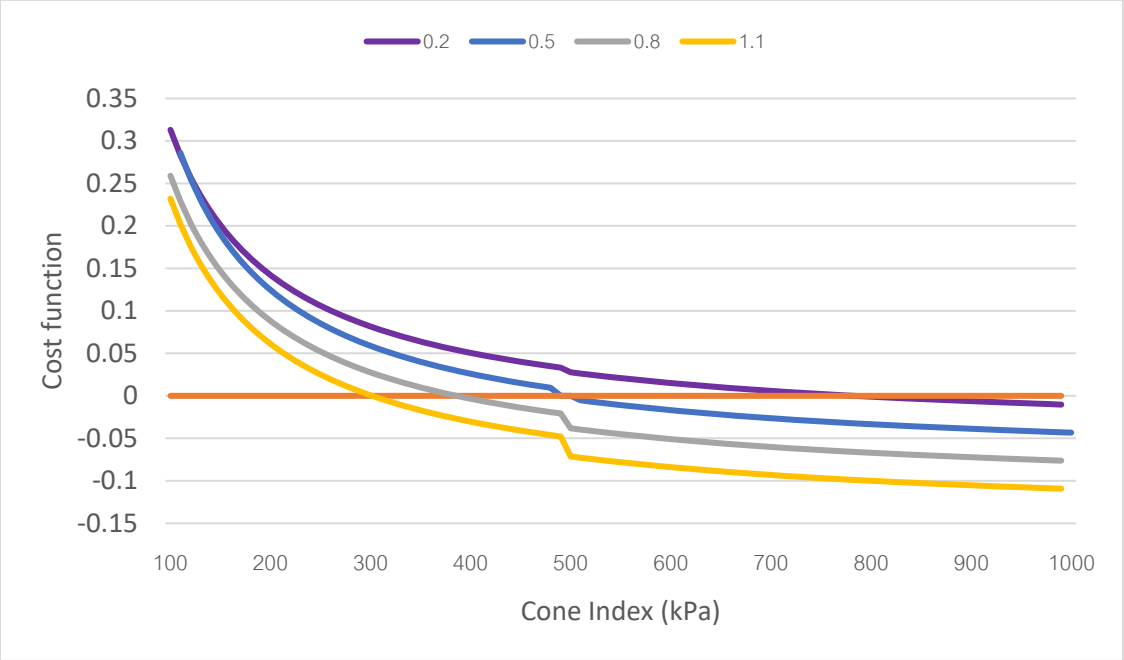

Figure 4-7 Selecting the weight of cost function

Finally, we define the dead zone. If the cost function is in the dead zone, the robot will not change the mode. If we don't define the dead zone, the robot will change mode many times in the experiment. The dead zone of the cost function is $-0.06 < C < 0.15$.

On the test, two different soil (soft and firm) conditions are prepared. First, we prepare soft and firm soil conditions. The robot moves on soft soil in track mode and switches to wheel mode autonomously when it moves on firm soil. Second, the robot moves on firm soil in wheel mode and switches to track mode autonomously when it moves on soft soil.

4.2. Experimental Results and Discussions

Figure 4-8 shows a video of the experiment switching from track to wheel mode autonomously. Figure 4-9 shows the cost function when the robot switches from track mode to wheel mode. The robot moves on soft soil in track mode and switches to wheel mode on firm soil. At a distance of 0–5 m, the robot moves in track mode on soft soil, as shown in Figure 4-8(1). At time 16 s, the cost function is lower than the dead zone, as

shown in Figure 4-9. So, the robot stops and switches to wheel mode, as shown in Figures 4-8(2) and 4-8(3). Finally, the robot moves in wheel mode, as shown in Figures 4–8(4). Figure 4-10 shows a comparison of sinkage between autonomous mode and track mode. Figure 4-11 shows the comparison of shear displacement between autonomous mode and single-track mode. Figure 4-12 shows the comparison power between autonomous mode and single-track mode. The sinkage and power of autonomous mode are similar to those of track mode. But the shear displacement in autonomous mode is lower than in track mode. Autonomous mode switches to wheel mode on firm soil to reduce shear displacement. Table 31 shows a summary of the results in firm soil for autonomous mode and track mode.

Figure 4-8 Experiment switch from track to wheel mode

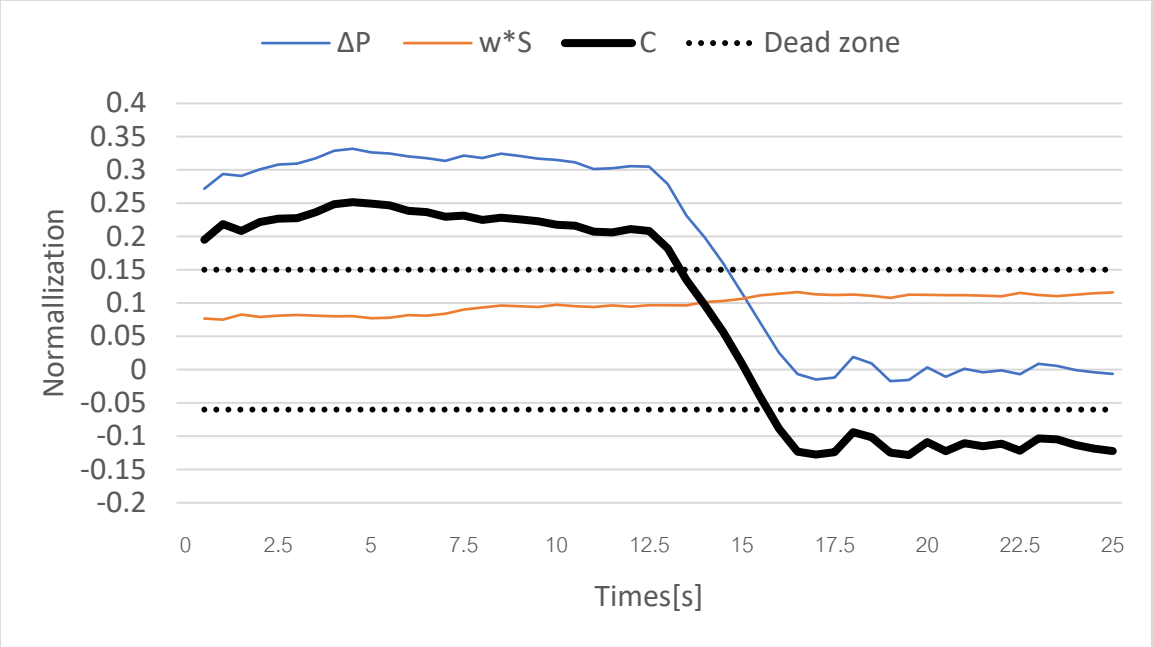

Figure 4-9 Cost function of experiment switch from track to wheel mode

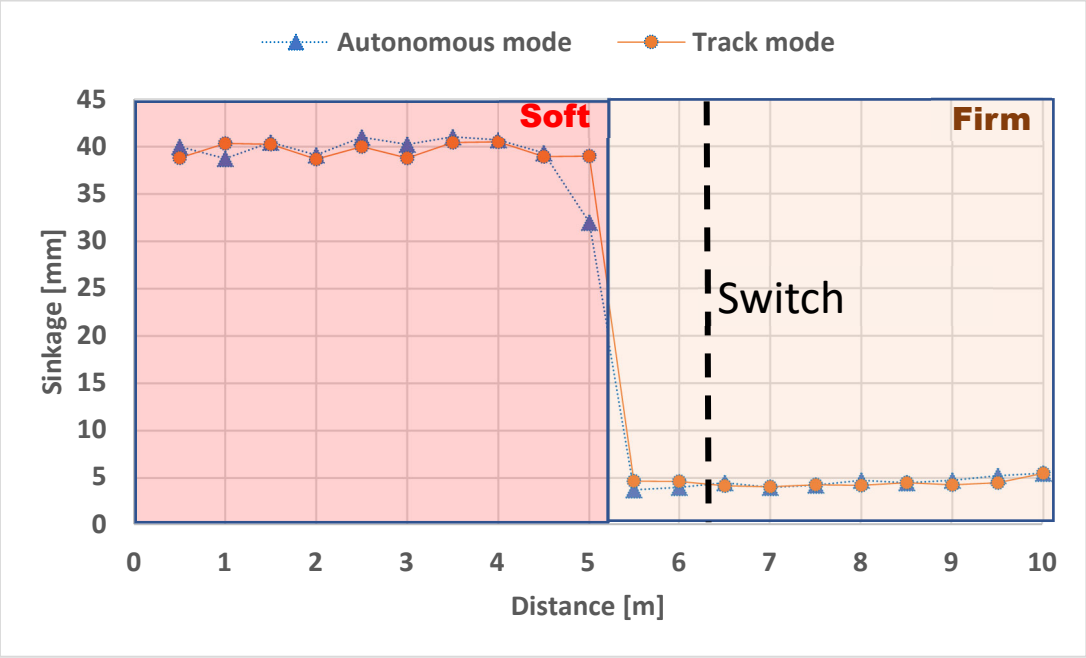

Figure 4-10 Sinkage between autonomous mode and track mode

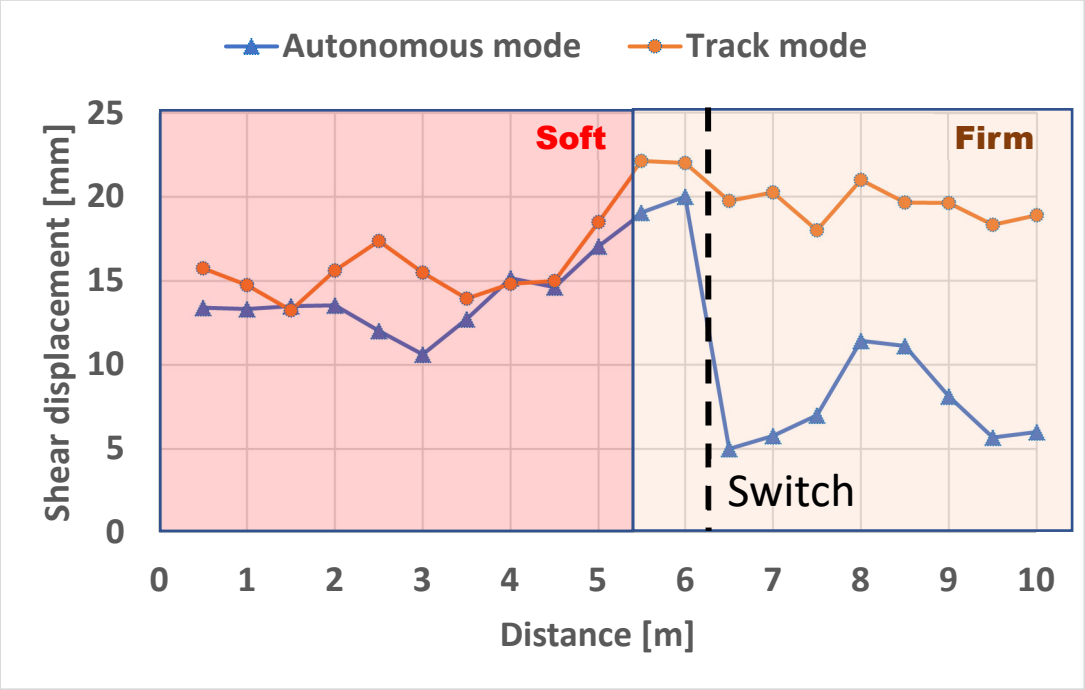

Figure 4-11 Shear displacement between autonomous mode and track mode

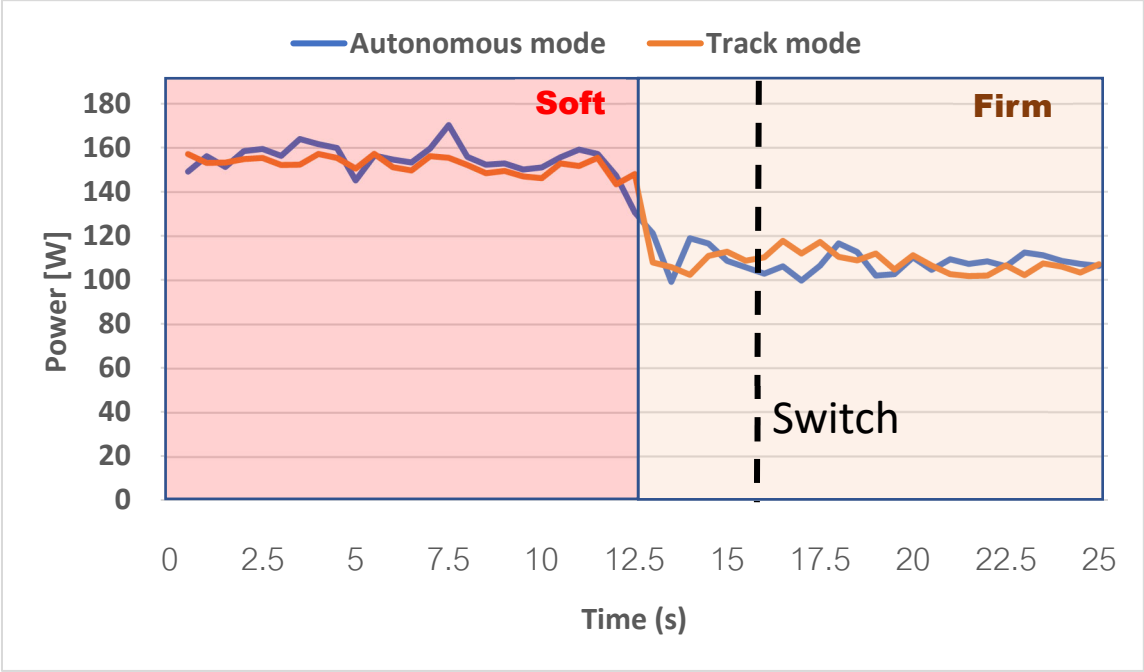

Figure 4-12 Power between autonomous mode and track mode

Mode	Sinkage [mm]	Power [W]	Shear displacement [mm]
Autonomous mode	4.5	108	9.8
Track	4.4	108	19.9

Table 31 Summary results in firm soil for autonomous mode and track mode.

Figure 4-13 shows a video of the experiment switching from wheel to track mode autonomously. Figure 4-14 shows the cost function when the robot switches from wheel mode to track mode. The robot moves on firm soil in wheel mode and switches to track mode on soft soil. At a distance of 0–5 m, the robot moves in wheel mode on firm soil, as shown in Figure 4-13(1). At time 16 s, the cost function is lower than the dead zone, as shown in Figure 4-14. So, the robot stops and switches to track mode, as shown in Figures 4-13(2) and 4-13(3). Finally, the robot moves in track mode, as shown in Figure 4-13(4). Figure 4-15 shows the comparison of sinkage between autonomous mode and single-wheel mode. Figure 4-16 shows the comparison of shear displacement between autonomous mode and single-wheel mode. Figure 4-17 shows the difference between autonomous mode and single-wheel mode. The sinkage and power of autonomous mode are lower than in wheel mode. So, the autonomous mode can reduce power and soil damage caused by sinkage. Table 32 shows a summary of the results in firm soil for autonomous mode and wheel mode. The average results of both firm and soft soil from Table 31 and 32 are shown in Table 33. Wheel mode has higher sinkage and power. Track mode has higher shear displacement. Autonomous switching mode can reduce sinkage and power if compared to wheel mode. Autonomous switching mode can reduce shear displacement if compared to track mode.

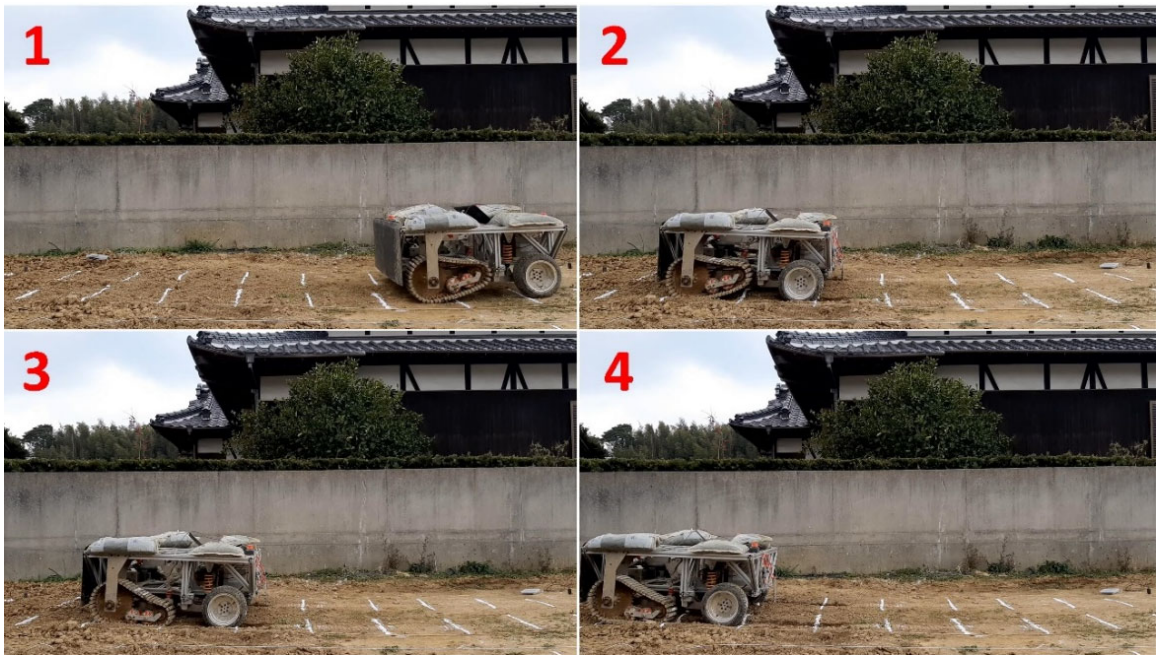

Figure 4-13 Experiment switch from wheel to track mode

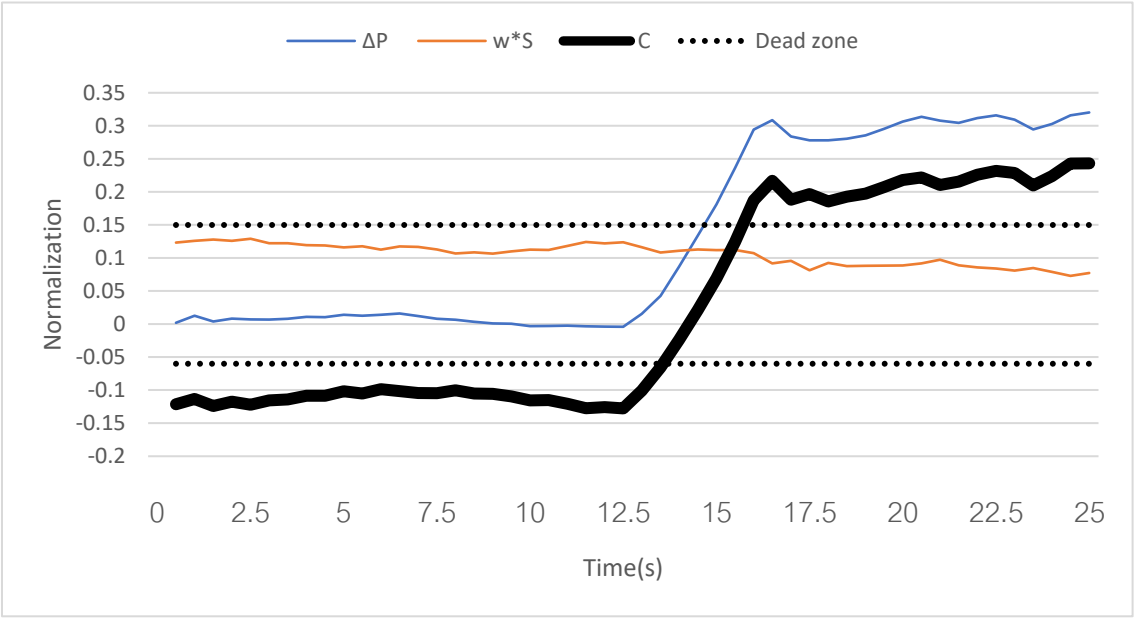

Figure 4-14 Cost function of experiment switch from wheel to track mode

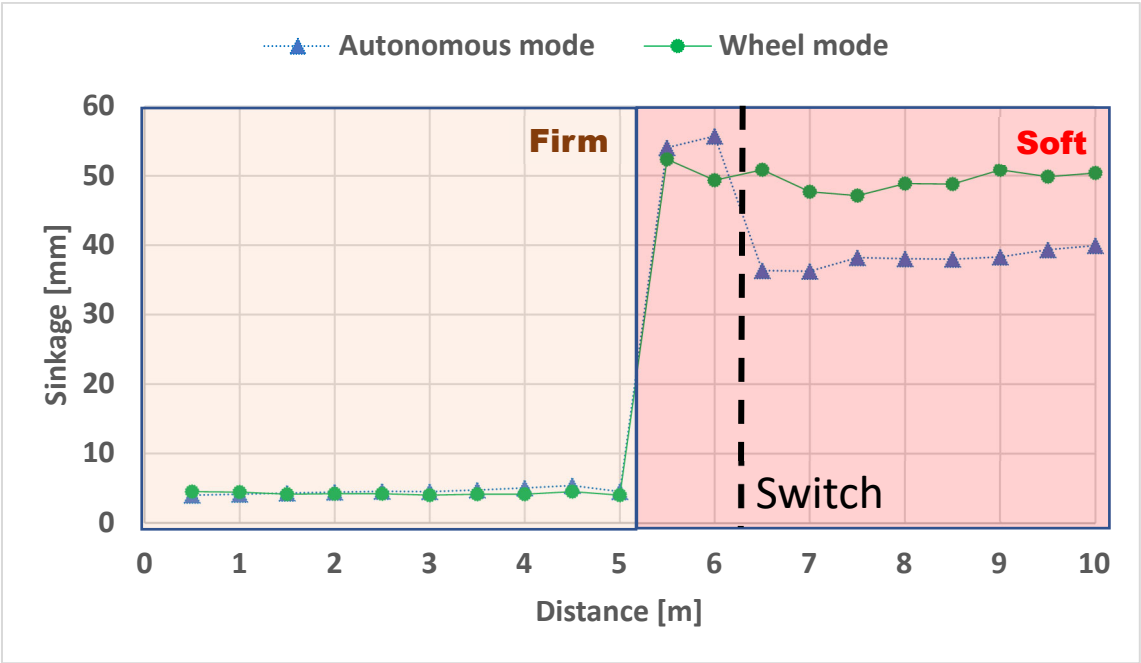

Figure 4-15 Sinkage between autonomous mode and wheel mode

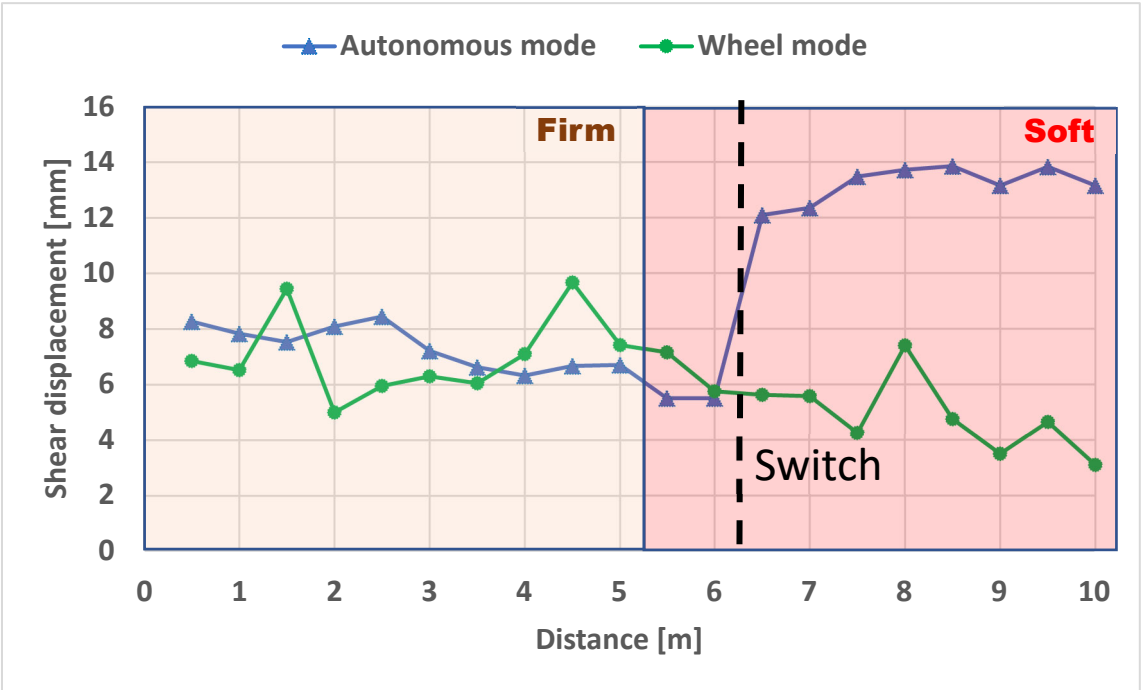

Figure 4-16 Shear displacement between autonomous mode and wheel mode

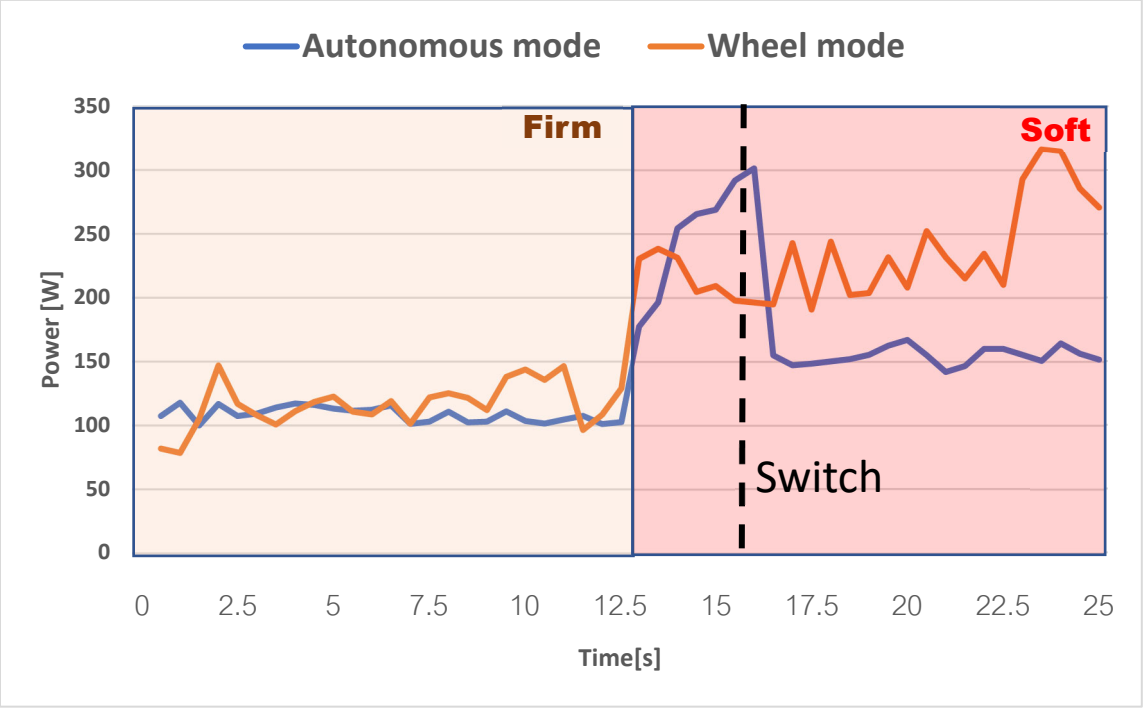

Figure 4-17 Power between autonomous mode and wheel mode

Mode	Sinkage [mm]	Power [W]	Shear displacement [mm]
Autonomous mode	41.4	181	11.6
Wheel	49.6	234	5.1

Table 32 summary results in firm soil for autonomous mode and wheel mode.

Mode	Sinkage [mm]	Power [W]	Shear displacement [mm]
Track to Wheel	21.9	132	10.8
Wheel to Track	22	140	11.1
Track	21.8	131	17.7
Wheel	27	175	6

Table 33 Summary results in firm/soft soil for autonomous mode and single mode.

Chapter 5
Conclusion

Chapter 5. Conclusion

The use of heavy machinery in agriculture has led to progressive soil degradation, a consequent reduction in crop yields, and an increase in maintenance costs. The soil damage is of two types: soil compaction (volume reduction) and distortion (shearing and deformation). Because this damage is affected by the state of the soil and by the contact area between the soil and running gear, the design of a vehicle able to change its contact area is here considered. The wheel/track reconfigurable mobile robot is developed to change contact area based on soil conditions to minimize soil damage and power. The robot has two modes, which are wheel mode and track mode. The robot is intended to transport the grapes into the vineyards and replace the use of heavy tractors during the harvesting period. The proposed system can pass from a wheeled vehicle, suited for hard, dry soil, to a half-tracked vehicle, suited for more soft and deformable soil.

The robot is tested on three agricultural soil conditions to compare soil damage and performance between wheel and track modes. Two conditions are considered: 1) without payload and 2) payload condition. The damage to the soil is caused by sinkage and soil distortion. The sinkage and power consumption of the payload condition are higher than without the payload condition because of the weight. The power is an indirect measure of the rolling resistance, sinkage, and soil compaction (on dry soil). For soil distortion, track mode causes higher shear displacement in three soil conditions because track has a longer contact area. The slip is an indirect measure of the soil distortion.

On firm soil, the power consumption of wheel mode and track mode is similar, but the shear displacement of track is higher than that of wheel mode. On soft soil and wet soil,

wheel mode causes higher sinkage and higher power consumption if compared with track mode.

After the results are obtained, we implement a cost function to switch modes autonomously. The graph between power and cone index in this experiment is proposed. We use this graph to estimate the difference power between wheel mode and track on each cone index. The results show autonomous switching modes can reduce sinkage and power if compared to wheel mode. Also, autonomous switching mode can reduce shear displacement if compared to track mode.

In our future work, we plan to use GPS to estimate the location and velocity of the robot because the laser distance sensor has the limitation that the robot needs to move in a straight line. Also, other methods, such as fuzzy logic and neural networks, will implement autonomous switching mechanisms.

Acknowledgements

I am extremely grateful to my supervisor, Prof. Ishii, for his invaluable advice, continuous support, and patience during my PhD study. His knowledge and plentiful experience have encouraged me in all my academic research and daily life. I'm extremely grateful to Prof. Nishida and Prof. Yasukawa, who generously provided expertise and knowledge. I would also like to thank Dr. Enrico and Dr. Raji for their technical support in my study. I would like to thank all the members of LAB ISHII. It is their kind help and support that have made my study and life in Japan a wonderful time. Finally, I would like to express my gratitude to my parents. Without their tremendous understanding and encouragement in the past few years, it would be impossible for me to complete my study.

References

[1] E. di Maria. "Running gear size selection of a wheel/track reconfigurable grape transporting vehicle by FEM analysis," phdthesis, Graduate School of Life Science and Systems Engineering, Kyushu Institute of Technology, March 2021.

[2] A. Maruyama, K. Naruse, “Development of small weeding robots for rice fields,” in 2014 IEEE/SICE International Symposium on System Integration, 13-15 December 2014, Japan, 2014.

[3] K. Nakamura, M. Kimura,T. Anazawa, T. Takahashi, K. Naruse ,“Investigation of weeding ability and plant damage for rice field weeding robots,” in 2016 IEEE/SICE International Symposium on System Integration (SII), 13-15 December 2016, Japan, 2016.

[4] A. Choudhary,Y. Kobayashi, F. J. Arjonilla,S. Nagasaka,M. Koike “Evaluation of mapping and path planning for non-holonomic mobile robot navigation in narrow pathway for agricultural application,” in 2021 IEEE/SICE International Symposium on System Integration (SII), 11-14 January 2021, Japan, 2021.

[5] H. Masuzawa, J. Miura, S. Oishi, “Development of a mobile robot for harvest support in greenhouse horticulture — Person following and mapping,” in 2017 IEEE/SICE International Symposium on System Integration (SII), 11-14 December 2017, Taiwan, 2017.

[6] T. Fujinaga, S. Yasukawa, K. Ishii, “Evaluation of Tomato Fruit Harvestability for Robotic Harvesting,” in 2021 IEEE/SICE International Symposium on System Integrations, January 11 - 14 2021, Japan, 2021.

[7] L. Yang, D. Gao, Y.Hoshino,“ Evaluation of the accuracy of an auto-navigation system for a tractor in mountain areas,” in 2017 IEEE/SICE International Symposium on System Integration (SII), 11-14 December 2017, Taiwan, 2017.

[8] H. Wang, N. Noguchi,“ Autonomous maneuvers of a robotic tractor for farming,” in 2016 IEEE/SICE International Symposium on System Integration (SII), 13-15 December 2016, Japan, 2016.

[9] J. Eriksson, I. Haekanson, and B. Danfors, "The effect of soil compaction on soil structure and crop yields," Swedish Institute of Agricultural Engineering, 1975.

[10] R. Lal, "Soil structure and sustainability," Journal of sustainable agriculture, pp. 67–92, 1991.

[11] Thomas Keller. Soil compaction and soil tillage-studies in agricultural soil mechanics, volume 489. 2004.

[12] T. Keller, M. Berli, S. Ruiz, M. Lamandé, J. Arvidsson, P. Schjønning, and Antony P. S. Selvadurai. Transmission of vertical soil stress under agricultural tyres: Comparing measurements with simulations. Soil and Tillage Research, 140:106–117, 2014.

[13] L. ten Damme, M. Stettler, F. Pinet, P. Vervaet, T. Keller, L. Juhl Munkholm, and M. Lamandé. The contribution of tyre evolution to the reduction of soil compaction risks. Soil and Tillage Research, 194:104283, 2019.

[14] Earth Observing System website. Soil types: A main aspect of agricultural productivity. https://eos.com/blog/soil-types-as-a-paramount-aspectof-agricultural-productivity/.

[15] A. Pires da Silva and B.D. Kay,"The sensitivity of shoot growth of corn to the least limiting water range of soils," Plant and Soil, vol.184,1996.

[16] A. Canarache, " PENETR — a generalized semi-empirical model estimating soil resistance to penetration," Soil and Tillage Research, vol. 16, pp. 51-70, 1990.

[17] M. T. De Moraes, A. L. Zwirtes, "Use of penetrometers in agriculture: A review," Article in Engenharia Agrícola, 2014.

[18] M. Lamandé, M. H. Greve, and P. Schjønning. Risk assessment of soil compaction in europe–rubber tracks or wheels on machinery. Catena, 167:353–362, 2018.

[19] T. Keller et al., "Historical increase in agricultural machinery weights enhanced soil stress levels and adversely affected soil functioning," Soil Tillage & Research, vol. 194, 2019.

[20] W.C. Chamen et al., "Mitigating arable soil compaction: A review and analysis of available cost and benefit data," Soil & Tillage Research, vol. 146, pp. 10-25, 2015.

[21] P. Hornback, "The Wheel Versus Track Dilemma," ARMOR, 1998.

[22] R. Galati and G. Reina, " Terrain Awareness Using a Tracked Skid-Steering Vehicle With Passive Independent Suspensions," Frontier in Robotics and AI, 2019.

[23] M. F. Nawaz, G. Bourrié, F. Trolardr, " Soil compaction impact and modelling. A review," Agron. Sustain. Dev, 2013.

[24] X. Huang, R. Horn, T. Renl, "Soil structure effects on deformation, pore water pressure, and consequences for air permeability during compaction and subsequent shearing," Geoderma, vol. 406, 2022.

[25] A. Battiato, E. Diserens, L. Laloui, L. Sartori " A Mechanistic Approach to Topsoil Damage due to Slip of Tractor Tyres," Journal of Agricultural Science and Applications, 2013.

[26] B.V. Iversen, P. Schjønning, "In Situ, on-Site and Laboratory Measurements of Soil Air Permeability: Boundary Conditions and Measurement Scale." Soil Science, vol. 166, 2001.

[27] M. Wang, X. Wang, Y. Sun, Z. Gu, " Tractive performance evaluation of seafloor tracked trencher based on laboratory mechanical measurements," in International Journal of Naval Architecture and Ocean Engineering, vol.8, pp. 177-187, 2016.

[28] Grazioso, A., di Maria, E., Giannoccaro, N.I., Ishii, K. Multibody Modeling of a New Wheel/Track Reconfigurable Loco-motion System for a Small Farming Vehicle. Machines, 2022, 10, 1-29.

[29] di Maria, E., Reina, G., Ishii, K., Giannoccaro, N.I. Rolling resistance and sinkage analysis by comparing FEM and ex-perimental data for a grape transporting vehicle. Journal of Terramechanics, 2021, 97, 59-70.

[30] Ojeda, L., Borenstein, J., Witus, G., Karlsen, R., 2006. Terrain characterization and classification with a mobile robot. J. Field Robot. 23 (2), 103–122.

[31] S. Khaleghian, S. Taheri, "Terrain classification using intelligent tire," Journal of Terramechanics, vol. 71, pp. 15-24, 2017.

[32] J. M. Solis, R. G. Longoria, " Modeling track–terrain interaction for transient robotic vehicle maneuvers," Journal of Terramechanics, vol. 45, pp. 65-78, 2008.

[33] Chetan J., Madhava Krishna, C. V. Jawahar, "Fast and Spatially-smooth Terrain Classification using Monocular Camera," 2010 International Conference on Pattern Recognition, 2010.

[34] G. Reina, A. Milella, R. Galati, " Terrain assessment for precision agriculture using vehicle dynamic modelling," Biosystems engineering, vol. 162, pp. 124-139, 2017.

[35] L.A. Zadeh,"Fuzzy logic," Computer,1988.

[36] P. Parikh, S. Sheth, R. Vasani Dr., J. K. Gohil, " Implementing Fuzzy Logic Controller and PID Controller to a DC Encoder Motor – "A case of an Automated Guided Vehicle"," Procedia Manufacturing, vol. 20, pp. 219-226, 2018.

[37] V. Stoian, M. Ivanescu, "Robot Control by Fuzzy Logic," Frontiers in Robotics, Automation and Control, 2008.

[38] J.M. Mendel, " Fuzzy logic systems for engineering: a tutorial," Proceedings of the IEEE, vol. 83, vol. 57, 1995.

[39] GeeksforGeeks, " Fuzzy Logic | Introduction," 2012. [Online]. Available: https://www.geeksforgeeks.org/fuzzy-logic-introduction.

[40] Electrical Technology, "What is Fuzzy Logic System – Operation, Examples, Advantages & Applications," 2012. [Online]. Available: https://www.electricaltechnology.org/2018/02/fuzzy-logic-system.html.

[41] SKL DOC, "eFLL - A Fuzzy Library for Arduino and Embedded Systems," 2012. [Online]. Available: https://blog.zerokol.com/2012/09/arduinofuzzy-fuzzy-library-for-arduino.html.

[42] D. Pattanaik, "Microcontroller based Implementation of A fuzzy knowledge based controller," bachelor thesis, Department of Electrical Engineering, National Institute of Technology, 2013

[43] Y. Tian, B. Shirinzadeh, D. Zhang, G. Alici, "Development and dynamic modelling of a flexure-basedScott–Russell mechanism for nano-manipulation," Mechanical Systemsand Signal Processing, vol. 23, pp. 957-978, 2009.

[44] Q. Xu, "Structure design of a new compliant gripper based on Scott-Russell mechanism," IEEE International Conference on Robotics and Biomimetics (ROBIO), 2013.

[45] Ching-Ming C., Rong-Fong F., "Dynamic modeling of a scott-russell amplifying mechanism driven by a piezoelectric actuator," IEEE ICCA, 2010.

[46] Adams, H. Chassis Engineering. Chassis design, building & tuning for high-performance cars. HP Books, 1992.

[47] S. S. Patel, "Modeling and Implementation of Intelligent Commutation System For BLDC Motor in Underwater Robotic Applications," International conference on Power Electronics, Intelligent control and Energy Systems (ICPEICES), 2016

[48] Myung-Jin C., "Development of in-wheel motor system using blushless DC motor of hall sensor type", International Conference on Control, Automation and Systems, 2008.

[49] T. Naruta, Y. Akiyama, Y. Niwa, "A study of cooling coefficient of the brushless DC motor for car air conditioner," International Conference on Electrical Machines and Systems (ICEMS), 2007

[50] N. Ishak, M. Tajjudin, "Real-time application of self-tuning PID in electro-hydraulic actuator," IEEE International Conference on Control System, Computing and Engineering, 2011.

[51] R. Kumar Gupta, L. Kumar, N. Pada Mandal"Displacement Control of an Electro-Hydraulic Actuator using Proportional Solenoid Valve," International Conference on Computing, Power and Communication Technologies (GUCON), 2019.

[52] X. Tian; H. An, Z. Zhang, X. Chang, H. Ma, Q. Wei, "Force Tracking Control for Electro-Hydraulic Actuators Based on Radial Basis Function Neural Networks," IEEE International Conference on Real-time Computing and Robotics (RCAR), 2021.

[53] O. Barybin, E. Zaitseva, V. Brazhnyi, "Testing the Security ESP32 Internet of Things Devices," IEEE International Scientific-Practical Conference Problems of Infocommunications, Science and Technology (PIC S&T), 2019.

[54] A. Maier, A. Sharp, Y. Vagapov, " Comparative Analysis and Practical Implementation of the ESP32 Microcontroller Module for the Internet of Things," 2017 Internet Technologies and Applications (ITA), 2017.

[55] R. Podder, R. Kumar Barai, "Hybrid Encryption Algorithm for the Data Security of ESP32 based IoT-enabled Robots," Innovations in Energy Management and Renewable Resources, 2021.

[56] R. Niranjana; Arvind S; Vignesh M; Vishaal S, "Effectual Home Automation using ESP32 NodeMCU," International Conference on Automation, Computing and Renewable Systems (ICACRS), 2022.

[57] A. Koushal, R. Gupta; F. Jan, K. Kamaldeep, V. Kumar, "Home Automation System Using ESP32 and Firebase," Seventh International Conference on Parallel, Distributed and Grid Computing (PDGC), 2022.

[58] I. Allafi, T. Iqbal, "Design and implementation of a low cost web server using ESP32 for real-time photovoltaic system monitoring," IEEE Electrical Power and Energy Conference (EPEC), 2017.

[59] RANDOM NERD TUTORIAL. (2020, April 14). ESP-NOW with ESP32: Receive Data from Multiple Boards (many-to-one). https://randomnerdtutorials.com/esp-now-many-to-one-esp32/.

[60] RealPars, Limit Switch Explained (2021) | Working Principles https://realpars.com/limit-switch/

[61] electronicshacks, Normally Open vs. Normally Closed: What Does it Mean? (2019) https://electronicshacks.com/normally-open-vs-normally-closed/

[62] Y. Soo Suh, "Laser Sensors for Displacement, Distance and Position," sensors (MDPI), 2019.

[63] K. Konolige; J. Augenbraun; N. Donaldson; C. Fiebig; Pankaj Shah,"A low-cost laser distance sensor," IEEE International Conference on Robotics and Automation, 2008.

[64] S. Chowdhury, S. Sen and S. Janardhanan, "Comparative Analysis and Calibration of Low Cost Resistive and Capacitive Soil Moisture Sensor," arXiv:2210.03019, 2022.

[65] C. I. M. Kulmány, Á. Bede-Fazekas, A. Beslin, "Calibration of an Arduino-based low-cost capacitive soil moisture sensor for smart agriculture," Journal of Hydrology and Hydromechanics, 2022.

[66] S. Nath, J. kumar Nath, Prof. K. C. Sarma, " IOT based system for continuous measurement and monitoring of temperature, soil moisture and relative humidity," International Journal of Electrical Engineering & Technology (IJEET), vol. 9, pp.106-113, 2018.

[67] N. Putjaikal, S. Phusael, A. Chen-Iml, " A Control System in an Intelligent Farming by using Arduino Technology," 2016 Fifth ICT International Student Project Conference (ICT-ISPC), 2016.

[68] S. L. Miller, B. Youngberg, A. Millie, P. Schweizer, J. C. Gerdes, " Calculating Longitudinal Wheel Slip and Tire Parameters Using GPS Velocity," Proceedings of the American Control Conference, 2001.

[69] S. Kareemulla, E. Prajwal "GPS based Autonomous Agricultural Robot," International Conference on Design Innovations for 3Cs Compute Communicate Control, 2018.

[70] Visual Basic documentation. Available online. https://learn.microsoft.com/en-us/dotnet/visual-basic/ (accessed on 20 June 2023)..

[71] L. Kaddour, J. Vareille, "Remote control on Internet,long distance experiment of remote practice works, measurements and results," International Review on Computers and Software (IRECOS), 2007.

[72] C. Vaida, D. Pisla, F. Covaciu, B. Gherman, A. Pisla, N. Plitea, "Development of a control system for a HEXA parallel robot," IEEE International Conference on Automation, Quality and Testing, Robotics (AQTR), 2016.

[73] Uteh Str.(2018, April 6). Visual Basic .NET | Receive Serial Data From Arduino [Video].YouTube. https://www.youtube.com/watch?v=T6b_K0ou6dA.

[74] ProgrammingKnowledge. (2014, Feb 14) Visual Basic .NET Tutorial 36 - How to use Chart /Graph in VB.NET [Video]. YouTube. https://www.youtube.com/watch?v=K31g-D7GaMM.

[75] Electronic Clinic.(2018, May 22). how to split a string message and access the sensors values sent from Arduino to visual Basic [Video]. YouTube. https://www.youtube.com/watch?v=Da9Llyn6nXU.

[76] G. R. Gerhart, “The Bekker model analysis for small robot vehicles”, US Army TACOM, 2004.

[77] A. Perrakis (2022, January 17). Spatial Calibration of a graph, with demo. https://jp.mathworks.com/matlabcentral/answers/1630745-spatial-calibration-of-a-graph-with-demo?s_tid=prof_contriblnk.
[78] E. di Maria, K. Ishii, " Soil Compaction and Rolling Resistance Evaluation of a Locomotion System with an Adjustable Contact Patch for a Grape Transporting Robot", Journal of Robotics, Networking and Artificial Life
Vol. 6(3); December (2019), pp. 148–151.